Pseudo Euler-Lagrange and Piecewise Affine Control Applied to Surge and Stall in Axial Compressors

Seyed Mohamad Amin Seyedahmady Zavieh

A Thesis

in

The Department

of

Electrical and Computer Engineering

Presented in Partial Fulfillment of the Requirements

for the Degree of Master of Applied Science (Electrical and Computer Engineering) at

Concordia University

Montréal, Québec, Canada

February 2013

CONCORDIA UNIVERSITY

School of Graduate Studies

This is to certify that the thesis proposal prepared

By: **Seyed Mohamad Amin Seyedahmady Zavieh**

Entitled: **Pseudo Euler-Lagrange and Piecewise Affine Control Applied to Surge and Stall in Axial Compressors**

and submitted in partial fulfilment of the requirements for the degree of

Master of Applied Science (Electrical and Computer Engineering)

complies with the regulations of this University and meets the accepted standards with respect to originality and quality.

Signed by the final examining committee:

_____ Dr. Xiupu Zhang, Chair

_____ Dr. Wahid Ghaly, Examiner, External

_____ Dr. Amir Aghdam, Examiner

_____ Dr. Mustafa Mehmet Ali, Examiner

_____ Dr. Khashayar Khorasani, Supervisor

_____ Dr. Luis Rodrigues, Supervisor

Approved by _____

Dr. W. E. Lynch, Chair

Department of Electrical and Computer Engineering

_____

Dr. Robin A. L. Drew

Dean, Faculty of Engineering and Computer Science

ABSTRACT

Pseudo Euler-Lagrange and Piecewise Affine Control Applied to Surge and Stall in Axial Compressors

Seyed Mohamad Amin Seyedahmady Zavieh

This thesis addresses the control of the axial compressor surge and stall phenomena using Pseudo Euler-Lagrange and Piecewise Affine (PWA) controller synthesis techniques. These phenomena are considered as major gas turbine compressor instabilities that may result in failures such as the engine flame-out or severe mechanical damages caused by high blade vibration. The common approach towards the detection of the rotating stall and surge is to install various types of pressure sensors, hot wires and velocity probes. The inception of the rotating stall and surge is recognized by the presence of pressure fluctuation and velocity disturbances in the gas stream that are obtained through sensors. The necessary measure is then taken by applying proper stall and surge stabilizing control actions. The Lyapunov stability of pseudo Euler-Lagrange systems in the literature is extended to include additional nonlinear terms. Although Lyapunov stability theory is considered as the cornerstone of analysis of nonlinear systems, the generalization of this energy-based method poses a drawback that makes obtaining a Lyapunov function a difficult task. Therefore, proposing a method for generating a Lyapunov function for the control synthesis problem of a class of nonlinear systems is of potential importance. A systematic Lyapunov-based controller synthesis technique for a class of second order systems is addressed in this thesis. It is shown, in terms of stability characteristics, that the

proposed technique provides a more robust solution to the compressor surge suppression problem as compared to the feedback linearization and the backstepping methods. The second contribution is a proposed new PWA approximation algorithm. Such an approximation is very important in reducing the complexity of nonlinear systems models while keeping the global validity of the models. The proposed method builds upon previous work on piecewise affine (PWA) approximation methods, which can be used to approximate continuous functions of n-variables by a PWA function. Having computed the PWA model of the stall and surge equations, the suppression problem is then solved by using PWA synthesis techniques. The proposed solution is shown to have higher damping characteristics as compared to the backstepping nonlinear method.

"At every step from the conception of a rational vision to the formulation of the theory, faith is necessary: faith in the vision as a rationally valid aim to pursue, faith in the hypothesis as a likely and plausible proposition, and faith in the final theory, at least until a general consensus about its validity has been reached."

— Erich Fromm, *The Art of Loving*

Dedicated to

My Parents

ACKNOWLEDGEMENTS

First of all, I extend my deep gratitude to my supervisors Dr. Luis Rodrigues and Dr. Khashayar Khorasani for awakening my interest in this particular field. This research, as one of my important life and academic goals, could not be accomplished without the invaluable and technical guidance and also generous support of them. I must thank Dr. W. Ghaly, Dr. A. Aghdam and Dr. M. Mehmet Ali as the defense examining committee members for their constructive comments, as well as the administrative and the technical staff of the department for their unstinting support and help.

I would like to heartily thank all my HYCONS family members and friends Miad Moarref, Hadi Karimi, Sina Kaynama, Camilo Ossa, Mehdi Abedinpour, Behzad Samadi, Mohsen Zamani, Azita Malek, Gavin Kenneally, Qasim Bhojani and Sahar Sedaghati, with whom I spent great moments during this period of my life. In particular, my profuse thanks goes to Miad Moarref, who I distracted a lot with my questions and who answered them unstintingly.

And of course, I owe my father Saeed, my mother Guiti and my sister Sarah a great dept of eternal gratitude for their continuous support and passionate love. I also would like to thank Sulmas for her help, understanding and patience.

Amin Zavieh

February 2013

TABLE OF CONTENTS

LIST OF FIGURES

LIST OF TABLES

LIST OF SYMBOLS

A. Nomenclature Used in The Compressor Modeling

Symbols Used in The Compressor Modeling

A	Stall amplitude
A_c	Compressor duct area
a	Dimensionless blade passage length reciprocal for N stages
a_s	Speed of sound
C_x	Axial component of the gas flow velocity
$F(\bar{\phi})$	Quasi-steady pressure rise coefficient
$F_T(\Phi_T)$	Throttle characteristic function
g	Axial velocity disturbance
H	Axisymmetric characteristic function constant
h	Circumferential velocity disturbance
K_G	Inlet Guide Vanes (IGVs) efficiency
l_{en}	Non-dimensional entrance duct length
l_{ex}	Non-dimensional exit duct length
l_{th}	Non-dimensional throttle duct length
l_c	Non-dimensional total aerodynamic duct length
L_c	$= \mathcal{R} l_c$ is the total aerodynamic duct length
m	Exit duct length integer coefficient

Symbols Used in The Compressor Modeling

N	Number of compressor stages
P	Pressure of the flow
P_i	Flow pressure at point $i \in \{1,2,\ldots,5\}$
$\mathscr{P}$	Dimensionless pressure coefficient
R	$= A^2$
$\mathcal{R}$	Compressor mean wheel radius
r	Phase angle
U	Wheel velocity at mean wheel radius
V_P	Plenum volume
W	Axisymmetric characteristic function constant
Y	Velocity potential of the disturbance at IGV entrance
β	Moore-Greitzer model parameter
η	Compression system axial axis
θ	Compression system circumferential axis
ξ	Dimensionless time parameter
ρ	Working fluid density
σ	Moore-Greitzer model constant
Φ	Averaged local axial flow coefficient
Φ_T	Flow coefficient of the throttle duct
ϕ	$= \Phi - 1$
$\bar{\phi}$	Local axial flow coefficient

Symbols Used in The Compressor Modeling

$\tilde{\phi}$	Velocity potential
$\tilde{\phi}'$	Velocity potential of the disturbance
Ψ	Dimensionless coefficient describing the difference of the free stream and the plenum pressure
ψ	$= \Psi - 1$
$\bar{\psi}_c$	Axisymmetric characteristic function

B. Nomenclature Used in Pseudo Euler-Lagrange Systems

Scripts and Operations

$f'(x),\ f'_x$	$= df/dx$, only for $x \in \mathbb{R}$
V_{x_i}	$= \partial V(x)/\partial x_i$, with $i \in \mathbb{N}$
$\nabla^2(\cdot)$	is the Hessian operator
$\Delta(\cdot)$	is used to denote the discriminant of a polynomial

Symbols Used in Pseudo Euler-Lagrange Systems

a_s	Speed of sound
A_c	Compressor duct area
$f,\ f(x_2)$	Nonlinear function of one variable used in Theorem 3.3.1
$\tilde{f},\ \tilde{f}(x_2)$	Generalized form of f defined in the equation set (3.21)
$f_1,\quad f_2,\quad f_1(x_2),$ $f_2(x_2)$	Nonlinear functions of one variable

Symbols Used in Pseudo Euler-Lagrange Systems

$F_1,\ F_1(x_2)$	Function defined in Theorem 3.2.1
$F^{LF},\ F^{LF}(V_1)$	Unknown term in Lyapunov function used in equation (3.50)
$g,\ g(x_1)$	Nonlinear function of one variable used in Theorem 3.3.1
$\tilde{g},\ \tilde{g}(x_1)$	Generalized form of g defined in the equation set (3.21)
$g_1,\ g_1(x_1)$	Nonlinear function of one variable
$g_2,\ g_2(x_1,x_2)$	Nonlinear function of two variables
$G_1,\ G_1(x_1)$	Function defined in Theorem 3.2.1
$h_i,\ h_i(x_1,x_2)$	with $i = 1,2$ are nonlinear functions of two variables used in Theorem 3.3.1
$\tilde{h}_i,\ \tilde{h}_i(x_1,x_2)$	Generalized form of h_i defined in the equation set (3.21)
$K = [k_1,k_2,k_3]$	State feedback gain vector
$k_1^f,\ k_2^f$	State feedback gains for feedback linearization control law
L_c	Total aerodynamic length of the compressor and duct
$p,\ p(\cdot)$	Used to denote polynomial functions of one variable
$\tilde{p},\ \tilde{p}(\cdot)$	Used to denote polynomial functions of one variable
q	Used to denote a nonlinear function in equation (3.37)
R_{air}	Specific gas constant for air
t	Time domain variable

Symbols Used in Pseudo Euler-Lagrange Systems

$t_0 < t_1 < t_2$	Moments of time
T	Medium temperature
u	Control input signal
$u_i,\ u_i(x_1, x_2)$	with $i = 1, 2$, is a state feedback control input
U	Compressor wheel speed at its mean diameter
$V,\ V(x)$	Candidate Lyapunov function
$V_1,\ V_1(x_1)$	Candidate Lyapunov function used in the first stage of backstepping design procedure
V_p	Volume of the compressor plenum
w	Error parameter, used in the backstepping design procedure
x	State vector of a second order system $x = [x_1, x_2]^T$
x_2^{des}	Desired value of the virtual control
y	Used for a change of variable in equation (3.60), as $y = [y_1, y_2]$
$y_1,\ y_2$	Scalar variables used as a change of variable
z	State vector defined prior to equation (3.10), as $z = [z_1, z_2]$
α	Constant coefficient used in the pseudo Euler-Lagrange control law
α_f	Constant coefficient used in the feedback linearization control law
α_b	Constant coefficient used in the backstepping control law

Symbols Used in Pseudo Euler-Lagrange Systems

β	Constant parameter used in the Moore-Greitzer model, and defined in equation (2.32)
$\bar{\beta}$	The same as β, but with uncertainty that is not constant any more
γ	Constant coefficient used in the pseudo Euler-Lagrange control law
γ_f	Constant coefficient used in the feedback linearization control law
γ_b	Constant coefficient used in the backstepping control law
γ_{air}	Air specific heat ratio
$\mu,\ \mu(x_1)$	Stabilizing function
ρ	Constant coefficient used in the pseudo Euler-Lagrange control law
ϕ	Mass flow rate through the throttle shifted by unity
ψ	Pressure rise in the compressor shifted by unity

C. Nomenclature Used in Piecewise Affine Systems

Scripts and Operations

Ω^o	Interior of the set Ω
$\overline{\Omega}$	Closure of the set Ω
$\partial\Omega$	$= \overline{\Omega} \setminus \Omega^o$
$\mathbb{R}^+$	$= \{x \in \mathbb{R} \mid x \geq 0\}$
x^+	$= x + \varepsilon$, where $\varepsilon \in \mathbb{R}^+$ is infinitesimally small
x^-	$= x - \varepsilon$

Symbols Used in Piecewise Affine Systems

A	State matrix: equation (4.3)
A_i	State matrix associated with each PWA region: equation (4.2)
$\mathcal{A}$	Linear algebraic system coefficient matrix: equation (4.70)
a_{ij}, a_0	Coefficients of x in polynomial $p(x)$
B	Input matrix: equation (4.3)
b_i	Offset term of the affine model associated with each PWA region: equation (4.2)
$\mathcal{b}$	Linear algebraic system offset matrix: equation (4.70)
$\mathcal{C}^k$	Set of class-k functions
C, $C(\hat{x})$	Representation of c in $(\hat{x}_1, \hat{x}_2, \ldots, \hat{x}_n)$ coordinates
$\tilde{C}$, $\tilde{C}(\hat{x})$	The same as C used to represent $\tilde{c}$
c, $c(t)$	Parameterized manifold of dimension $n-1$. In case of $n=2$ this manifold represents a curve
$\tilde{c}$, $\tilde{c}(t)$	specified as $\tilde{c} = \{(x,y) \mid y = \tilde{h}_{aux}(x)\} \cap \{(x,y) \mid y = f(x)\}$
D	A set defined in Lemma 4.4.1
$\tilde{D}$	The same as D, defined is equation (4.58)
$D_{\mathbf{v}}$	The same as D, specified as $D_{\mathbf{v}} = \mathcal{E}(\Delta) \cap \mathcal{P}_{\mathbf{v}}$
d	Segment connecting point V_1 to V_2

Symbols Used in Piecewise Affine Systems

d^s	Sequence of consecutive points in Γ defined in equation (4.7)
$\mathcal{E}(f)$	Epigraph of f
$\mathbf{e}_\xi$	Unit vector along ξ
e_{max}	Maximum error between f and $\bar{f}$
$\hat{F}$, $\hat{F}(\hat{x},\hat{y})$	Implicit function representing $f(x)$ in $(\hat{x},\hat{y})$ coordinate system. See equation (4.53) for the definition
F_A, F_B	Points $F_A \in \partial D$ illustrated in Fig 4.5
$\mathcal{F}_r$	Flat of dimension r
f, $f(x)$	Nonlinear function of states which is specified everywhere used. It is defined as $f : \Omega \to \mathbb{R}$, where $\Omega \subset \mathbb{R}^n$
f_{nl}, $f_{nl}(x)$	Nonlinear vector function of states defined as $f_{nl} : \Omega \to \mathbb{R}^n$, where $\Omega \subset \mathbb{R}^n$. : equation (4.3)
$\bar{f}$, $\bar{f}(x)$	PWA approximation of f_{nl}: Def 4.2.2
$\hat{f}$, $\hat{f}(\hat{x},\hat{y})$	Is equal to $f(x)$ with x being replaced by equation (4.51)
g, $g(\hat{x}_1,\hat{x}_2,\ldots,\hat{x}_{n-1})$	A function that maps $\mathbb{R}^{n-1}$ to $\mathbb{R}$
H	Hyperplane as a set
$\bar{H}_\Omega(f)$	Mean curvature of f over Ω
$\mathcal{H}(f)$	Hypograph of f
h, $h(x)$	Notation for the function of hyperplanes. See Def 4.3.1
h_i, $h_i(x)$	Hyperplane obtained by linearization of f at $x_0^i \in \mathscr{R}_i$

Symbols Used in Piecewise Affine Systems

$\bar{h}$, $\bar{h}(x)$	Hyperplane defined for f as a function of one variable, as in equation (4.10)
h_{aux}, $\tilde{h}_{aux}$	Auxiliary hyperplanes that cut the graph of f through specific points. See Lemma 4.4.3 and the proof of Lemma 4.4.5
$h_{aux}^{(1)}, h_{aux}^{(2)}$	The same as h_{aux}. See Lemma 4.4.4
h_i^j	Hyperplane defined over $\mathscr{R}_i^j$
h_{N_u}	Hyperplane of the current linearization stage
$\mathscr{I}$	Index set $\mathscr{I} = \{1, 2, \ldots, N\}$
i	Index for variables defined locally where used
j	Index for variables defined locally where used
L_{int}	Intersection of two hyperplanes. equation (4.67)
L_{pj}	Represents the projection of L_{int} onto Ω
$L_{int}^{i,j}$	Intersection of h_i with h_i^j
$L_{pj}^{i,j}$	Represents the projection of $L_{int}^{i,j}$ onto Ω
l_i	$= h_i \cap h_{aux}$
$l_i^{(1)}, l_i^{(2)}$	The same as l_i. Used in the proof of Lemma 4.4.4
$\tilde{l}_i$	The same as l_i, with $i = 1, 2$, and h_{aux} replaced by $\tilde{h}_{aux}$. Used in the proof of Lemma 4.4.5
M	A point in Ω used for the proof of Lemma 4.4.5. See equation (4.73)
M'	A point in Ω' used for the proof of Lemma 4.4.5. See equation (4.80)

Symbols Used in Piecewise Affine Systems

$\mathcal{M}$	Set of points in segment d that do not belong to $\mathscr{R}_i$. See equation (4.120)
m	Dimension of the space where the graph of f is located
N	Number of regions: equation(4.3))
N_u	Number of regions in the u^{th} linearization loop
n	Dimension of the function domain space
P_i	Arbitrary point with $i = 1,2$ and $P_1 \neq P_2$.
$\hat{P}_i$	Representation of P_i in the $(\hat{x},\hat{y})$ coordinate system
P_0	Arbitrary point in Ω.
P_{0_ξ}	Representation of P_0 in the ξ axis
P_{N_u}	Point of maximum error, used for the current linearization stage
$\mathcal{P}_\mathbf{v}$	A plane such that $\mathcal{P}_\mathbf{v} \perp \Omega$ and $\mathbf{v}_{P_0} \in \mathcal{P}_\mathbf{v}$
$p,\ p(x)$	Stands for polynomials
p	(As index) $p \in \{1,2,\ldots,n\}$ is used for x and $\hat{x}$, e.g. x_p
Q_i	Flats of dimension $(m-3)$, with $i = 1,2$
$\hat{Q}_i$	Representation of Q_i in the $(\hat{x},\hat{y})$ coordinate system
q	$q \in \{1,2,\ldots,n\}$ is an index used for x and $\hat{x}$, e.g. x_q
q_i	$q_i \in \{1,2,\ldots,n\}$ with $i \in \{1,2,\ldots,n\}$ is a double index used for x and $\hat{x}$, e.g. x_{q_i}
$q_{k,\lambda}$	λ^{th} vertex of a region $\mathscr{R}_k$
$\mathbb{R}$	Real numbers set

Symbols Used in Piecewise Affine Systems

$\mathscr{R}_i$	i$^{\text{th}}$ PWA Region
$\mathscr{R}_i^j$	j$^{\text{th}}$ neighboring region of $\mathscr{R}_i$
$\mathscr{R}_{N_u}$	Region of the current linearization stage
$S, S(a)$	Integral of the squares of the errors
$s_1,\ s_2$	$\in \mathbb{R}^+$ are two constants such that $s_1 < s_2$
s	$\in \mathbb{R}$ is a variable
T	Coordinate transformation function defined in Lemma 4.4.2
$T_{(\xi,\zeta)}$	Coordinate transformation function from $\{(x,y) \in \mathscr{P}_{\mathbf{v}}\}$ to (ξ,ζ)
t	$t \in \mathbb{R}$ or $t \in [0,1]$ is a variable used for parameterization
t_1, t_2, t_3, t_4	Points along the parameterization axis t
u	Input signal: equation(4.3)
u	As an index, used as the number of the algorithms loop
$V_1,\ V_2$	Two points in Ω used in the proof of Lemma 4.4.4
$V,\ V(t)$	Function determining points in segment d. See equation (4.119)
$\mathbf{v}_{P_0},\ \mathbf{v}_{P_0}(x)$	A unit vector lying in Ω, pointing from P_0, and defined in equation (4.88)
$\mathbf{v}_{P_0\xi},\ \mathbf{v}_{P_0\xi}(\xi)$	A unit vector coinciding $\mathbf{v}_{P_0}$ in the ξ axis. See equation (4.97)

Symbols Used in Piecewise Affine Systems

$\mathbf{v}_{P_i},\ \mathbf{v}_{P_i}(x)$	Two unit vectors, with $i = 1,2$, lying in Ω, pointing from P_i, and defined in equation (4.102)
$\mathbf{v}_{x^\star},\ \mathbf{v}_{x^\star}(x)$	A unit vector lying in Ω, pointing from $x^\star$, and defined in equation (4.113)
x	Function argument: equation(4.3)
$x_1, x_2, \ldots, x_n$	Defined for $x \in \mathbb{R}^n$ as $x = [x_1, x_2, \ldots, x_n]^T$
x_0^i	A nominal point belonging to $\mathscr{R}_i$ used for linearization of f
$x^{(1)}, x^{(2)}$	Nominal points(scalars) in Γ
x_b	Arbitrary point(scalar) in Γ°
$x_{11},\ x_{12},\ \ldots$	Sequence of scalars in Γ
x_{int}	Intersection point defined in Lemma 4.3.2
$x_c,\ x_c(t)$	Parameterized coordinate used for the definition of $c(t)$
$\hat{x}$	Vector defined as $\hat{x} = [\hat{x}_1, \hat{x}_2, \ldots, \hat{x}_n]^T$
$\hat{x}_1, \hat{x}_2, \ldots, \hat{x}_n$	Axes associated with the frame $\{\hat{x}, \hat{y}\}$ defined in Lemma 4.4.2
$x_j^{\phi_0(j-1)}$	Updated axis orientation after some rotations (See the proof of Lemma 4.4.2)
$x^I,\ x^{II}$	Two collinear points that belong to Ω. See equation (4.89)
$x^I_{(s)},\ x^{II}_{(s)}$	The same as x^I and x^{II}. Where the index s shows that the variables are functions of s

Symbols Used in Piecewise Affine Systems

$x_m(\mathscr{R}_i)$	The point of maximum error associated with each region $\mathscr{R}_i$
x_0	Vector defined as $x_0 = [x_{1_0}, x_{2_0}, \ldots, x_{n_0}]^T$ addressing a nominal point in Ω
$x^\star$	$\in L_{pj} \cap \Omega$ is an arbitrary point
y	Coordinate representing the range of f
y_c, $y_c(t)$	Parameterized coordinate used for the definition of $c(t)$
$\hat{y}$	Axis, associated with the frame $\{\hat{x}, \hat{y}\}$ defined in Lemma 4.4.2
α_i, α_0	Coefficients of linear equation (4.72), with $i = \{1, 2, \ldots, n\}$
δ	A real infinitesimally small number
$\delta_{\mathbf{v}}$	A curve defined in equation (4.93) (refer to Figure 4.12)
$\bar{\delta}$, $\bar{\delta}(\xi)$	Representation of $\delta_{\mathbf{v}}$ in the (ξ, ζ) coordinates
ε	A sufficiently small positive real number
$\bar{\varepsilon}$	A sufficiently small positive real number
ζ	Axis associated with the frame $\{\xi, \zeta\}$
$\eta_{(\cdot)}$	Constant coefficient used in equation (4.54)
λ	$\in \{1, 2, \ldots, \lambda_k^{max}\}$ is an index, with λ_k^{max} denoting the number of vertices of region $\mathscr{R}_k$
ξ	Axis associated with the frame $\{\xi, \zeta\}$
ξ_1, ξ_2	Representation of $x^{(I)}$ and $x^{(II)}$, respectively in the (ξ, ζ) coordinates

Symbols Used in Piecewise Affine Systems

$\phi^{(i)}$	Rotation angle about x_i axis
$\phi_0^{(i)}$	Rotation angle about x_i axis that results in construction of axes $\{\hat{x}, \hat{y}\}$
$\varphi, \varphi(x)$	A curve that is contained in $f(x)$, and defined by equation (4.122)
ψ	Rotation angle about y axis
Γ	Domain of a function of one variable. Lemma 4.3.1
Δ	See Def 4.3.2
Δ_i	See Def 4.3.2
$\Lambda_{(\cdot)}$	Rotation matrix about only one axis by the amount indicated in the subscript
Λ	Rotation matrix defined in equation (4.45)
$\bar{\Lambda}$	The same as the rotation matrix Λ with $\phi^{(i)}$ replaced by $\phi_0^{(i)}$
$\bar{\Lambda}_{j,i}$	The element of matrix $\bar{\Lambda}$ located in the j^{th} row and the i^{th} column
Υ	A closed subset of Γ
Ω	Domain of functions $f, f_{nl}, \ldots$, that maps $\mathbb{R}^n$ to $\mathbb{R}$
Ω'	Domain of a function that maps $\mathbb{R}^{n-1}$ to $\mathbb{R}$

Chapter 1

Introduction

1.1 Motivation

For the time being, majority of human needs is met by using technological systems, such that any new machine may easily become an indispensable part of our lives. From the basic tasks as warming up our lunch to traveling intercontinental paths modern machines are inevitable. These machines become more and more complex with time. Nevertheless the primary human concern − health and safety − has been violated repeatedly through this mechanized life. Due to the significance of safety, reliability and cost efficiency of such systems, health monitoring, fault detection and recovery of modern systems play a crucial role in this era. In particular, the consequences of occurrence of a fault in a class of systems called safety-critical, may result in sever health problems as injuries or death, cost penalties, or lack of security. Safety-critical systems, including aircraft, nuclear reactors, power plants, robotic surgery machines, or even an amusement ride, are of major concern.

Aircraft, as a complex safety-critical system, have received great attention in the fault diagnosis and recovery field. Therefore, numerous successful attempts have been made to provide more reliable flights. The flight safety is dependent on the reliability of many different parameters from the aircraft subsystems, such as structure, flight controls,

oxygen and ventilation, the power plant and the fuel systems, up to the Air Traffic Control that includes a number of external equipments as VOR/DME [1] stations and control tower, to name a few.

The combustion of fuel in jet engines, as an example, occurs at around $1200K$. Hence, for a typical subsonic airliner with more than 200 passengers, the health monitoring, fault avoidance strategies and fault tolerance of the propulsion system are of great importance. The main failures of jet engines include compressor blade damage, turbine blade erosion, engine flame-out, foreign object damages, engine mechanical vibration, worn seals, and plugged nozzle. Many factors may result in these failures or malfunctions that occasionally occur during flight. For instance, the ambient atmospheric conditions abruptly change as the aircraft switches different flight profiles, such as take-off, climb, or cruise. The engine governor thus has to adjust the amount of fuel to the combustor to prevent any potential failure, such as engine flame-out, and to make sure that the thrust generation is maintained at high performance. In addition, another important factor that causes compressor vibration, blade damages and engine flame-out is the instabilities of the gas stream that passes through the compressor. These instabilities are referred to as compressor rotating stall and surge. In this case, a stabilizing control action to the compressor actuator has to be applied as soon as the surge and stall inception is recognized. This measurement is referred to as fault avoidance strategy. Based on the aforementioned points, any attempt that improves the reliability of jet engine subsystems enhances the flight and the passenger safety.

With the increased production of science and technology and the motivation for the reliability and safety, fault detection, isolation and recovery (FDIR) of systems has been widely improved, such that different methodologies from different points of view are developed. There are two major approaches towards FDIR: model-based and data driven. The **model-based** FDIR technique, in the case of availability of an accurate mathematical

[1] VOR and DME are acronyms standing for *VHF Omnidirectional Range* and *Distance Measuring Equipment*, respectively.

model of the system, has been used since 1970s [4]. Using the thermodynamic and the gas dynamic laws several models have been developed for the engine components individually as well as for the power plant, as an integrated system [5]. Reference [6] studied the real-time fault diagnosis and isolation of jet engines by using a multiple model approach. Having modeled the fouling and erosion damages for a single spool engine, the authors of [7] investigated the low fatigue cycle and the creep on the turbine blades.

More specifically, Moore and Greitzer in [3] proposed an accurate approximation of the axial compressor dynamics in the form of ODEs. Based on this model the authors of references [8, 9, 10, 11, 12, 13, 14, 15, 16] tackled the surge and stall control problems, as a fault avoidance technique. These works will be thoroughly reviewed in Chapter 2, Section 2.3.2. In the absence of an accurate model, **data driven** FDIR technology, in many cases, gives a reliable solution to the fault diagnostics and recovery problems. As in the case of jet engines, a wide spectrum of data can be obtained by both on-line flight data recording that is produced in each flight as well as the off-line engine maintenances. References [17, 18, 19, 20, 21, 22] tackled data driven FDIR for jet engines by using machine learning and competitive learning methods in addition to statistical techniques. Reference [23] investigated the mechanical damages in the turbine components due to high gas stream temperature. This research used condition-based health management, as an FDIR technique, which provides a diagnostic scheme development by monitoring the deviation of the measured system parameters.

In contrast to the fault diagnosis and prognosis that deal with the monitoring and analysis of the system health and the detection of a fault, the fault tolerance and recovery provide the necessary measurements to maintain the system operating at a reasonable performance, in addition to reducing the propagation of the fault to the other operating subsystems. In fault avoidance strategies the objective is to monitor the system health as well as take the measurements to avoid potential faults.

Unfortunately, the occurrence of stall in the compression component of the engine

has the consequences of engine flame-out and high mechanical vibrations. Therefore, maintaining the engine at its performance, avoiding potential severe damages, reducing the maintenance cost, and of course increasing the flight safety are the important results of installing stall and surge stabilizing controllers on jet engines. This thesis addresses the model-based suppression of the compressor surge and stall by enhancing the control law of the compressor model.

1.2 On The Proposed Methodologies

1.2.1 Pseudo Euler-Lagrange Systems

A class of physical systems in nature exhibit second order nonlinear behavior, thus they can be mathematically modeled by second order differential equations. One dimensional motions including rotation or translation that is caused by exertion of force or torque, servomotor systems, and pneumatic valves are cases described in [24]. Therefore, any technique that deals with the stabilization of these systems is of potential importance. In the case of nonlinear systems, the well-known Lyapunov theory, upon which the control theory of such systems is based, poses a setback due to the difficult problem of finding the Lyapunov function itself. Consequently, determining separate classes of Lyapunov functions on various types of systems makes the stability analysis more systematic [25].

Pseudo Euler-Lagrange systems, as a class of second order systems, have shown an increasing capability in controller synthesis [25]. Chapter 3 studies a more general form of this class of second order systems. By adding a nonlinear term, in contrast to previous work, the dynamics of both states are nonlinear functions of both states. By doing so, a more general class of nonlinear systems can be analyzed, such as stability analysis of the Moore-Greitzer compression surge model, which does not fit the theorem given in reference [25]. As pointed out earlier, pseudo Euler-Lagrange systems can be a good candidate for second order systems. As will be explained later in Chapter 2, the surge phenomenon

can be reasonably approximated by a second order system. Therefore, control synthesis technique of pseudo Euler-Lagrange systems are used in this thesis for the stabilization of the surge. The main advantages of the proposed theory for stability of the Moore-Greitzer no-stall surge model as compared to the current two nonlinear techniques − the feedback linearization and the backstepping − are as follows:

1. The pseudo Euler-Lagrange controller is more robust as compared to the feedback linearization and the backstepping controllers in the stabilization of the Moore-Greitzer model, in the sense that the wide margin in choosing the coefficients of the controller allows us to avoid potential instability of the system due to the disturbances.

2. The uncertainty in the available model, that is discussed in Chapter 3, motivates us to avoid the cancelation of the useful nonlinear terms that enhances the stability of the system. This cancelation is the essence of the feedback linearization method that, at least in the case of the Moore-Greitzer model with uncertainties, may lead to instability.

The alternative techniques for stabilization of rotating stall and surge performed in literature are provided in Chapter 2.

1.2.2 Piecewise Affine Systems

Piecewise affine (PWA) techniques are shown to be a powerful approach in analysis and synthesis of nonlinear systems [26, 27, 28]. The key concept behind this idea is that the nonlinearities appearing in a dynamical system can be reasonably approximated by PWA functions. The work done in this thesis builds upon previous work on approximation of functions of n-variables using a piecewise affine method [29], emphasizing the elements that increase the effectiveness of the approximation algorithm in terms of elimination of

the need to search for points of maximum error and decreasing the error between the exact function and its approximation.

Although the concept of PWA systems was initially researched in the late 1940's, the first optimal algorithm to approximate nonlinearities with PWA functions appears, to the best of the author's knowledge, in 1970's by Cantoni [30] and Tomek [31]. Many different attempts have been made to produce suitable PWA models in references [32, 26, 33, 34], and [29]. Reference [32] addresses PWA approximation of continuous functions by using uniform simplicial partitions. Later in [26], the idea of refinement of the partitions around the origin is introduced. The least squares technique as an optimization over simplicial partitions is addressed in [33]. In references [32] and [26], the domain of the nonlinearity was uniformly divided into a number of simplices. A point in each simplicial region was then selected for the linearization of the function.

The main disadvantage of these methods lies in the fact that the number of regions exponentially grows as the dimension of the domain of approximation is increased. This drawback can be avoided if the curvature or the variation of the nonlinear function is considered, as done recently in [34] and [29]. Reference [34] addresses a novel methodology in PWA approximation of functions that uses the concept of Lebesgue integration partitioning. However, the resulting PWA approximation is not guaranteed to be continuous. Uniform grid approximation techniques have been extensively used in the literature [35, 36, 37, 38, 39, 40, 41]. The authors of [29] address the approximation problem by considering the curvature of the function. Moreover the continuity problem has been solved in their work, which, nevertheless, has never been proved. Reference [29] provides the reader with an interesting and heuristic idea to find the PWA model of a micro air vehicle. Although, the proposed concept is shown to be efficient as compared to the work done in this area, the details of the approximation and the supporting theory are missing, which is a reason for motivating the work on the current thesis.

The method proposed in this thesis is used to find a PWA model of the Moore-Greitzer stall and surge models. The resulting PWA models can later be used for the analysis and/or synthesis problems that have been addressed in reference [28]. Moreover, it is suggested in [34] that PWA models may be used for piecewise affine identification with a clustering approach [42], mixed logical dynamics (MLD) model based technique [43], system verification of conflict maneuvers [44], automated symbolic reachability analysis [45], and probabilistic controllability/observability analysis of discrete-time piecewise affine systems [46, 47].

With the intersection-based Piecewise Affine (IPWA) models, the following properties can be achieved:

1. Continuity of the vector fields,

2. Optimality of the linearization of the nonlinear function relative to the maximum approximation error,

3. Increased reduction of the approximation error for a fixed number of regions (as compared to the Voronoi-based and the uniform grid PWA models for the motivating Moore-Greitzer system in Section 5.2),

4. Consistency of the derivative of the nonlinear function with the derivative of its approximation at the linearization points.

The continuity of the vector field may play a crucial role in controller synthesis for PWA systems [48]. By the optimality of the linearization we mean that the nonlinear function is linearized at the points of maximum approximation error. By doing so, not only the number of approximation stages is reduced, but also the number of regions is decreased. Note that the smaller the number of regions we have in the PWA model, the more the computation size of the controller synthesis problem is reduced [28]. Finally, if the user is required to have zero error at specific points as well as minimum amount of error in the neighborhood of those points, the IPWA method can serve as a good solution

to such problems. The reason, as will be shown in Section 4.4.1, is that the algorithm starts by linearizing the function at a set of user-defined points. Since the function is linearized at the user-defined points, the approximation error is zero at these points. Moreover, since the derivative of the exact and the derivative of the IPWA functions are equal, the error in the neighborhood of the user-defined points is small.

The importance of these properties is well-understood when the PWA synthesis method is applied to the Moore-Greitzer PWA model, which results in a set of bilinear matrix inequalities (BMIs). For instance, due to the large number of regions of the PWA approximation by the current PWA techniques, the solution to the BMIs could not be obtained by using the PenBMI [49] toolbox while PenBMI successfully solved the BMIs by using the proposed IPWA method as the number of regions is reduced.

1.3 Contributions of the Thesis

The contributions of this work consist of proposing the following two methodologies:

1. A new controller synthesis formulation for pseudo Euler-Lagrange systems is proposed, giving a more general form of this class of second order systems. By adding a nonlinear term, in contrast to the previous work, the dynamics of both states are nonlinear functions of both states. In this regard, a more general class of physical nonlinear systems can be analyzed.

2. A new PWA approximation methodology for functions of n-variables is developed. It is shown that continuity of the vector field and the increased reduction in the approximation error are two important properties that can be achieved by using this technique. These advantages help to reduce the computation complexity of the PWA controller synthesis method.

1.4 Structure of the Thesis

The thesis is organized as follows. Axial compressors, a fundamental piece of machinery in jet engines, are introduced in Chapter 2. In that chapter, the equations governing the dynamical behavior of axial compressors including surge and stall are developed, according to [3]. The pseudo Euler-Lagrange system formulation is given in Chapter 3. Chapter 4 addresses the Intersection-based Piecewise Affine approximation theory with a focus on functions of one variable in Section 4.3 and functions of n-variables in Section 4.4. The application of the proposed methodologies to the axial compressor surge and stall models are then given in Chapter 5, followed by the conclusions in Chapter 6.

Chapter 2

Gas Turbines Compressors

2.1 Introduction

The principles and methods in the generation of thrust and power in aircraft are involved in the study of propulsion. In particular, the thrust force produced for jet aircraft (refer to Figure 2.1) is considered in this context. This force is produced as the difference in the momentum of the gas passing through the jet engine, as depicted in Figure 2.2a. The main components of a gas turbine are intake, compressor, combustion chamber, turbine and nozzle. These components are illustrated in Figure 2.2b.

This chapter briefly introduces axial compressors in Section 2.2. Later in Section 2.3 rotating stall and surge, two important instabilities in compressors, are discussed followed by derivation of the governing equations.

2.2 Axial Compressors

The working fluid in compressors is pressurized through a change from kinetic to potential energy through each compression stage. Each stage consists of two parts, a rotor and a stator. The rotor disc, as its name imparts, rotates by the shaft coming from the turbine, conveying the kinetic energy to the fluid while the stator is fixed with diverging channels,

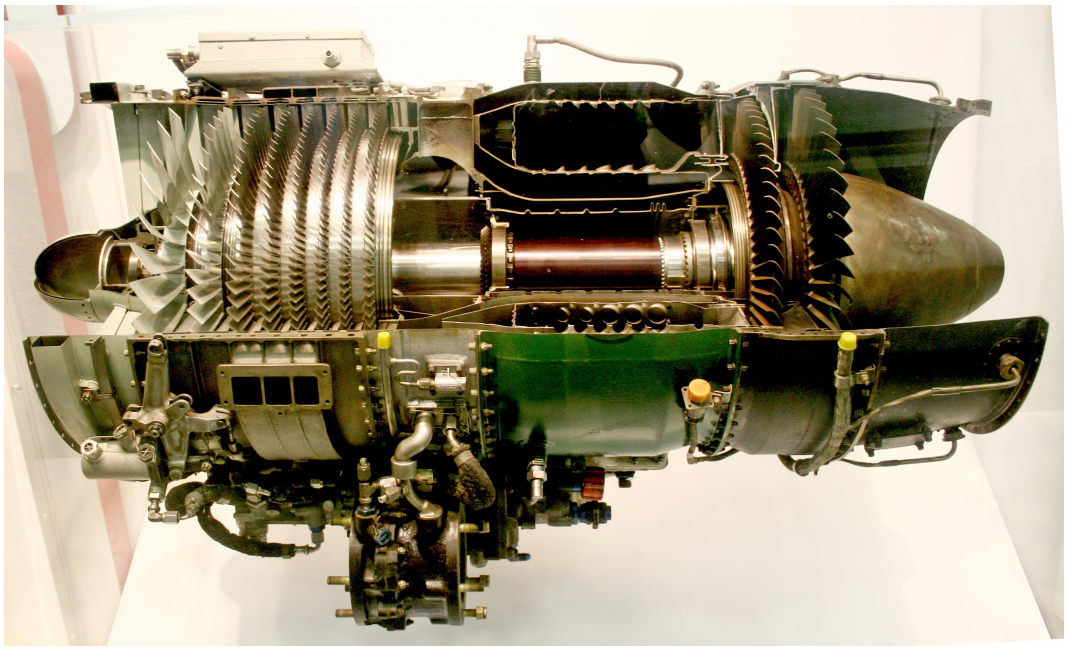

Figure 2.1: Typical tubojet with an axial compressor. This picture refers to GE-J85 engine, adapted from [1].

converting the kinetic energy of the fluid to potential energy. By doing so the added energy is stored in the working fluid in the form of pressure.

The performance of a compressor is characterized by the compressor maps. Compressor maps usually consist of curves representing the relation of the *rotor rotational speed*, the fluid *mass flow rate* and the *pressure ratio* through the compressor. As shown in Figure 2.3 representing a generic plot of a compressor map, the operating region of a compressor is limited to a bounded region. The lower bound, called compressor capacity, restricts the compressor operation for the high mass flow range. However, the upper bound provides a limitation in the low mass flow range. The entrance of the working fluid in the compressor to the upper inoperable region causes aerodynamic instabilities on the compressor operation called rotating stall and surge, as stated in [51].

These instability issues regarding the stable operation of a compressor − namely the rotating stall and surge − are discussed in the next section.

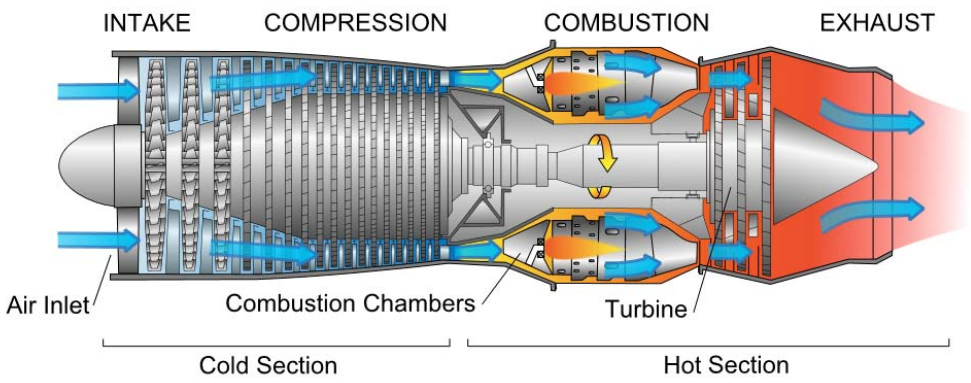

(a) Air stream through a turbojet, taken from [1].

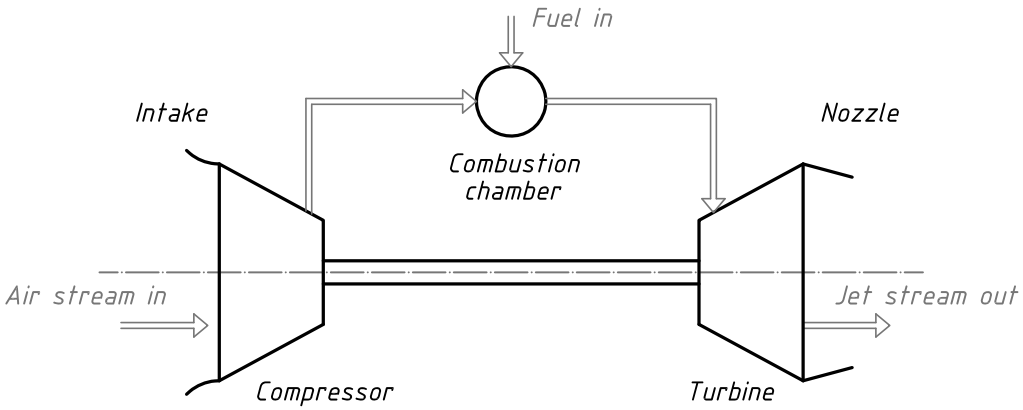

(b) Gas turbine simple block diagram.

Figure 2.2: A schematic representation of a turbojet functionality.

2.3 Rotating Stall and Surge

2.3.1 Basic Concept

Rotating stall is characterized by the local instability in a compressor in which the disturbance occurs in the uniform circumferential flow, that causes stagnant flow in one or more regions. The stalled regions propagate along the annulus of the compressor at a fraction of the rotor speed, normally between 20% and 70% of the wheel velocity [52]. The occurrence of rotating stall, depending on its magnitude, can severely limit the performance of the compressor in the sense of the design compression ratio. Moreover, this phenomenon

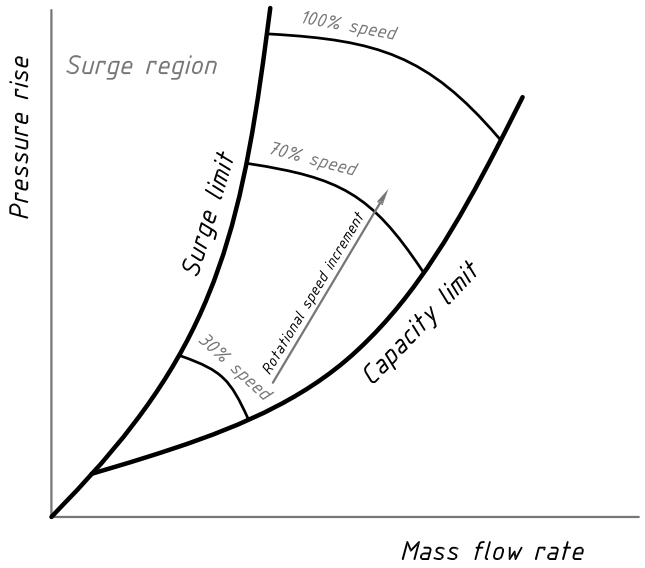

Figure 2.3: Single-stage compressor map. The diagram is inspired from [2].

is a nonlinear limit cycle, resulting in high blade vibration that cannot be tolerated by the compressor. The third potential side effect, includes the thermal load on the turbine caused by the flow rate reduction, which with the presence of surge may result in engine flame-out.

Surge is a phenomenon in compressors in which the pressure rise exhibits large amplitude oscillation, and consequently, the axial average mass flow rate becomes unsteady. In contrast to the rotating stall, which is two dimensional, the surge has the one dimensional instability property. However, similar to the rotating stall, this instability phenomenon results in a drastic loss of compression efficiency and high blade and structure vibrations. By the magnitude of the pressure rise oscillation amplitude, surge is categorized into mild surge, classic surge, modified surge, and deep surge, according to [52].

Contrary to the rotating stall where the average axial flow is steady and the circumferential flow has non-uniformities, in the surge, the axial flow is not steady in time at all, but it has a uniform pattern in the circumferential direction. In accordance with this fact, rotating stall sticks locally to the rotating cell while the surge infests the entire compressor

due to its instability in the axial direction, as argued in [53].

2.3.2 A Brief Survey on the Compressor Instability Problem

A typical industrial strategy to prevent surge and stall is to keep the compressor operation far enough from the surge limit as depicted in Figure 2.3. This is referred to as avoidance control action. Note that the term *avoidance control* should not be confused with the term *fault avoidance strategies*. The former action avoids surge and stall while the later refers to the suppression of the surge and stall in order to avoid further faults such as engine flame-out, mechanical vibration, or compressor blade damages. However, the maximum performance of a compressor is achieved sufficiently close to the surge line. This fact motivates researchers to look for different solutions.

For this purpose, the control synthesis problem of the compressor instabilities by using feedback control was first addressed in [8] by Epstein and co-authors. Using the Fourier decomposition of the measured parameters coming from sensors (hot wires installed upstream of the compressor), the authors of [9] developed a model for rotating stall. The control action, according to the model, is applied to the system via a set of wiggly IGVs [1] that transmit a wave at an appropriate amplitude and phase to the inlet stream. In [11], the inception of the rotating stall of axial compression system is suppressed by using pulse air injection. The instability in their case is diagnosed via the pressure sensors installed close to the rotor face.

Using modulated air injectors, [12] proposes an active feedback control law to stabilize the rotating stall and surge in a transonic single stage axial compressor. By computing the compressor output and comparing it with the output of the linearized model, reference [13] addresses the use of linear-based fault identification filter to detect the surge and rotating stall. A high-gain type adaptive control of compressor instabilities is addressed in [14], the design of which is based on the second order model. Reference [15] proposes a

[1] IGV is an acronym for *Inlet Guide Vane*.

high gain feedback control law, which improves the bifurcation control performance such that for a larger range of operating conditions the steady state pressure rise is sustained.

The detection of the aerodynamic instabilities in compressors, i.e. rotating stall and surge, as well as the use of feedback control action inevitably requires the presence of sensors and measurements of the key parameters (pressure, velocity disturbance, mass flow rate, temperature rise). Pressure sensors and hot wires are the most effective sensors noted in the literature. The onset of both surge and rotating stall is diagnosed by the use of diffusor pressure sensor and hot wire in [54] and [55], respectively. Inlet pressure sensors are used by [56] to suppress rotating stall only. The authors of [57] and [58] implemented plenum and duct pressure sensors, respectively, to control the pure surge instability. [59] also used pressure sensor to apply a surge avoidance control. Besides, [60] employed axial velocity probes near the rotor blade to measure the circumferential disturbances. By this means, the author applied a CFD [2] technique to compute and simulate the rotating stall inception.

In the following section, the equations governing the operation of the axial compressors are derived, due to the work done by Moore and Greitzer [3]. Using the final set of equations, the rotating stall and surge can be described.

2.3.3 Compressor Model

An axial compression system can be schematically represented as shown in Figure 2.4, according to [3]. It consists of an intake, an entrance duct with length l_{en}, inlet guide vanes (IGVs), a compression actuator comprised of rotor-stator stages, an exit duct of length l_{ex}, a plenum, which is a reservoir where the compressed fluid is accumulated, a throttle duct of length l_{th}, and a throttler. Note that lengths l_{en}, l_{ex} and l_{th} are made non-dimensional with respect to the mean radius of the compressor wheel $\mathcal{R}$.

[2] CFD is an acronym for *Computational Fluid Dynamics*.

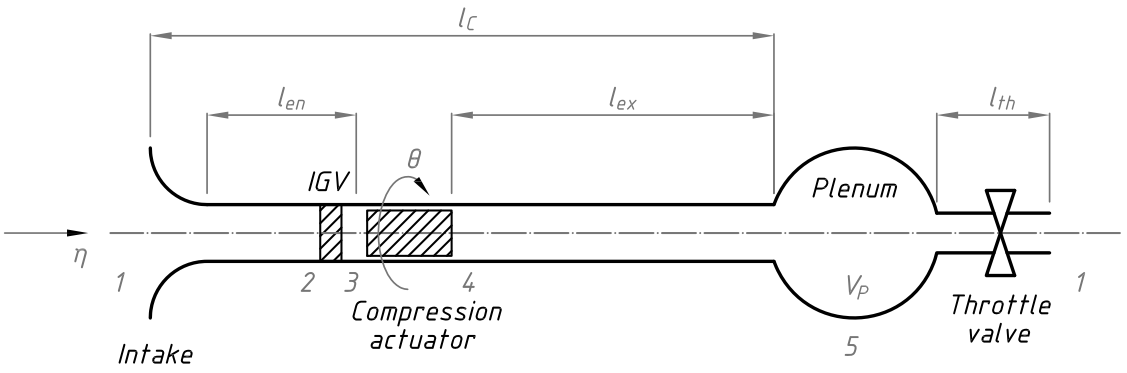

Figure 2.4: Schematic representation of a non-dimensional axial compression system with respect to $\mathcal{R}$, adapted from [3].

In this section, the model of the compression system will be developed. The equations governing such a system are derived by Moore himself [61] and by Moore and Greitzer in [3]. This model is then approximated by a third order ordinary differential equations, however, the procedure is not given here. For details on the approximation, the reader is encouraged to refer to the main articles [3, 61].

Assumptions: Following the work done in [3, 61], the next assumptions are made.

1. The plenum size is large enough as compared to the duct cross section area such that the gas speed can be neglected in the plenum. By this assumption, the plenum pressure can be considered spatially uniform.

2. The flow through the compressor is considered incompressible. This is a reasonable assumption since the Mach number through the rotor and stator is small. This fact results in the gas molecules oscillations to be much below the acoustic resonance. However, the overall process from intake to the plenum is conceived to be compressible.

3. In order to use the two dimensional flow theory, the hub-to-tip radius ratio of the blades is assumed to be high.

4. The flow through the entrance duct is irrotational and inviscid.

5. The IGVs are assumed to guide the flow to the rotor ideally.

In order to determine the net pressure rise through the compression system, the four components, i.e. entrance duct, IGVs, compressor, and exit duct to the plenum are studied separately [3]. Before proceeding further, we define $\bar{\phi}$ as the local axial flow coefficient equal to $\bar{\phi} = C_x/U$ with C_x denoting the axial component of the flow velocity vector and U denoting the wheel speed at mean wheel radius $\mathcal{R}$. The average value of $\bar{\phi}$, denoted by Φ, is then defined as

$$\Phi(\xi) = \frac{1}{2\pi}\int_0^{2\pi} \bar{\phi}(\xi,\theta)d\theta, \tag{2.1}$$

where θ is the rotational axis about the system symmetric axis η, as show in Figure 2.4, and ξ is the dimensionless time parameter defined as

$$\xi = Ut/\mathcal{R}. \tag{2.2}$$

With the definition of Φ in equation (2.1), the parameter $\bar{\phi}$ can be written as the summation of the average value and the disturbances. This is done by means of velocity potential $\tilde{\phi}$, the gradient of which with respect to η and θ provides us with the axial and circumferential velocity coefficients, i.e.

$$\tilde{\phi}_\eta = \Phi(\xi) + g(\xi,\theta) \tag{2.3}$$

$$\tilde{\phi}_\theta = h(\xi,\theta) \tag{2.4}$$

where subscripts designate the partial derivatives, and g and h are the axial and circumferential velocity disturbances, respectively. Obviously we have

$$\int_0^{2\pi} g(\xi,\theta)d\theta = 0, \text{ and } \int_0^{2\pi} h(\xi,\theta)d\theta = 0. \tag{2.5}$$

Entrance duct: According to the assumptions, the flow is considered irrotational through the entrance duct. This assumption allows us to define the velocity potential $\tilde{\phi}$, which satisfies the Laplace's equation. Using the Bernouilli's equation, the following pressure balance can be written

$$\frac{P_1 - P_2}{\rho U^2} = \frac{1}{2}(\bar{\phi}^2 + h^2) + (\tilde{\phi}_\xi)_2, \tag{2.6}$$

where ρ stands for density, and the numeric indices indicate the variables evaluated at the associated points in Figure 2.4. Following [3], the velocity potential is written as

$$\tilde{\phi} = (\eta + l_{en})\Phi(\xi) + \tilde{\phi}'(\xi, \eta), \tag{2.7}$$

where $\tilde{\phi}'$ is the velocity potential of the disturbance, and l_{en} is the entrance duct length. Noting that

$$(\tilde{\phi}'_{\eta})_2 = g(\xi, \theta), \tag{2.8}$$

$$(\tilde{\phi}'_{\theta})_2 = h(\xi, \theta), \tag{2.9}$$

the parameter $(\tilde{\phi}_{\xi})_2$ is then computed, according to [3], as

$$(\tilde{\phi}_{\xi})_2 = l_{en}\frac{d\Phi}{d\xi} + (\tilde{\phi}'_{\xi})_2. \tag{2.10}$$

IGVs: As the disturbed flow passes though the IGVs, the circumferential velocity disturbance is transformed into the incremental pressure form. This pressure rise can be written as

$$\frac{P_3 - P_2}{\rho U^2} = \frac{1}{2}K_G h^2, \tag{2.11}$$

where K_G is related to the efficiency of the IGVs. For ideal IGVs, as in this case, we have $K_G = 1$.

Compressor dynamics: The pressure rise across rotor and stator blades is, according to [61], assumed to attain the form

$$\frac{P_4 - P_3}{\rho U^2} = NF(\bar{\phi}) - \frac{1}{2a}\left(2\frac{\partial \bar{\phi}}{\partial \xi} + \frac{\partial \bar{\phi}}{\partial \theta}\right), \tag{2.12}$$

where N is the number of compression stages, a designates the dimensionless blade passage length reciprocal, and F is the quasi-steady pressure rise coefficient as a function of $\bar{\phi}$.

Exit duct and plenum: The pressure at point 5 in Figure 2.4 is assumed to be spatially uniform. Moreover, the flow velocity at this point is considered to be negligible.

However, the exit flow from the compressor is rotational, for which the velocity potential does not exit. Accordingly, assuming that the difference between P_5 and P_4 is small, the author of [61] considers a dimensionless coefficient $\mathscr{P}$ defined as

$$\mathscr{P} = \frac{P_5(\xi) - P}{\rho U^2}, \tag{2.13}$$

which satisfies the Laplace's equation $\nabla^2 \mathscr{P} = 0$. Applying the Euler's equation in the exit duct gives

$$(\mathscr{P}_\eta)_4 = (\tilde{\phi}_{\eta\xi})_2 = \frac{d\Phi}{d\xi} + (\tilde{\phi}'_{\eta\xi})_2. \tag{2.14}$$

Solving equation (2.14) and combining it with equation (2.13) yields

$$\frac{P_5 - P_4}{\rho U^2} = (\mathscr{P})_4 = -l_{ex}\frac{d\Phi}{d\xi} - (m-1)(\tilde{\phi}'_\xi)_2, \tag{2.15}$$

where l_{ex} is the exit duct length and m is a coefficient determined by the length of the exit duct.

Overall pressure rise: Combining equations (2.6), (2.10), (2.11), (2.12) and (2.15) results in the following equation that gives the net pressure rise through the compression system with ideal IGVs

$$\begin{aligned}\frac{P_5 - P_1}{\rho U^2} = &\left(NF(\bar{\phi}) - \frac{1}{2}\bar{\phi}^2\right) - \left(l_{en} + \frac{1}{a} + l_{ex}\right)\frac{d\Phi}{d\xi} - m(\tilde{\phi}'_\xi)_2 \\ &- \frac{1}{2a}\left(2\tilde{\phi}'_{\xi\eta} + \tilde{\phi}'_{\theta\eta}\right)_2\end{aligned} \tag{2.16}$$

Let us denote the dimensionless net pressure rise in the left hand side of (2.16) by Ψ, as

$$\Psi(\xi) \triangleq \frac{P_5 - P_1}{\rho U^2}. \tag{2.17}$$

The following notations

$$\bar{\Psi}_c(\bar{\phi}) \triangleq NF(\bar{\phi}) - \frac{1}{2}\bar{\phi}^2, \tag{2.18}$$

$$l_c \triangleq l_{en} + \frac{1}{a} + l_{en}, \tag{2.19}$$

$$Y(\xi,\theta) \triangleq (\tilde{\phi}')_2 \tag{2.20}$$

are also used. Using the Laplace's equation for the velocity potential disturbance, and solving it with the Fourier series yields

$$\Psi(\xi) = \bar{\psi}_c(\Phi - Y_{\theta\theta}) - l_c\frac{d\Phi}{d\xi} - mY_\xi + \frac{1}{2a}\left(2Y_{\xi\theta\theta} + Y_{\theta\theta\theta}\right). \tag{2.21}$$

Applying the conservation of mass law to the flow passing through the plenum we have

$$l_c\frac{d\Psi}{d\xi} = \frac{1}{4\beta^2}\left(\Phi(\xi) - F_T^{-1}(\Psi)\right), \tag{2.22}$$

where $F_T(\Phi_T) = \Psi$ is the throttle characteristic function, Φ_T is the flow coefficient of the throttle duct, and β is a parameter that will be given later.

In order to complete the system of three unknowns Y, Φ and Ψ, and three equations, one more equation, besides equations (2.21) and (2.22), is still needed, which can be obtained by integrating equation (2.21) over θ form 0 to 2π, resulting in

$$\Psi(\xi) + l_c\frac{d\Phi}{d\xi} = \frac{1}{2\pi}\int_0^{2\pi}\bar{\psi}_c(\Phi - Y_{\theta\theta})d\theta. \tag{2.23}$$

The final set of partial differential equations describing the compressor dynamics are given here together as

$$\Psi(\xi) = \bar{\psi}_c(\Phi - Y_{\theta\theta}) - l_c\frac{d\Phi}{d\xi} - mY_\xi + \frac{1}{2a}\left(2Y_{\xi\theta\theta} + Y_{\theta\theta\theta}\right) \tag{2.24a}$$

$$l_c\frac{d\Psi}{d\xi} = \frac{1}{4\beta^2}\left(\Phi(\xi) - F_T^{-1}(\Psi)\right) \tag{2.24b}$$

$$\Psi(\xi) + l_c\frac{d\Phi}{d\xi} = \frac{1}{2\pi}\int_0^{2\pi}\bar{\psi}_c(\Phi - Y_{\theta\theta})d\theta \tag{2.24c}$$

The basis of the Moore-Greitzer model was first initiated by Greitzer in 1976 in reference [62], which described the surge phenomenon only. Later in 1983, Moore provided the model for the rotating stall [63]. The combination of these two models was then published as the Moore-Greitzer model in [3] that was derived in this section. In addition to the this model, other researchers provided different models for the axial compressor that can be found in the literature [64, 65, 66, 67, 68].

2.3.4 Simplified Moore-Greitzer Model

As mentioned earlier, compressor surge is one of the major engine failures that may result in flame-out or severe mechanical damages caused by high blade vibration. The equations governing this phenomenon are the set of complicated PDEs (2.24), which can be simplified in the form of ODEs due to the work done by Moore and Greitzer in [3]. As the authors of [3] are inspired by the work done on stalled performance of axial compressors and vibrations [69] and [70], the axisymmetric characteristic function $\bar{\psi}_c(\phi)$ has the form

$$\bar{\psi}_c(\bar{\phi}) = \bar{\psi}_{c_0} + H\left[1 + \frac{3}{2}\left(\frac{\bar{\phi}}{W} - 1\right) - \frac{1}{2}\left(\frac{\bar{\phi}}{W} - 1\right)^3\right], \tag{2.25}$$

where $\bar{\psi}_{c_0}$, H, and W are parameters. Using a Galerkin procedure, explained in the reference [3], Y is represented as a harmonic function, as

$$Y = WA(\xi)\sin(\theta - r(\xi)), \tag{2.26}$$

where A is the unknown stall amplitude and r is the phase angle that is found to be, according to [3], equal to

$$r = \xi\frac{1}{2(1+ma)}. \tag{2.27}$$

Continuing with the Galerkin procedure, and setting $R = A^2$, $\phi = \Phi - 1$, and $\psi = \Psi - 1$, we have the following approximation of the system (2.24) in the form of a set of three first order ODEs, as

$$\dot{\phi} = -\psi + \frac{3}{2}\phi + \frac{1-(1+\phi)^3}{2} - 3R(1+\phi) \tag{2.28a}$$

$$\dot{\psi} = \frac{1}{\beta^2}(\phi - u) \tag{2.28b}$$

$$\dot{R} = -\sigma R^2 - \sigma R\left(2\phi + \phi^2\right) \tag{2.28c}$$

where R is the normalized rotational velocity amplitude in the stalled cell, ϕ is the mass flow rate shifted by unity, ψ is the pressure rise shifted by unity, u is a function of the flow through the throttle considered as the control input, and $\sigma = f(H,W,m,a)$, and β are both

system parameters. Note that the parameters description is addressed in [3]. Moreover, one can refer to the reference [71] for the experimental results that are obtained for axial compressors.

The set of equations (2.28) is simply called *MG model*. Replacing ϕ, ψ and R by x_1, x_2 and x_3, respectively, results in

$$\dot{x}_1 = -x_2 + \frac{3}{2}x_1 + \frac{1-(1+x_1)^3}{2} - 3x_3(1+x_1) \tag{2.29a}$$

$$\dot{x}_2 = \frac{1}{\beta^2}(x_1 - u) \tag{2.29b}$$

$$\dot{x}_3 = -\sigma x_3^2 - \sigma x_3\left(2x_1 + x_1^2\right) \tag{2.29c}$$

The last equation in (2.28) describes the stall of the compressor blade while the two remainder equations provide the surge dynamics in the cells of the compression stage. It is observed that the zero input response of the system is oscillatory (see Figure 2.5). If this undesirable oscillation is not damped out in a sufficiently short time period, it can make the engine enter the vibrating condition resulting in severe mechanical damages or engine flame-out. ıer word suppresses

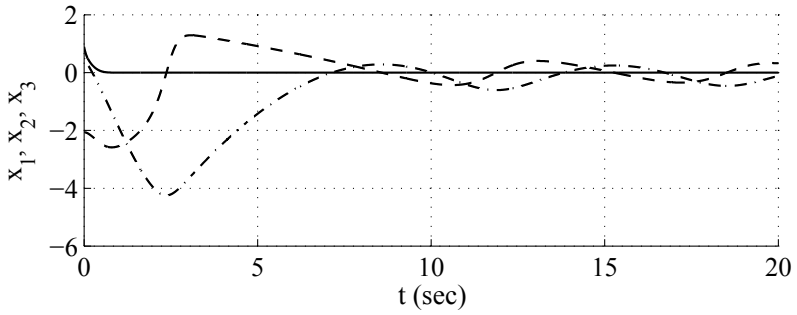

Figure 2.5: Simulation result of the open loop nonlinear system. The dashed, dash-dot, and the solid lines represent x_1, x_2 and x_3, respectively.

With respect to Figure 2.5, the stall oscillation, as the initiator of the surge, over-damps as fast as $0.3sec$ compared to the oscillation period of the surge states (ϕ and ψ) that is about $9.0sec$. Therefore, considering $R = 0$ in (2.28), as done by Krstić and coauthors

[10], is a reasonable approximation to decouple the surge states from the stall states. By doing this, the following second order system is derived

$$\dot{\phi} = -\psi - \frac{3}{2}\phi^2 - \frac{1}{2}\phi^3 \tag{2.30a}$$

$$\dot{\psi} = \frac{1}{\beta^2}(\phi - u). \tag{2.30b}$$

Using the same notation, i.e. $x_1 = \phi$ and $x_2 = \psi$ results in

$$\dot{x}_1 = -x_2 - \frac{3}{2}x_1^2 - \frac{1}{2}x_1^3 \tag{2.31a}$$

$$\dot{x}_2 = \frac{1}{\beta^2}(x_1 - u). \tag{2.31b}$$

Common nonlinear approaches to tackle both problems may be feedback linearization, as done in [16] for (2.29), or the backstepping method [10] used for both the third order and the second order systems ((2.29) and (2.31)). Although these methods have been shown to be effective for numerous applications, they may have some drawbacks, such as cancelation of useful nonlinear terms in the feedback linearization method.

2.3.5 Uncertainty in a Parameter

The parameter β in equation (2.29) is defined as

$$\beta = \frac{U}{a_s}\sqrt{\frac{V_p}{A_c L_c}}, \tag{2.32}$$

where U is the compressor wheel speed at its mean diameter, a_s is the speed of sound, V_p is the volume of the compressor plenum, A_c is the compressor duct area, and L_c is the total aerodynamic length of the compressor and duct (refer to Figure 2.4). A deeper observation of these parameters is given now.

1. V_c, A_c and L_c are geometric parameters that are considered constants.

2. a_s is the speed of sound in the air, which is a function of temperature T. We have $a_s = \sqrt{\gamma_{air} R_{air} T}$, where γ_{air} and R_{air} are the air specific heat ratio and the specific

gas constant for air. Therefore, any slight change in the compressor temperature can lead to a change in β.

3. U is the speed of the compressor wheel that can be changed slightly and can be oscillatory when the surge is growing in the compression cells. Such changes in U directly changes β.

From what was mentioned, one reaches the conclusion that β as a coefficient of system (2.29) may change due to the changes in temperature or compressor wheel speed. Using sensitivity analysis one can determine how much β is vulnerable to the change of the wheel velocity and the temperature. For this purpose, with respect to the definition of β from equation (2.32), we have

$$\begin{aligned}\frac{\partial \beta}{\partial U} =& \frac{1}{a_s}\sqrt{\frac{V_p}{A_c L_c}} \\ =& \frac{\beta}{U}\end{aligned}$$

Using $\Delta\beta$ and ΔU as slight changes in β and U, one may write

$$\Delta\beta = \left(\frac{\Delta U}{U}\right)\beta. \tag{2.33}$$

Similarly, the same analysis can be done for T, as

$$\begin{aligned}\frac{\partial \beta}{\partial T} =& \frac{-\gamma_{air} R_{air} U}{2\sqrt{(\gamma_{air} R_{air})^3 T}}\sqrt{\frac{V_p}{A_c L_c}} \\ =& -\frac{1}{2}\frac{\beta}{T}\end{aligned}$$

Denoting ΔT as a slight change in the air temperature, one may write

$$\Delta\beta = \left(-\frac{1}{2}\frac{\Delta T}{T}\right)\beta \tag{2.34}$$

Two independent proposals are given in this thesis to solve the surge and stall problem. Our first proposal consists of the use of pseudo Euler-Lagrange systems to suppress the states of the second order system (2.31) to the origin. Towards this end, the pseudo

Euler-Lagrange system in [25] is extended to fit system (2.31) in Chapter 3, and the simulation results are presented in Chapter 5, Section 5.1. The second proposal is to design a state feedback intersection-based PWA controller, which makes the states of system (2.29) converge to the origin. To design a PWA controller, a PWA model is required. To the best of the author's knowledge, a PWA controller has never been used for systems (2.29) and (2.31). In Chapter 4, the theory to produce a suitable PWA approximation of a nonlinear system is developed. The proposed novel method is called Intersection-based Piecewise Affine (IPWA) approximation. The results of IPWA approximation as well as the results of the PWA controller synthesis problem for the Moore-Greitzer Model (2.29) are then shown in Chapter 5, Section 5.2.

2.4 Conclusions

Using the laws governing the thermodynamic and fluid behavior of gas stream in each component, as adapted from [3], the modeling of axial compressors of gas turbines was addressed in this chapter. The obtained set of equations were in form of PDEs, which are difficult to tackle with. Using a Galerkin procedure, as addressed in the literature, these equations were simplified to the form of a set of third order ODEs. Moreover, since the amplitude of the rotating stall is damped out quickly comparing to the mass flow and pressure rise states, following [10], the third order ODE was reduced to a second order ODE. Furthermore, the uncertainty of the parameter β in the set of governing equations was studied in detail. With the obtained equations in this chapter, one can apply nonlinear stability analysis and control synthesis techniques for the rotating stall and surge in axial compressors.

Chapter 3

Lyapunov Stability of Pseudo Euler Lagrange Systems

3.1 Introduction

In this chapter, pseudo Euler-Lagrange systems introduced in [25] are extended to a system of the same order, but with additional nonlinear terms. The proposed method enables us to fit a more general class of second order systems for the Lyapunov-based control synthesis problems, such as the second order axial compression surge phenomenon in jet engines. Section 3.2 briefly explains the recent work on pseudo Euler-Lagrange systems. The stability analysis of the extended pseudo Euler-Lagrange systems is addressed in Section 3.3. Section 3.4 provides the reader with the technique used to formulate a second order system as an extended pseudo Euler-Lagrange system. In Section 3.5, the theory suggested in this thesis is applied to the Moore-Greitzer compression surge model as a motivating example. Moreover, the control synthesis problem of the Moore-Greitzer model is addressed by using two current nonlinear methods − namely the feedback linearization and the backstepping, followed by the conclusions.

3.2 Review of Pseudo Euler-Lagrange Systems

According to [25], the pseudo Euler-Lagrange systems are described by the following set of differential equations

$$\dot{x}_1(t) = f_1(x_2) \tag{3.1a}$$

$$\dot{x}_2(t) = -g_1(x_1) + g_2(x_1) f_2(x_2) \tag{3.1b}$$

where, $f_1, f_2, g_1, g_2 \in \mathcal{C}^1$ and satisfy inequalities (3.4) and (3.5). The lemma giving the Lyapunov stability analysis of such systems and its proof are given here from [25] to make the thesis self-contained. However, the reader is always encouraged to refer to the reference [25].

Lemma 3.2.1. *[25] For system* (3.1) *define a class* $\mathcal{C}^1$ *function*

$$V(x_1, x_2) = F_1(x_2) + G_1(x_1) \tag{3.2}$$

where

$$G_1(x_1) = \int g_1(x_1) dx_1, \quad F_1(x_2) = \int f_1(x_2) dx_2 \tag{3.3}$$

Then if

$$f_1(x_2) g_2(x_1) f_2(x_2) \leq 0, \tag{3.4}$$

and

$$f_1'(x_2) > 0, \;\; x_2 \neq 0, \tag{3.5a}$$

$$g_1'(x_1) > 0, \;\; x_1 \neq 0, \tag{3.5b}$$

the system (3.1) *is stable and* V *is a Lyapunov function provided it is radially unbounded. If furthermore*

- $f_1(x_2) = 0$ *implies* $x_2 = 0$,
- $f_2(0) = 0$,

- $g_i(x_1) = 0$ *implies* $x_1 = 0$ *for* $i = 1, 2,$

then the system (3.1) *is asymptotically stable to the origin.*

Proof. Using V as a candidate Lyapunov function and computing its derivative over time using (3.1) yields

$$\dot{V} = \frac{\partial V}{\partial x_1}\dot{x}_1 + \frac{\partial V}{\partial x_2}\dot{x}_2 \tag{3.6}$$

$$= g_1 f_1 + f_1[g_2 f_2 - g_1] \tag{3.7}$$

$$= g_2 f_1 f_2 \leq 0 \tag{3.8}$$

which shows that the system is globally stable since V is positive definite under the constraints (3.5) and it is assumed to be radially unbounded. Let the following three sets be defined

$$M_1 = \{(x_1, x_2) \mid f_1(x_2) = 0\},$$

$$M_2 = \{(x_1, x_2) \mid f_2(x_2) = 0\},$$

$$M_3 = \{(x_1, x_2) \mid g_1(x_1) = 0\}.$$

Using LaSalle's Invariance Principle (refer to Theorem 3.4 in [72]), we define the set

$$M = M_1 \cup M_2 \cup M_3.$$

If $f_1(x_2) = 0$ then $x_2 = 0$ (constant) and $\dot{x}_1, \dot{x}_2, f_2(0)$ are zero. This implies that $g_1(x_1) = 0$, which in turn implies that $x_1 = 0$. If $f_2(x_2) = 0$ then $x_2 = 0$, and x_2 is zero, which implies that $g_1(x_1) = 0$, and consequently $x_1 = 0$. Finally, if $g_2(x_1) = 0$ then $x_1 = 0$, $x_1 = 0$ and consequently $f_1(x_2) = 0$, which implies $x_2 = 0$. Therefore, the largest invariant set of system (3.1) contained inside M is the origin and system (3.1) is asymptotically stable to the origin. This completes the proof of the lemma. □

Note that the Lyapunov stability of the pseudo Euler-Lagrange systems addressed in Lemma 3.2.1 has been generalized for higher order systems with specific structure [25].

To tackle system (3.1) we start with the analysis of the surge part of the Moore-Greitzer model, as a motivating example. Reconsider equation (2.30) describing the surge phenomenon in gas turbines, taken from [10].

$$\dot{\phi} = -\psi - \frac{3}{2}\phi^2 - \frac{1}{2}\phi^3 \tag{3.9a}$$

$$\dot{\psi} = \frac{1}{\beta^2}(\phi - u) \tag{3.9b}$$

where ϕ is the mass flow rate through the throttle shifted by unity, ψ is the pressure rise shifted by unity, u is a function of the flow through the throttle considered as the control input, and β is considered as a constant. In order to represent (3.9) in the form of (3.1), the substitution of ϕ by z_2 and ψ by z_1 is proposed.

This results in the following state space representation

$$\dot{z}_1 = \frac{1}{\beta^2} z_2 - \frac{1}{\beta^2} u \tag{3.10a}$$

$$\dot{z}_2 = -z_1 - \frac{3}{2} z_2^2 - \frac{1}{2} z_2^3 \tag{3.10b}$$

Comparing (3.10) with (3.1), one can distinguish the pseudo Euler-Lagrange components associated with Lemma 3.2.1, as

$$f_1(z_2) = \frac{1}{\beta^2} z_2 + \frac{1}{\beta^2} u(z_2) \tag{3.11a}$$

$$f_2(z_2) = -\frac{3}{2} z_2^2 - \frac{1}{2} z_2^3 \tag{3.11b}$$

$$g_1(z_1) = z_1 \tag{3.11c}$$

$$g_2(z_1) = 1 \tag{3.11d}$$

Even though conditions in (3.4)-(3.5) are easily satisfied, the conditions for asymptotic stability cannot be satisfied. This can be realized since $g_2(z_1) = 1$, and therefore $\{z_1 \mid g_2(z_1) = 0\} = \emptyset$. Moreover, there is no control authority over $\dot{z}_2$ to manipulate $g_2(z_1)$.

This drawback has led us to explore more opportunities by adding more nonlinear terms to the structure of (3.1), which is addressed in the next section.

3.3 Stability Analysis

Let us consider the second order dynamical system of the form

$$\dot{x}_1 = h_1(x_1, x_2) - f(x_2) \tag{3.12a}$$

$$\dot{x}_2 = g(x_1) + h_2(x_1, x_2) \tag{3.12b}$$

The main theory associated with the Lyapunov stability of this class of second order systems is provided in the following theorem.

Theorem 3.3.1. *Consider the second order system* (3.12). *Furthermore, consider* $V(x_1, x_2)$ *as a candidate Lyapunov function defined as*

$$V(x_1, x_2) = G(x_1) + F(x_2) \tag{3.13}$$

where

$$F(x_2) = \int f(x_2)dx_2, \quad G(x_1) = \int g(x_1)dx_1 \tag{3.14}$$

If the following conditions

$$G(x_1) > 0, \quad x_1 \neq 0 \tag{3.15a}$$

$$F(x_2) > 0, \quad x_2 \neq 0 \tag{3.15b}$$

$$g(x_1)h_1(x_1, x_2) \leq 0 \tag{3.15c}$$

$$f(x_2)h_2(x_1, x_2) \leq 0 \tag{3.15d}$$

are satisfied, $V(x_1, x_2)$ *is a Lyapunov function for* (3.12) *and system* (3.12) *is stable. In addition, if* V *is continuously differentiable and radially unbounded and if*

$$\{x \in \mathbb{R}^2 \mid g(x_1)h_1(x_1, x_2) + f(x_2)h_2(x_1, x_2) = 0\} = \{(0,0)\}, \tag{3.16}$$

system (3.12) *is asymptotically stable.*

Proof. Since there are no cross terms in the right hand side of (3.13), positive definiteness of the candidate Lyapunov function is guaranteed by (3.15a) and (3.15b). Taking the time derivative of the candidate Lyapunov function yields

$$\begin{aligned}\dot{V}(x_1,x_2) =& V_{x_1}\dot{x}_1 + V_{x_2}\dot{x}_2 \\ =& g(x_1)\left(h_1(x_1,x_2) - f(x_2)\right) \\ &+ f(x_2)\left(g(x_1) + h_2(x_1,x_2)\right) \\ =& g(x_1)h_1(x_1,x_2) - g(x_1)f(x_2) + g(x_1)f(x_2) \\ &+ f(x_2)h_2(x_1,x_2) \\ =& g(x_1)h_1(x_1,x_2) + f(x_2)h_2(x_1,x_2) \end{aligned} \tag{3.17}$$

Regarding conditions (3.15c) and (3.15d) we have

$$g(x_1)h_1(x_1,x_2) + f(x_2)h_2(x_1,x_2) \leq 0 \tag{3.18}$$

implying $\dot{V}(x_1,x_2) \leq 0$, which implies that $V(x_1,x_2)$ is indeed a Lyapunov function for system (3.12). According to the Lyapunov stability theorem [72], (3.12) is then stable.

Moreover, equations (3.16) and (3.18) imply

$$\{x \in \mathbb{R}^2 \mid \dot{V}(x) = 0\} = \{(0,0)\}.$$

Since V is a positive definite, continuously differentiable and radially unbounded function, the LaSalle's invariance principle [72] guarantees the global asymptotic stability of this system to the origin. This completes the proof of the theorem. □

3.4 Controller Synthesis

Although many mathematical models do not seem to satisfy conditions (3.15), the presence of a control input signal, in some cases, can indeed transform the original second order system in such a way that these conditions are satisfied. This can be done by adding

control signals u_1 and u_2 to (3.12), as

$$\dot{x}_1 = h_1(x_1,x_2) - f(x_2) + u_1(x_1,x_2) \tag{3.19a}$$

$$\dot{x}_2 = g(x_1) + h_2(x_1,x_2) + u_2(x_1,x_2) \tag{3.19b}$$

The structure of u_1 and u_2 has to have specific characteristics such that the nonlinear terms in (3.12) can be manipulated. With this idea in mind, the following structure is proposed

$$u_1(x_1,x_2) = u_{11}(x_1,x_2) + u_{12}(x_2) \tag{3.20a}$$

$$u_2(x_1,x_2) = u_{21}(x_1) + u_{22}(x_1,x_2), \tag{3.20b}$$

where u_{11}, u_{12}, u_{21} and u_{22} are the components of the control input. Note that (3.20) represents only two nonlinear controllers. The new pseudo Euler-Lagrange components can thus be defined as

$$\tilde{f}(x_2) = f(x_2) - u_{12}(x_2) \tag{3.21a}$$

$$\tilde{g}(x_1) = g(x_1) + u_{21}(x_1) \tag{3.21b}$$

$$\tilde{h}_1(x_1,x_2) = h_1(x_1,x_2) + u_{11}(x_1,x_2) \tag{3.21c}$$

$$\tilde{h}_2(x_1,x_2) = h_2(x_1,x_2) + u_{22}(x_1,x_2) \tag{3.21d}$$

which are used to present the *generalized pseudo Euler-Lagrange* system. The candidate Lyapunov function attains the form

$$V = \int \tilde{f}(x_2)dx_2 + \int \tilde{g}(x_1)dx_1 \tag{3.22}$$

$$\dot{x}_1 = \tilde{h}_1(x_1,x_2) - \tilde{f}(x_2) \tag{3.23a}$$

$$\dot{x}_2 = \tilde{g}(x_1) + \tilde{h}_2(x_1,x_2). \tag{3.23b}$$

By properly choosing $u_1(x_1,x_2)$ and $u_2(x_1,x_2)$, one can satisfy (3.15), and system (3.23) is thus guaranteed to be Lyapunov stable. However, we may have restrictions in the

control action, as an instance, not all the states may be observable, or not all modes may be controllable. Moreover, note that the two control channels in the full format given in equations (3.20) are not usually used simultaneously. Control signals u_{ij}, where $i, j \in \{1,2\}$, are given to provide the reader with the various options that can be used to manipulate the original system. For instance, if there is no control authority over the dynamics of the first state, one needs to leave $\tilde{f}(x_2) = f(x_2)$ and $\tilde{h}_1(x_1,x_2) = h_1(x_1,x_2)$ as they are, hence make an attempt to drive $\dot{x}_2 = \tilde{g}(x_2) + \tilde{h}_2(x_1,x_2)$ with u_2 to a condition such that the assumptions of Theorem 3.3.1 are satisfied.

To illustrate this technique, a controller is designed for the nonlinear no-stall Moore-Greitzer model. In order to show the benefits of the proposed methodology that is applied to this system, the problem is also solved by using the feedback linearization and the backstepping techniques for comparison.

3.5 Compressor Surge Stabilization

In this section, the no-stall part of the Moore-Greitzer model is considered as a physical phenomenon described by a second order ODE. In Subsections 3.5.1 and 3.5.2 the Moore-Greitzer surge model is controlled by using the feedback linearization as well as the backstepping techniques, respectively. Later in Subsection 3.5.3 the same problem is solved by the proposed pseudo Euler Lagrange nonlinear control synthesis method.

3.5.1 Input-Output Feedback Linearization Technique

One of the most common controller design techniques in nonlinear systems is the well-known *feedback linearization*. In this section the Moore-Greitzer model is stabilized by using this technique. For this purpose, consider the set of second order nonlinear equations in (3.9) representing the surge phenomenon in gas turbines. Using the substitutions $x_1 = \phi$,

$x_2 = \psi$ and $u_2 = u$ yields the following representation

$$\dot{x}_1 = -\frac{3}{2}x_1^2 - \frac{1}{2}x_1^3 - x_2 \tag{3.24a}$$

$$\dot{x}_2 = \frac{1}{\beta^2}(x_1 - u_2) \tag{3.24b}$$

Using the change of variables

$$y_1 = x_1 \tag{3.25}$$

for system (3.24), we have

$$\begin{aligned}\ddot{y}_1 =& \ddot{x}_1 \\ =& -3x_1\dot{x}_1 - \frac{3}{2}x_1^2\dot{x}_1 - \dot{x}_2 \\ =& -3x_1\dot{x}_1 - \frac{3}{2}x_1^2\dot{x}_1 - \frac{1}{\beta^2}(x_1 - u_2).\end{aligned} \tag{3.26}$$

Replacing x_1 and $\dot{x}_1$ by y_1 and $\dot{y}_1$, respectively we may write

$$\ddot{y}_1 = -3y_1\dot{y}_1 - \frac{3}{2}y_1^2\dot{y}_1 - \frac{1}{\beta^2}(y_1 - u_2). \tag{3.27}$$

According to [72], in the input/output linearization approach, the control signal must be such that all of the nonlinearities are canceled, resulting in a linear map between the input and the output. The signal u_2 must then have the following form

$$u_2 = \beta^2(3y_1\dot{y}_1 + \frac{3}{2}y_1^2\dot{y}_1 + \frac{1}{\beta^2}y_1 + k_1^f\dot{y}_1 + k_2^f y_1), \tag{3.28}$$

where k_1^f and k_2^f are gains to be designed to achieve desirable pole location for the linear system

$$\ddot{y}_1 - k_1^f\dot{y}_1 - k_2^f y_1 = 0. \tag{3.29}$$

This will ensure global asymptotic stability of the closed-loop system. The above controller can be realized by substituting for y_1 as x_1 and for $\dot{y}_1$ as

$$\dot{y}_1 = -\frac{3}{2}x_1^2 - \frac{1}{2}x_1^3 - x_2, \tag{3.30}$$

resulting in the following nonlinear controller.

$$\boxed{\begin{aligned} u_2 = -\beta^2 \Bigg[& \frac{3}{4}x_1^5 + \frac{15}{4}x_1^4 + \left(\frac{1}{2}k_1^f + \frac{9}{2}\right)x_1^3 + \frac{3}{2}x_1^2 x_2 \\ & + \frac{3}{2}k_1^f x_1^2 + 3x_1 x_2 - \left(\frac{1}{\beta^2} + k_2^f\right)x_1 + k_1^f x_2 \Bigg] \end{aligned}} \tag{3.31}$$

Although this controller with gains k_1^f and k_2^f seems to be powerful in the sense that any oscillation and damping specification (natural frequency and damping ratio) can be achieved, what this solution lacks is the robustness of the closed-loop system. The following case is studied.

Following the uncertainty analysis of the parameter β from Chapter 2, consider equations (2.33) and (2.34). If the speed U at time $t_1 > t_0$ is increased by 2% and at time $t_2 > t_1$ the temperature is decreased by 3%, according to equations (2.33) and (2.34), we have

$$\left.\frac{\Delta\beta}{\beta}\right|_{t_1} = 0.02. \tag{3.32}$$

resulting in

$$\beta|_{t_1} = \beta|_{t_0} \times 1.02. \tag{3.33}$$

After a fraction of time we will have

$$\left.\frac{\Delta\beta}{\beta}\right|_{t_2} = -\frac{1}{2}(-0.03), \tag{3.34}$$

which leads to

$$\beta|_{t_2} = \beta|_{t_1} \times 1.015. \tag{3.35}$$

The overall change in β is now given by

$$\beta|_{t_2} = \beta|_{t_0} \times 1.0353, \tag{3.36}$$

which implies 3.53% of increment in β due to slight changes in temperature and compressor wheel speed, that are not unlikely to happen.

Now, following [16], let $\beta = 0.707$. With the above sensitivity analysis and using the same changes due to the uncertainty in the temperature and the compressor wheel speed, β can easily grow up to 0.732. On the other hand, u_2 expressed in (3.28), as the feedback linearization controller for the nonlinear second order system (3.27), is proportional to β^2, which indeed is multiplied by the canceling term of the nonlinearities.

Denoting $\bar{\beta}$ as the disturbed value of β due to the changes in T and U, and the nonlinear function $q(y_1, \dot{y}_1)$ as

$$q(y_1, \dot{y}_1) = -3y_1\dot{y}_1 - \frac{3}{2}y_1^2\dot{y}_1, \tag{3.37}$$

the closed-loop form of equation (3.27) can be written as

$$\ddot{y}_1 = q(y_1, \dot{y}_1) - \frac{1}{\bar{\beta}^2}\left(y_1 - \beta^2\left[-q(y_1, \dot{y}_1) + \frac{1}{\beta^2}y_1 + k_1^f\dot{y}_1 + k_2^f y_1\right]\right) \tag{3.38}$$

Simplifying (3.38) yields

$$\ddot{y}_1 = \left[1 - \left(\frac{\beta}{\bar{\beta}}\right)^2\right]q(y_1, \dot{y}_1) + \left(\frac{\beta}{\bar{\beta}}\right)^2\left(-k_1^f y_1 - k_2^f\dot{y}_1\right) \tag{3.39}$$

It can be seen from equation (3.39) that the feedback linearization works perfectly as long as $\bar{\beta} = \beta$. Once this condition is violated, $\pm\delta q(y_1, \dot{y}_1)$, where $\delta = |1 - (\beta/\bar{\beta})^2|$, appears in the equation, for which the feedback linearization stability analysis is no longer valid. This term, with a potential positive or negative sign, may render the no-stall Moore-Greitzer model unstable.

3.5.2 Backstepping Technique

In this subsection a backstepping controller is designed for the no-stall part of the Moore-Greitzer model. The design methodology and the procedure are adapted with a minor variation from the model in [10], page 70. Considering system (3.24), let x_2 denote the virtual control parameter. The candidate Lyapunov function for the first step of the design is selected quadratically as follows

$$V_1(x_1) = \frac{1}{2}x_1^2. \tag{3.40}$$

The time derivative of V_1 is then computed as

$$\begin{aligned}\dot{V}_1 =& x_1\dot{x}_1 \\ =& x_1\left(-\frac{3}{2}x_1^2-\frac{1}{2}x_1^3-x_2\right)\end{aligned} \tag{3.41}$$

Note that to the benefit of avoiding useful nonlinear term cancelation, $\dot{x}_1$ taken from (3.24a), can be recast as

$$\dot{x}_1 = -\frac{1}{2}\left(x_1+\frac{3}{2}\right)^2 x_1+\frac{9}{8}x_1-x_2 \tag{3.42}$$

so that $\dot{V}$ will then take the form

$$\dot{V}_1 = x_1\left(-\frac{1}{2}\left(x_1+\frac{3}{2}\right)^2 x_1+\frac{9}{8}x_1-x_2\right).$$

Since x_2 acts as the virtual controller, its desired value can then be suggested as

$$x_2^{des} = \left(\alpha_b+\frac{9}{8}\right)x_1 \tag{3.43}$$

$$\triangleq \mu(x_1), \qquad \alpha_b > 0, \tag{3.44}$$

such that $\dot{V}_1$ is guaranteed to be negative definite, where $\mu(x_1)$ is called stabilizing function. Note that without recasting (3.24a) into the form of (3.42), the stabilizing function would contain a squared term to render $\dot{V}_1$ negative definite, which is contradicting our objective to keep the nonlinearities that are stabilizing terms. Given (3.44), $\dot{V}_1$ can then be rewritten as

$$\begin{aligned}\dot{V}_1 =& x_1\left(-\frac{1}{2}\left(x_1+\frac{3}{2}\right)^2 x_1+\frac{9}{8}x_1-x_2+\mu(x_1)-\mu(x_1)\right) \\ =& -\frac{1}{2}\left(x_1+\frac{3}{2}\right)^2 x_1^2-\alpha_b x_1^2-(x_2-\mu(x_1))x_1\end{aligned} \tag{3.45}$$

The error parameter w is defined to be the deviation of x_2 from its desired value as

$$w = x_2 - x_2^{des} = x_2-\mu(x_1). \tag{3.46}$$

Using w, equation (3.45) can be recast as

$$\dot{V}_1 = -\frac{1}{2}\left(x_1 + \frac{3}{2}\right)^2 x_1^2 - \alpha_b x_1^2 - w x_1 \tag{3.47}$$

Since $\dot{\mu}(x_1) = (\alpha_b + 9/8)\dot{x}_1$, using equation (3.24a), $\dot{w}$ is then computed as

$$\dot{w} = \frac{1}{\beta^2}(x_1 - u_2) - (\alpha_b + \frac{9}{8})\left(-\frac{3}{2}x_1^2 - \frac{1}{2}x_1^3 - x_2\right) \tag{3.48}$$

Going to the next step, as done in the backstepping technique, the candidate Lyapunov function $V_2(x_1, x_2)$ is introduced as

$$V_2(x_1, w) = V_1(x_1) + \frac{1}{2}w^2, \tag{3.49}$$

and using equation (3.47), its time derivative is given by

$$\begin{aligned}
\dot{V}_2 =& \dot{V}_1 + w\dot{w} \\
=& -\frac{1}{2}\left(x_1 + \frac{3}{2}\right)^2 x_1^2 - \alpha_b x_1^2 - w x_1 \\
&+ w\left[\frac{1}{\beta^2}(x_1 - u_2) - (\alpha_b + \frac{9}{8})\left(-\frac{3}{2}x_1^2 - \frac{1}{2}x_1^3 - x_2\right)\right] \\
=& -\frac{1}{2}\left(x_1 + \frac{3}{2}\right)^2 x_1^2 - \alpha_b x_1^2 \\
&+ w\left[x_1\left(\frac{1}{\beta^2} - 1\right) - \frac{1}{\beta^2}u_2 - (\alpha_b + \frac{9}{8})\left(-\frac{3}{2}x_1^2 - \frac{1}{2}x_1^3 - x_2\right)\right]
\end{aligned}$$

At this stage, u_2 could be selected such that the multiplier of w in the parentheses is made equal to zero. However, adding a term $F_L(V_1)$ to V_2, where F_L is an unknown to be determined, can help avoid cancelation of the nonlinearities that enhances the stability of the system. Doing this, a new candidate Lyapunov function can be suggested as

$$V(x_1, w) = V_1(x_1) + F_L(V_1) + \frac{1}{2}w^2, \tag{3.50}$$

for which we have

$$\begin{aligned}
\dot{V} =& \dot{V}_1 + F'_{L_{V_1}}\dot{V}_1 + w\dot{w} \\
=& \dot{V}_1(1 + F'_{L_{V_1}}) + w\dot{w}
\end{aligned}$$

Substituting $\dot{V}_1$ and $\dot{w}$ from equations (3.47) and (3.48) yields

$$\begin{aligned}\dot{V} = &\left[-\frac{1}{2}\left(x_1+\frac{3}{2}\right)^2 x_1^2 - \alpha_b x_1^2 - w x_1\right](1+F'_{L_{V_1}}) \\ &+ w\left[\frac{1}{\beta^2}(x_1-u_2) - (\alpha_b+\frac{9}{8})\left(-\frac{3}{2}x_1^2 - \frac{1}{2}x_1^3 - x_2\right)\right] \\ = &\left[-\frac{1}{2}\left(x_1+\frac{3}{2}\right)^2 x_1^2 - \alpha_b x_1^2\right](1+F'_{L_{V_1}}) \\ &+ w\left(-x_1 - x_1 F'_{L_{V_1}} + \frac{1}{\beta^2}x_1 - \frac{1}{\beta^2}u_2 + \frac{3\gamma_b}{2}x_1^2 + \frac{\gamma_b}{2}x_1^3 + \gamma_b x_2\right),\end{aligned}$$

where $\gamma_b = (\alpha_b + 9/8)$. In order to avoid the cancelation of $\gamma_b x_1^3/2$ with the control input u_2, one needs to cancel it by using $F'_{L_{V_1}}$ by setting

$$F'_{L_{V_1}} = \frac{\gamma_b}{2}x_1^2 = \gamma_b V_1(x_1), \tag{3.51}$$

Integrating both sides results in

$$\begin{aligned}F_L(V_1) =& \frac{\gamma_b}{2}V_1^2 \\ =& \frac{\gamma_b}{8}x_1^4,\end{aligned} \tag{3.52}$$

Consequently, the final expression for V, using equations (3.40), (3.50) and (3.52), has the form

$$V(x_1,w) = \frac{1}{2}x_1^2 + \frac{\gamma_b}{8}x_1^4 + \frac{1}{2}w^2 \tag{3.53}$$

$$>0, \quad (x_1,w) \neq (0,0) \tag{3.54}$$

By equations (3.46) and (3.44) we have $w = x_2 - (\alpha_b + 9/8)x_1$, resulting in

$$V(x_1,x_2) = \frac{1}{2}x_1^2 + \frac{\gamma_b}{8}x_1^4 + \frac{1}{2}\left[x_2 - (\alpha_b+\frac{9}{8})x_1\right]^2 \tag{3.55}$$

Accordingly, $\dot{V}$ becomes

$$\begin{aligned}\dot{V} = &\left[-\frac{1}{2}\left(x_1+\frac{3}{2}\right)^2 x_1^2 - \alpha_b x_1^2\right](1+\frac{\gamma_b}{2}x_1^2) \\ &+ w\left(-x_1 + \frac{1}{\beta^2}x_1 - \frac{1}{\beta^2}u_2 + \frac{3\gamma_b}{2}x_1^2 + \gamma_b x_2\right).\end{aligned}$$

Rearranging yields

$$\begin{aligned}\dot{V} =& -\frac{1}{2}\left(x_1+\frac{3}{2}\right)^2 x_1^2(1+\frac{\gamma_b}{2}x_1^2)-\alpha_b x_1^2(1+\frac{\gamma_b}{2}x_1^2)\\ &+w\left(-x_1+\frac{1}{\beta^2}x_1-\frac{1}{\beta^2}u_2+\frac{3\gamma_b}{2}x_1^2+\gamma_b x_2\right)\\ =& -\frac{1}{2}\left(x_1+\frac{3}{2}\right)^2 x_1^2(1+\frac{\gamma_b}{2}x_1^2)-\alpha_b x_1^2-\alpha_b\frac{\gamma_b}{2}x_1^4\\ &+w\left(-x_1+\frac{1}{\beta^2}x_1-\frac{1}{\beta^2}u_2+\frac{3\gamma_b}{2}x_1^2+\gamma_b x_2\right)\end{aligned}$$

Adding and subtracting the term $\frac{9\gamma_b}{8\alpha_b}w^2$, we have

$$\begin{aligned}\dot{V} =& \left[-\frac{1}{2}\left(x_1+\frac{3}{2}\right)^2 x_1^2(1+\frac{\gamma_b}{2}x_1^2)-\alpha_b x_1^2\right]\\ &-\left[\alpha_b\frac{\gamma_b}{2}x_1^4-\frac{3\gamma_b}{2}x_1^2w+\frac{9\gamma_b}{8\alpha_b}w^2\right]\\ &+w\left(-x_1+\frac{1}{\beta^2}x_1-\frac{1}{\beta^2}u_2+\gamma_b x_2+\frac{9\gamma_b}{8\alpha_b}w\right)\end{aligned}\tag{3.56}$$

Since $\alpha_b>0$ and $\gamma_b>0$, the term in the square brackets can be shown to be positive definite as

$$\alpha_b\frac{\gamma_b}{2}x_1^4-\frac{3\gamma_b}{2}x_1^2w+\frac{9\gamma_b}{8\alpha_b}w^2=\frac{\gamma_b\alpha_b}{2}\left[x_1^2-\frac{3w}{2\alpha_b}\right]^2.\tag{3.57}$$

This term multiplied by the negative unity and its preceding terms (in the square brackets) are negative definite. Therefore, our job is to design u_2 such that the last term in (3.56) becomes zero. Towards this end, u_2 is selected as

$$\boxed{u_2=(1-\beta^2)x_1+\beta^2\gamma_b x_2+\beta^2\frac{9\gamma_b}{8\alpha_b}w,}\tag{3.58}$$

where $w=x_2-\gamma_b x_1$ and $\gamma_b=(\alpha_b+9/8)$. This is a linear controller that guarantees the asymptotic stability of the Moore-Greitzer no-stall model.

Investigating the designed backstepping controller, the following conclusion is drawn. Similar to the input/output feedback linearization controller that was designed in Subsection 3.5.1 (see equation (3.31)), the control input is a function of β^2, as it can be seen from equation (3.58). Performing a perturbation on the value of $\bar{\beta}$, as done for the feedback

linearization, the disturbed value of $\bar{\beta}$ will be considered for system (3.24). Following equation (3.56), by replacing u_2 with the obtained value in (3.58), the time derivative of the Lyapunov function of the disturbed close loop system takes the form

$$\begin{aligned}\dot{V} = &-\frac{1}{2}\left(x_1+\frac{3}{2}\right)^2 x_1^2(1+\frac{\gamma_b}{2}x_1^2) - \alpha_b x_1^2 \\ &-\left[\alpha_b\frac{\gamma_b}{2}x_1^4 - \frac{3\gamma_b}{2}x_1^2 w + \frac{9\gamma_b}{8\alpha_b}w^2\right] \\ &+\left[1-\left(\frac{\beta}{\bar{\beta}}\right)^2\right]\left[-x_1+\gamma_b x_2+\frac{9\gamma_b}{8\alpha_b}w\right]w \end{aligned} \tag{3.59}$$

Although the stabilizing nonlinearities have been preserved with the backstepping, one can still study what happens as the parameter $\bar{\beta}$ is varied. To have equation (3.59) negative definite, one needs $\bar{\beta} = \beta$. For instance, for 8% disturbance in $\bar{\beta}$, $\alpha_b = 2$, and $(x_1, x_2) = (-2.1, 2.0)$ we obtain $\dot{V} = 0.85 > 0$. Further increment in α_b, leads to a positive value for $\dot{V}$. Therefore, a slight change in $\bar{\beta}$ results in the violation of the negativity of $\dot{V}$. Consequently, the control input (3.58), which is based on (3.59), will not be guaranteed to asymptotically stabilize the no-stall Moore-Greitzer model with the Lyapunov function of form (3.55). Yet, one needs to consider the fact that the Lyapunov theory provides sufficient conditions for stability of a control system. Therefore, the positivity of $\dot{V}$ in (3.59) does not nevertheless impart an instability property to the closed-loop Moore-Greitzer system.

3.5.3 Pseudo Euler-Lagrange Technique

Consider again system (3.24). By letting

$$\begin{aligned} f(x_2) &= x_2 \\ g(x_1) &= \frac{1}{\beta^2}x_1 \\ h_1(x_1,x_2) &= -\frac{3}{2}x_1^2 - \frac{1}{2}x_1^3 \\ h_2(x_1,x_2) &= 0 \end{aligned}$$

one can recognize that $g(x_1)h_1(x_1,x_2) = \frac{-1}{2\beta^2}x_1^2(x_1^2+3x_1) \not\leq 0$, implying that the condition (3.15c) is violated. Accordingly, our task is to design a feedback controller using $u_2(x_1,x_2)$, such that the set of conditions (3.15) is met. Since there is no control authority over $h_1(x_1,x_2)$ (i.e. $u_1 = 0$), using u_2 we need to manipulate $g(x_1)$ such that (3.15a), (3.15b) and (3.15c) are satisfied.

Further investigation of this problem led us to use a change of variables, in order to convert equations in (3.24) into the form of (3.12). In what follows, the next coordinate transformation is suggested

$$y_1 = x_1 \tag{3.60a}$$

$$\begin{aligned} y_2 &= -\dot{x}_1 - x_1 \\ &= \frac{3}{2}x_1^2 + \frac{1}{2}x_1^3 - x_1 + x_2 \end{aligned} \tag{3.60b}$$

where y_1 represents the mass flow rate and y_2 the negative of the sum of the mass flow rate and acceleration through the compressor. The Jacobian of y in (3.60) is given by

$$\mathfrak{J} = \begin{bmatrix} 1 & 0 \\ \frac{3}{2}x_1^2 + 3x_1 - 1 & 1 \end{bmatrix} \tag{3.61}$$

which is full rank, and according to the implicit function theorem given in reference [73], x_1 and x_2 are locally invertible with respect to y_1 and y_2. Nonetheless y is not a global diffeomorphism. Substituting the change of variables (3.60), into system (3.24) yields

$$\dot{y}_1 = -y_1 - y_2 \tag{3.62a}$$

$$\begin{aligned} \dot{y}_2 = &\left(-\frac{3}{2}y_1^3 - 3y_1^2 + (1+\beta^{-2})y_1\right) \\ &- y_2\left(\frac{3}{2}y_1^2 + 3y_1 - 1\right) - \beta^{-2}u_2 \end{aligned} \tag{3.62b}$$

Comparing (3.62) with (3.19) yields

$$g(y_1) = -\frac{3}{2}y_1^3 - 3y_1^2 + (1+\beta^{-2})y_1 \tag{3.63a}$$

$$f(y_2) = y_2 \tag{3.63b}$$

$$h_1(y_1, y_2) = -y_1 \tag{3.63c}$$

$$h_2(y_1, y_2) = -y_2\left(\frac{3}{2}y_1^2 + 3y_1 - 1\right) \tag{3.63d}$$

With the assignments (3.63), condition (3.15b) is given by

$$\int f(y_2)dy_2 = \int y_2 dy_2 = \frac{1}{2}y_2^2 \geq 0$$

In order to verify the conditions (3.15a), (3.15c) and (3.15d), one needs to manipulate $g(y_1)$ and $h_2(y_1, y_2)$ using $u_2(y_1, y_2) = u_{21}(y_1) + u_{22}(y_1, y_2)$. This implies to determine the generalized components of the pseudo Euler-Lagrange system, as expressed in (3.21). Let us choose u_{21} as

$$u_{21}(y_1) = -\beta^2\alpha(-\frac{1}{2}y_1^3 - \frac{3}{2}y_1^2) - \beta^2\gamma y_1 \tag{3.64}$$

where α and γ are constant coefficients. Note that the intuition behind choosing the nonlinear terms in $u_{21}(y_1)$ is the fact that according to the proposed substitution law in equation (3.60), we have $-(1/2)y_1^3 - (3/2)y_1^2 = \dot{x}_1 + x_2$, which is the algebraic sum of the linear terms. We thus have

$$\begin{aligned}\tilde{g}(y_1) = &\left(-\frac{3}{2} - \alpha\frac{1}{2}\right)y_1^3 + \left(-3 - \alpha\frac{3}{2}\right)y_1^2 \\ &+ (1 + \beta^{-2} + \gamma)y_1\end{aligned} \tag{3.65}$$

With no control action on $\dot{y}_1$, the functions $\tilde{f}$ and $\tilde{h}_1$ remain unchanged as

$$\begin{aligned}\tilde{f}(y_2) &= f(y_2) &&= y_2 \\ \tilde{h}_1(y_1, y_2) &= h_1(y_1, y_2) &&= -y_1\end{aligned}$$

To construct the first part of the candidate Lyapunov function, as shown in equation (3.22), we are to find

$$\begin{aligned}\int \tilde{g}(y_1)dy_1 =& \left(-\frac{3}{8}-\alpha\frac{1}{8}\right)y_1^4+\left(-1-\alpha\frac{1}{2}\right)y_1^3\\ &+\frac{1}{2}(1+\beta^{-2}+\gamma)y_1^2\\ =&y_1^2\left[\left(-\frac{3}{8}-\alpha\frac{1}{8}\right)y_1^2+\left(-1-\alpha\frac{1}{2}\right)y_1\right.\\ &\left.+\frac{1}{2}(1+\beta^{-2}+\gamma)\right]\end{aligned} \tag{3.66}$$

Since the factor $y_1^2 \geq 0$, we need to find the conditions for α and γ, under which the second order polynomial in equation (3.66) is non-negative according to (3.15a), i.e.

$$\begin{aligned}p(y_1) =& \left(-\frac{3}{8}-\alpha\frac{1}{8}\right)y_1^2+\left(-1-\alpha\frac{1}{2}\right)y_1\\ &+\frac{1}{2}(1+\beta^{-2}+\gamma)\geq 0\end{aligned}$$

Towards this end, the properties of the second order polynomials are used, as

$$\nabla^2 p(y_1) \geq 0 \tag{3.67a}$$

$$\Delta(p(y_1)) \leq 0 \tag{3.67b}$$

where $\Delta(p(y_1))$ is the discriminant of $p(y_1)$ and $\nabla^2(\cdot)$ is the Hessian operator. Condition (3.67a) restricts $p(y_1)$ to be convex while constraint (3.67b) forces $p(y_1)$ not to have a real root, implying that $p(y_1) > 0$. Accordingly we have

$$\nabla^2 p(y_1) \geq 0 \quad (=) \quad \alpha < -3 \tag{3.68}$$

$$\Delta(p(y_1)) \leq 0 \quad (=) \quad \gamma \geq \frac{\alpha^2+(5+\beta^{-2})\alpha+(7+3\beta^{-2})}{-(\alpha+3)} \tag{3.69}$$

Note that we need $\alpha \neq 0$ since otherwise the right hand side term in equation (3.69) is rendered infinity. Furthermore, to satisfy condition (3.15c) we have

$$\begin{aligned}\tilde{g}(y_1)\tilde{h}_1(y_1,y_2) =& \left(\frac{3}{2}+\alpha\frac{1}{2}\right)y_1^4+\left(3+\alpha\frac{3}{2}\right)y_1^3\\ &-(1+\beta^{-2}+\gamma)y_1^2\end{aligned} \tag{3.70}$$

To make (3.70) non-positive, the same argument is used as for (3.66). Factorizing $-y_1^2$ in (3.70) yields a second order polynomial

$$\tilde{p}(y_1) = -\left(\frac{3}{2}+\alpha\frac{1}{2}\right)y_1^2 - \left(3+\alpha\frac{3}{2}\right)y_1 + (1+\beta^{-2}+\gamma)$$

for which conditions (3.67) have to be verified. As a result, we have

$$\nabla^2\tilde{p}(y_1) \geq 0 \quad (=) \quad \alpha < -3 \tag{3.71}$$

$$\Delta(\tilde{p}(y_1)) \leq 0 \quad (=) \quad \gamma \leq \frac{9/4\alpha^2+(11+2\beta^{-2})\alpha+(15+6\beta^{-2})}{-2(\alpha+3)} \tag{3.72}$$

Comparing (3.69) and (3.72) irrespective of β, we have

$$\frac{\alpha^2+(5+\beta^{-2})\alpha+(7+3\beta^{-2})}{-(\alpha+3)} \leq \frac{9/4\alpha^2+(11+2\beta^{-2})\alpha+(15+6\beta^{-2})}{-2(\alpha+3)}, \tag{3.73}$$

for $\alpha < -3$, by which one can conclude that γ has to be determined by (3.72). Noting that $-(\alpha+3) \geq 0$, condition (3.73) can be validated by being equivalent to

$$2\alpha^2+2(5+\beta^{-2})\alpha+2(7+3\beta^{-2}) \leq 9/4\alpha^2+(11+2\beta^{-2})\alpha+(15+6\beta^{-2})$$

The above inequality can then be recast as

$$-\frac{1}{4}\alpha^2-\alpha-1 \leq 0, \tag{3.74}$$

which can be trivially verified.

Now, let

$$u_{22}(y_1,y_2) = \beta^2\rho y_2 \tag{3.75}$$

where ρ is a constant. Given equation (3.21d) we have

$$\tilde{h}_2(y_1,y_2) = -y_2\left(\frac{3}{2}y_1^2+3y_1-1+\rho\right) \tag{3.76}$$

Accordingly, condition (3.15d) becomes

$$f(y_2)\tilde{h}_2(y_1,y_2) = -y_2^2\left(\frac{3}{2}y_1^2+3y_1-1+\rho\right) \leq 0 \tag{3.77}$$

for which it is required from the non-positivity of the discriminant of the second order polynomial in parentheses that

$$\rho \geq \frac{5}{2} \tag{3.78}$$

Note that from (3.64) and (3.75), the control input attains the form

$$\begin{aligned} u_2(y_1,y_2) =& u_{21}(y_1,y_2)+u_{22}(y_1,y_2) \quad (=) \\ (=) \quad u_2(y_1,y_2) =& \beta^2\left[\alpha\left(\frac{1}{2}y_1^3+\frac{3}{2}y_1^2\right)-\gamma y_1+\rho y_2\right] \end{aligned} \tag{3.79}$$

Replacing y_1 and y_2 by (3.60) yields in

$$\begin{aligned} u_2(x_1,x_2) &= \beta^2\left[\alpha\left(\frac{1}{2}x_1^3+\frac{3}{2}x_1^2\right)-\gamma x_1-\rho\left(\dot{x}_1+x_1\right)\right] \\ &= \beta^2\left[\alpha\left(\frac{1}{2}x_1^3+\frac{3}{2}x_1^2\right)-\gamma x_1+\rho\left(\frac{3}{2}x_1^2+\frac{1}{2}x_1^3-x_1+x_2\right)\right] \end{aligned} \tag{3.80}$$

Rearranging results in the following nonlinear controller.

$$\boxed{u_2(x_1,x_2) = \beta^2(\alpha+\rho)(\frac{3}{2}x_1^2+\frac{1}{2}x_1^3)-\beta^2(\gamma+\rho)x_1-\beta^2\rho x_2} \tag{3.81}$$

where α, γ and ρ are constants to be determined by (3.68), (3.72) and (3.78), respectively. Note that according to (3.22), the Lyapunov function of the system (3.62) has the form

$$V(y_1,y_2) = y_1^2\left[\left(-\frac{3}{8}-\alpha\frac{1}{8}\right)y_1^2+\left(-1-\alpha\frac{1}{2}\right)y_1+\frac{1}{2}(1+\beta^{-2}+\gamma)\right]+y_2^2, \tag{3.82}$$

which using (3.60), can be transformed into the (x_1,x_2) coordinates as

$$\begin{aligned} V(x_1,x_2) =& x_1^2\left[\left(-\frac{3}{8}-\alpha\frac{1}{8}\right)x_1^2+\left(-1-\alpha\frac{1}{2}\right)x_1+\frac{1}{2}(1+\beta^{-2}+\gamma)\right] \\ &+\left[\frac{3}{2}x_1^2+\frac{1}{2}x_1^3-x_1+x_2\right]^2. \end{aligned} \tag{3.83}$$

Moreover, the values of α, γ and ρ are determined in such a way that

$$\{y \mid \dot{V}(y_1, y_2) = 0\} = \{(0,0)\}.$$

In other words the origin is the only equilibrium point of system (3.62). The Lyapunov function obtained in this example is a polynomial that is continuously differentiable and radially unbounded. Furthermore, the coefficients α, γ and ρ are such that $V > 0$. Satisfying the assumptions of Theorem 3.3.1, system (3.62), and thus system (3.24) are guaranteed to be globally asymptotically stable to the origin.

Note that inequalities (3.68), (3.72) and (3.78) give a very wide margin for choosing α, γ and ρ. In practice, they can be chosen such that stability is preserved under small changes in $\bar{\beta}$. To show this, the control law of the form of equation (3.79) is given here again

$$u_2(y_1, y_2) = \beta^2(\alpha(\frac{1}{2}y_1^3 + \frac{3}{2}y_1^2) - \gamma y_1 + \rho y_2) \tag{3.84}$$

Let $\tilde{\alpha}$, $\tilde{\gamma}$ and $\tilde{\rho}$ be the parameters which yields the system to remain stable. Now, consider the above controller in the following form as

$$u_{rob}(y_1, y_2) = (\beta^2\tilde{\alpha})(\frac{1}{2}y_1^3 + \frac{3}{2}y_1^2) - (\beta^2\tilde{\gamma})y_1 + (\beta^2\tilde{\rho})y_2 \tag{3.85}$$

In order to maintain the disturbed closed-loop system robust using u_{rob}, the following conditions are required

$$\beta^2\tilde{\alpha} = \bar{\beta}^2\alpha, \tag{3.86a}$$

$$\beta^2\tilde{\gamma} = \bar{\beta}^2\gamma, \tag{3.86b}$$

$$\beta^2\tilde{\rho} = \bar{\beta}^2\rho, \tag{3.86c}$$

Conditions (3.86) yield

$$\tilde{\alpha} = \left(\frac{\bar{\beta}}{\beta}\right)^2 \alpha, \tag{3.87a}$$

$$\tilde{\gamma} = \left(\frac{\bar{\beta}}{\beta}\right)^2 \gamma, \tag{3.87b}$$

$$\tilde{\rho} = \left(\frac{\bar{\beta}}{\beta}\right)^2 \rho, \tag{3.87c}$$

which implies that for $[\bar{\beta}/\beta - 1] \times 100$ percentage disturbance in $\bar{\beta}$, the marginal conditions for coefficients $\tilde{\alpha}$, $\tilde{\gamma}$ and $\tilde{\rho}$ must be subject to the shift of $[(\bar{\beta}/\beta)^2 - 1] \times 100$ percent. Therefore, if $\tilde{\alpha}$, $\tilde{\gamma}$ and $\tilde{\rho}$ are chosen according to (3.87) and α, γ, and ρ by the inequalities (3.68), (3.72) and (3.78), the system is guaranteed to be stable. For instance, let $\bar{\beta}$ is found out to change by $\pm 8\%$ maximum in some experiments. By conditions (3.87), $\tilde{\alpha}$, $\tilde{\gamma}$ and $\tilde{\rho}$ we have

	For $+8\%$ variation in $\bar{\beta}$	For -8% variation in $\bar{\beta}$
$\tilde{\alpha} =$	1.1664α	0.8464α
$\tilde{\gamma} =$	1.1664γ	0.8464γ
$\tilde{\rho} =$	1.1664ρ	0.8464ρ

Combining conditions (3.68), (3.72) and (3.78) to the above criteria one reaches the new set of conditions $\tilde{\alpha} < -3.50$, $\tilde{\gamma} > 1.664 \times \frac{9/4\alpha^2 + (11+2\beta^{-2})\alpha + (15+6\beta^{-2})}{-2(\alpha+3)}$, and $\rho > 2.92$ that guarantees the stability of the Moore-Greitzer surge system (3.24) for a maximum disturbance of $\pm 8\%$ in $\bar{\beta}$.

Furthermore, note that the only parameter among these, where the condition for which depends on β is γ. The allowable values for γ, as a function of α and β are studied with respect to the changes in $\bar{\beta}$. For this purpose Figure 3.1 shows the plot of γ by using the inequality (3.72). It can be seen that having the selected α, the parameter γ can be chosen from the epigraph of the plotted curve. This epigraph, providing a large area, allows the designer to pick up a safe enough value for γ such that the variation of $\bar{\beta}$ from -10.0% to $+10.0\%$ does not violate the stability of the Moore-Greitzer model.

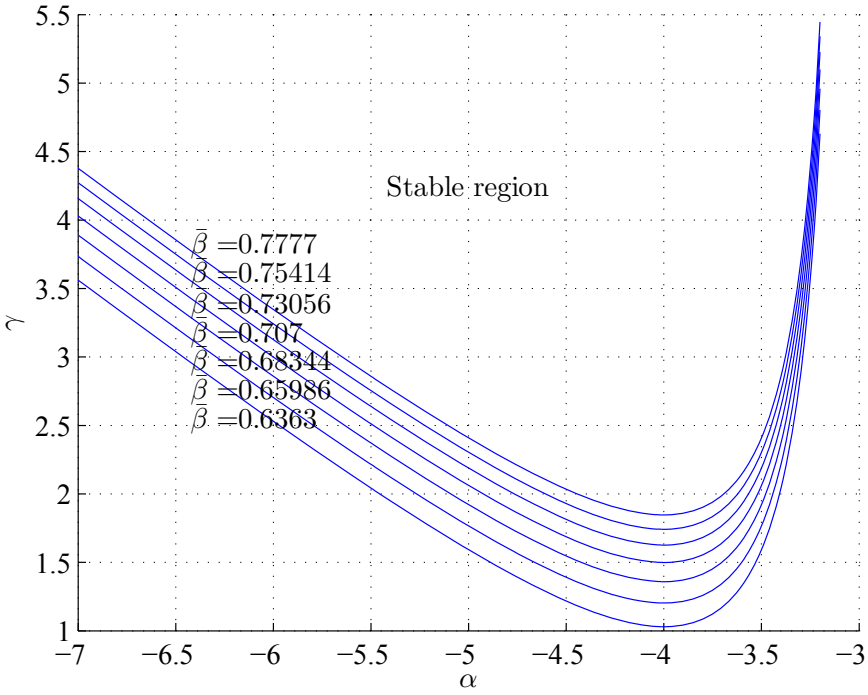

Figure 3.1: Plot of minimum allowable values for γ according to the inequality (3.72) with $\bar{\beta}$ being varied from $-10\%\beta$ to $+10\%\beta$.

Additionally, in the feedback linearization approach, the nonlinearities are canceled by the same term with an opposite sign to render a linear system for stability issues. Nevertheless, using pseudo Euler Lagrange technique, as done for the Moore-Greitzer model, the closed-loop system reaches stability by adding a portion of the nonlinear terms, which is determined by α, γ and ρ. This fact provides the system with a robust property that not necessarily any potential uncertainty in the model makes the system unstable.

3.6 Conclusions

In this chapter, a new Lyapunov-based control synthesis methodology was proposed based on previous work done by Rodrigues [25]. This method that is called pseudo Euler-Lagrange, suits a class of second order systems. The proposed technique was applied to

the stabilization problem of the no-stall Moore-Greitzer axial compressor model. In order to compare the stabilization properties of the proposed method, a feedback linearization and a backstepping controllers were designed. A summary of the controllers designed for the surge part of the Moore-Greitzer model as well as the proposed Lyapunov functions are outlined in Tables 3.1 and 3.2, respectively.

Nonlinear Method	**Control Law**
Input / Output Feedback Linearization	$u_2 = -\beta^2\left[\frac{3}{4}x_1^5+\frac{15}{4}x_1^4+\left(\frac{1}{2}k_1^f+\frac{9}{2}\right)x_1^3+\frac{3}{2}x_1^2x_2 + \frac{3}{2}k_1^f x_1^2+3x_1x_2-\left(\frac{1}{\beta^2}+k_2^f\right)x_1+k_1^f x_2\right]$
Backstepping	$u_2 = (1-\beta^2)x_1+\beta^2\gamma_b x_2+\beta^2\frac{9\gamma_b}{8\alpha_b}(x_2-\gamma_b x_1)$
Pseudo Euler-Lagrange	$u_2 = \beta^2(\alpha+\rho)(\frac{3}{2}x_1^2+\frac{1}{2}x_1^3)-\beta^2(\gamma+\rho)x_1-\beta^2\rho x_2$

Table 3.1: Summary of the controllers for the MG model.

Nonlinear Method	**Lyapunov Function**
Input / Output Feedback Linearization	Lyapunov theory is not used.
Backstepping	$V = \frac{1}{2}x_1^2+\frac{\gamma_b}{8}x_1^4+\frac{1}{2}(x_2-\gamma_b x_1)^2$
Pseudo Euler-Lagrange	$V = x_1^2\left[\left(-\frac{3}{8}-\alpha\frac{1}{8}\right)x_1^2+\left(-1-\alpha\frac{1}{2}\right)x_1+\frac{1}{2}(1+\beta^{-2}+\gamma)\right] + \left[\frac{3}{2}x_1^2+\frac{1}{2}x_1^3-x_1+x_2\right]^2$

Table 3.2: Summary of the Lyapunov functions for the closed-loop MG model.

As discussed earlier, the main advantages of the pseudo Euler-Lagrange for the suppression of the Moore-Greitzer model oscillation are found to be the following:

- The pseudo Euler-Lagrange technique provides the designed controller with a broad margin for choosing the control law coefficients such that the stability of the system

is guaranteed for a range of disturbances.

- During the design procedure, nonlinearities that may enhance the stability quality of the system are not canceled out as is done in the feedback linearization procedure.

Since there may be uncertainty in the model as well as potential variations of the coefficients, these advantages help one to have a safe margin of stability. Future suggested work in this area may include the extension of the pseudo Euler-Lagrange technique to higher order systems.

Chapter 4

Intersection-based Piecewise Affine Approximation of Functions of n-Variables

4.1 Introduction

This chapter proposes and develops the Intersection-based Piecewise Affine (IPWA) approximation method. The results will later be used in Chapter 5 to approximate the third order axial compressor stall and surge system equations. The PWA control synthesis tools, adapted from [28] can be applied to this model afterwards.

The chapter is organized as follows. Section 4.2 briefly reviews PWA systems. The approximation theory for functions of one variable is addressed in Section 4.3. Later, in Section 4.4, the proposed methodology is extended to functions of n-variables, with geometric results shown for functions of two variables The development of results in Section 4.3 for functions of one variable is necessary from two important points of view. First, it gives a good intuition for understanding the basis of the theory, since the domain of such functions is a subset of the real number coordinate axis. Second, the proofs of the

lemmas and theorems in Section 4.4 are based on induction, which inevitably requires the approximation theory for functions of one variable.

4.2 Review of PWA Systems

Consider the state space representation of a dynamical system as

$$\dot{x} = Ax + f_{nl}(x) + Bu \tag{4.1}$$

where $A \in \mathbb{R}^{n\times n}$, $x \in \mathbb{R}^n$ is the state vector, $B \in \mathbb{R}^{n\times \bar{n}}$, $u \in \mathbb{R}^{\bar{n}}$ is the control input, and f_{nl} is a nonlinear continuous function defined as $f_{nl} : \Omega \to \mathbb{R}^n$, where $\Omega \subset \mathbb{R}^n$. By computing a PWA approximation for (4.1), Ω is partitioned into a finite number of regions, in each of which an affine function serves as the approximation of f_{nl}. Let us denote $\mathscr{R}_i$ as the i^{th} PWA region, $i \in \mathscr{I} = \{1,2,...,N\}$ such that $\bigcup_{i=1}^{N} \overline{\mathscr{R}}_i = \Omega$. In what follows, the subsequent concepts will be used.

Definition 4.2.1. *A PWA system that has N regions is called N-modal. In particular, a bimodal system refers to a system with two regions.*

Remark 4.2.1. *Consequently, an N-modal PWA system has N pieces of affine functions.*

Definition 4.2.2. *The function $\bar{f} : \Omega \to \mathbb{R}^n$, where $\Omega \subset \mathbb{R}^n$, is defined to be the PWA approximation of the nonlinear function f_{nl}, and is given by*

$$\bar{f}(x) = A_i x + b_i, \quad x \in \mathscr{R}_i \tag{4.2}$$

where $i \in \mathscr{I} = \{1,2,...,N\}$ is the index indicating the region.

Note that by replacing $f_{nl}(x)$ in (4.1) by $\bar{f}(x)$ one obtains the PWA approximation of the nonlinear system (4.1) as

$$\dot{x} = (A + A_i)x + b_i + Bu, \quad x \in \mathscr{R}_i \tag{4.3}$$

Definition 4.2.3. *Intersection-based Piecewise Affine (IPWA) systems are a subset of PWA systems, that consist of the coefficients A_i and b_i being obtained by the methodology that is proposed in Sections 4.3 and 4.4.*

4.3 Approximation Theory For Functions of One-Variable

We begin this section by introducing the main idea of the approximation algorithm. The first stage of the IPWA approximation is performed by linearizing the nonlinear function around specific operating points which are given by the user. If, for instance, the task is to solve a PWA controller synthesis problem for the obtained IPWA system, these points can be chosen to be the equilibrium points of the nonlinear system. Therefore, the selection of such points varies depending on the nature of the problem. Each linearization will be called by tangent hyperplanes. The regions are created by projecting the intersection points of the hyperplanes onto the domain of the nonlinearity. In the next approximation stage, the function will be linearized at the intersection points that are obtained in the previous stage. This process is continued until the desired approximation error is met.

Definition 4.3.1. *Consider a nonlinear function $f : \Omega \to \mathbb{R}$, where $\Omega \subset \mathbb{R}^n$. A linearization hyperplane is denoted by H and is defined to be*

$$H = \{(x,y) \mid y = h(x)\}, \quad h(x) = h_i(x), \quad x \in \mathscr{R}_i, \tag{4.4}$$

where

$$h_i(x) = f(x_0^i) + \nabla f(x_0^i)(x - x_0^i), \tag{4.5}$$

and $x_0^i \in \mathscr{R}_i$, with $i = 1,2,\ldots,N$ are nominal points.

As given in equation (4.1), the nonlinear component of a dynamical system is described by $f_{nl}(x) = [f_1(x),\ f_2(x), ..., f_n(x)]^T$. If $f_{nl}(x)$ is a continuous function of only one variable, say x_j with j being a fixed number in $\{1,2,...,n\}$, satisfying the conditions given

subsequently in Theorem 4.3.2, the proposed IPWA algorithm for continuous functions can be used to construct the IPWA model. For this purpose $\bar{f}(x)$ is first obtained as in (4.2) for all $f_i(x_j)$, where $i = \{1,2,...,n\}$. This approximation will later be added to the linear components, as in equation (4.3). Therefore, the PWA regions produced during any linearization stage will take the form of

$$\mathscr{R}_i = \{x \in \mathbb{R} \mid d_i^s < x_j < d_{i+1}^s\}, \tag{4.6}$$

where

$$d^s = [q_1,\ x_{int}^{(1)},\ ...,x_{int}^{(k)},\ q_2], \tag{4.7}$$

where q_1 and q_2 are the domain boundaries, and $x_{int}^{(k)}$, as shown in Figure 4.1 is the projection of the intersection of the linearization hyperplanes $H_1, H_2, \ldots, H_{k+1}$ in a sequence onto Ω with k referring to the number of intersections.

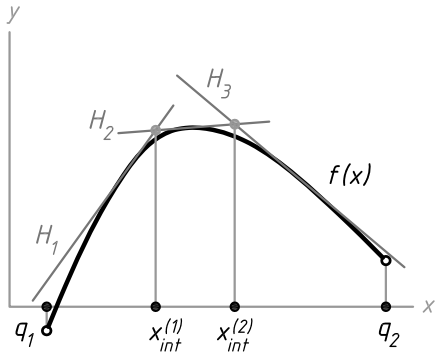

Figure 4.1: Representation of $x_{int}^{(1)}$, $x_{int}^{(2)}$, q_1, and q_2.

The regions of type (4.6) that can be defined with only one variable are called *slabs*. PWA systems with slab regions are thus called PWA slab systems [28]. Accordingly, as Rodrigues and Boyd [28] have shown, for PWA slab systems the state feedback controller synthesis with a quadratic Lyapunov function can be formulated as a convex optimization problem subject to an infinite set of LMIs. Although the solution to the synthesis problem

is not addressed in [28], the resulting approximation of the nonlinear system introduced can be used to design a PWA controller.

Henceforth, the Greek letter Γ is used as the domain of a function if $n = 1$ while Ω is generally used for $n > 1$. Moreover, in order to denote a point in Γ, two indices with the first index being always 1, are used as $x_{11}, x_{12}, \ldots \in \Gamma$ (instead of $x_1, x_2, \ldots$). This is done to avoid any potential confusion of a sequence of points in $\Gamma \subset \mathbb{R}$ with the components of the vector $x = [x_1, x_2, \ldots, x_n] \in \Omega$, where $\Omega \subset \mathbb{R}^n$.

The supporting hyperplane theorem, taken form [73], is presented here since it is used frequently in this section.

Theorem 4.3.1. *[73] Let D be a convex set and let $P \in \partial D$ be a point. Then there is a hyperplane containing P and containing D in one of its closed half spaces.*

The following proposition can be derived from the supporting hyperplane theorem, adapted form [73], Section 7.4.

Proposition 4.3.1. *Let $f : \Omega \to \mathbb{R}$ be a concave function, and $P \in \Omega$ be an arbitrary point. Suppose that $f \in \mathcal{C}^1$ in the neighborhood of P. Then*

$$f(x) \leq f(P) + \nabla f(P)(x - P) \tag{4.8}$$

for all $x \in \Omega$.

Note that given Γ as a set, the notation Γ° is used to denote the interior set of Γ.

Lemma 4.3.1. *Consider a concave function $f : \Gamma \to \mathbb{R}$, $\Gamma \subset \mathbb{R}$. Suppose that f is class $\mathcal{C}^1$ in a neighborhood of two distinct points x_{11}, x_{12} with $x_{11} < x_{12} \subset \Gamma^\circ$. Then*

$$f'(x_{12}) \leq f'(x_{11}). \tag{4.9}$$

Proof. Given two points x_{11} and x_{12}, let $x_b \in \Gamma^\circ$ be an arbitrary point. Note that f as a concave function is absolutely continuous in $\Upsilon = [x_b - \varepsilon, x_b + \varepsilon] \subset \Gamma$, for $\varepsilon > 0$ sufficiently small [74]. Using this property, $f'(x)$ exists almost in Υ. Therefore, if $f'(x_b)$ does not exist,

one concludes $f'(x_b-\varepsilon)$ and $f'(x_b+\varepsilon)$ exist, or simply $\exists\{f'(x_b^-), f'(x_b^+)\}$. Consequently, for $x_b^- < x_b$ a tangent hyperplane $\bar{h}(x)$ can be constructed as

$$\bar{h}(x) = f(x_b^-) + f'(x_b^-)(x - x_b^-) \tag{4.10}$$

Using the continuity of f, we have

$$\lim_{\varepsilon\to 0} x_b^- = \lim_{\varepsilon\to 0} x_b - \varepsilon = x_b,$$
$$\lim_{\varepsilon\to 0} f(x_b^-) = \lim_{\varepsilon\to 0} f(x_b - \varepsilon) = f(x_b).$$

There is no assumption on the existence of $f'(x_b)$. Noting that $\varepsilon > 0$ is sufficiently small, one may write

$$\lim_{\varepsilon\to 0} f'(x_b^-) \approx f'(x_b^-).$$

Therefore, taking the limit from equation (4.10) one may write

$$\bar{h}(x)\big|_{\varepsilon\to 0} = f(x_b) + f'(x_b^-)(x - x_b). \tag{4.11}$$

The function $f(x)$ can be approximated at $x_b^+ > x_b$ using the Taylor series as

$$f(x)|_{x_b^+} \approx f(x_b^+) + f'(x_b^+)(x - x_b^+) \tag{4.12}$$

Since f is continuous, we have

$$\lim_{\varepsilon\to 0} x_b^+ = \lim_{\varepsilon\to 0} (x_b + \varepsilon) = x_b,$$
$$\lim_{\varepsilon\to 0} f(x_b^+) = \lim_{\varepsilon\to 0} f(x_b + \varepsilon) = f(x_b).$$

Let us assume f may not be differentiable at x_b. With sufficiently small $\varepsilon > 0$, we have

$$\lim_{\varepsilon\to 0} f'(x_b^+) \approx f'(x_b^+).$$

Taking the limit from both sides of (4.12), we have

$$f(x)|_{x_b^+} \approx f(x_b) + f'(x_b^+)(x - x_b). \tag{4.13}$$

Note that the function f is concave, and by Proposition 4.3.1 we have

$$f(x) \leq \bar{h}(x), \quad \forall x \in \Gamma. \tag{4.14}$$

Let $x = x_b + \delta$, where $\delta > 0$ is an infinitesimally small number. Using (4.13) to approximate $f(x_b + \delta)$ and (4.11) to evaluate $\bar{h}(x_b + \delta)$, the inequality (4.14) becomes

$$f(x_b) + f'(x_b^+)(x_b + \delta - x_b) \leq$$
$$f(x_b) + f'(x_b^-)(x_b + \delta - x_b)$$

Simplifying the left and the right hand side terms yields

$$f'(x_b^+) \leq f'(x_b^-) \tag{4.15}$$

so that inequality (4.15) in a sequence including f' implies that (4.9) is held, no matter if f is differentiable at x_b or not. □

Remark 4.3.1. *A lemma with a similar result to Lemma 4.3.1 is provided in [74] (Chapter 5, Section 5, Lemma 15).*

Lemma 4.3.2. *Consider a concave function $f : \Gamma \to \mathbb{R}$, $\Gamma \subset \mathbb{R}$, and assume that f is class $\mathcal{C}^1$ in a neighborhood of x_{11}, x_{12} with $x_{11} < x_{12} \subset \Gamma^\circ$. Let the function f be linearized around x_{11} and x_{12} with lines $h_1(x)$ and $h_2(x)$, respectively. Assuming $h_1'(x) \neq h_2'(x)$, the intersection of $H_1 = \{(x,y) \mid y = h_1(x)\}$ and $H_2 = \{(x,y) \mid y = h_2(x)\}$ is a singleton, i.e,*

$$\{x_{int}\} = \{x \mid h_1(x) = h_2(x)\} \tag{4.16}$$

Furthermore, $x_{11} \leq x_{int} \leq x_{12}$.

Proof. From the assumption, since $\{x_{11}, x_{12}\} \subset \Gamma^\circ$ and since f is concave and locally of class $\mathcal{C}^1$ around x_{11} and x_{12}, we have $h_1'(x) = f'(x_{11}) \neq \infty$ and $h_2'(x) = f'(x_{12}) \neq \infty$. Moreover, $h_1'(x) \neq h_2'(x)$ implies that H_1 and H_2 are not parallel, and therefore they intersect with each other at some point equal to x_{int}. To prove that H_1 and H_2 intersect and x_{int} is the unique solution for the intersection of h_1 and h_2, one is required to show that $h_1(x) \neq h_2(x)$

for $x \neq x_{int}$. Note that $h_1(x)$ and $h_2(x)$ are determined by the linearization of f around x_{11} and x_{12}, as

$$h_1(x) = f(x_{11}) + f'(x_{11})(x - x_{11}), \tag{4.17a}$$

$$h_2(x) = f(x_{12}) + f'(x_{12})(x - x_{12}), \tag{4.17b}$$

Let us assume $h_1(x) = h_2(x)$ for $x \neq x_{int}$. This results in

$$x = \frac{[f(x_{11}) - f(x_{12})] + [f'(x_{12})x_{12} - f'(x_{11})x_{11}]}{f'(x_{12}) - f'(x_{11})} = x_{int}. \tag{4.18}$$

Since from the assumption of the lemma $h_1'(x) \neq h_2'(x)$, we therefore conclude that $f'(x_{11}) \neq f'(x_{12})$ as well as $x_{11} \neq x_{12}$. Therefore, equation (4.18) provides a unique value for x being $x = x_{int}$. Consequently, $h_1(x) = h_2(x)$ only for $x = x_{int}$ or in other words $h_1(x) \neq h_2(x)$ for $x \neq x_{int}$, which implies that x_{int} is a singleton.

By Proposition 4.3.1 we have

$$h_1(x) \geq f(x) \tag{4.19a}$$

$$h_2(x) \geq f(x) \tag{4.19b}$$

From this point, the proof of $x_{11} \leq x_{int} \leq x_{12}$ follows by contradiction. First, let $x_{12} < x_{int}$. Since H_1 and H_2 intersect with each other, we have

$$h_1(x_{int}) = h_2(x_{int})$$

Using (4.17), this implies that

$$f(x_{12}) + f'(x_{12})(x_{int} - x_{12}) = f(x_{11}) + f'(x_{11})(x_{int} - x_{11})$$

This in turn implies that

$$f(x_{12}) - f(x_{11}) - f'(x_{12})x_{12} + f'(x_{11})x_{11} = -x_{int}(f'(x_{12}) - f'(x_{11})) \tag{4.20}$$

On the other hand

$$\begin{aligned} h_2(x) - h_1(x) =& f(x_{12}) + f'(x_{12})(x - x_{12}) - f(x_{11}) - f'(x_{11})(x - x_{11}) \\ =& \left[f(x_{12}) - f(x_{11}) - f'(x_{12})x_{12} + f'(x_{11})x_{11}\right] \\ &+ x(f'(x_{12}) - f'(x_{11})) \end{aligned} \tag{4.21}$$

Substituting (4.20) into (4.21) yields

$$\begin{aligned} h_2(x) - h_1(x) &= -x_{int}(f'(x_{12}) - f'(x_{11})) + x(f'(x_{12}) - f'(x_{11})) \\ &= (f'(x_{12}) - f'(x_{11}))(x - x_{int}) \end{aligned} \tag{4.22}$$

Finally, using (4.9) (the result of Lemma 4.3.1), it is concluded from (4.22) that

$$h_2(x) \geq h_1(x), \quad \forall x < x_{int} \tag{4.23}$$

It was assumed that $x_{12} < x_{int}$ which, by using (4.23), implies that

$$h_2(x_{12}) \geq h_1(x_{12}), \quad x_{12} < x_{int} \tag{4.24}$$

By substituting x_{12} into (4.17b) we have

$$h_2(x_{12}) = f(x_{12}) \tag{4.25}$$

Combining (4.24) and (4.25) results in the following condition

$$f(x_{12}) \geq h_1(x_{12}), \quad \forall x < x_{int}$$

by which equation (4.19a), and consequently Proposition 4.3.1 are violated, implying that $x_{int} \leq x_{12}$. Similarly, the same argument can be used to show that $x_{int} \geq x_{11}$, confirming that $x_{11} \leq x_{int} \leq x_{12}$. □

Definition 4.3.2. *The distance function $\Delta : \Omega \to \mathbb{R}$ is defined as*

$$\Delta(x) = \Delta_i(x), \;\; x \in \mathscr{R}_i, \;\; i \in \mathscr{I}, \tag{4.26}$$

where

$$\Delta_i(x) = \begin{cases} |h_i(x) - f(x)| & , \;\; h_i(x) < f(x), \\ h_i(x) - f(x) & , \;\; h_i(x) \geq f(x). \end{cases} \tag{4.27}$$

Lemma 4.3.3. *Let $f : \Gamma \to \mathbb{R}$, $\Gamma \subset \mathbb{R}$ be a class $\mathcal{C}^1$ concave function. Consider an arbitrary point $x_0 \in \Gamma$. Assume that the linearization of f around the point x_0 is described by a*

hyperplane H defined by equations (4.4) *and* (4.5)*. Then for any direction pointing from x_0, $\Delta(x)$ defined by* (4.26) *and* (4.27) *is monotonically increasing, i.e.*

$$\nabla\Delta(x)\cdot\mathbf{v}_{x_0}(x)\geq 0,\quad x\in\Gamma, \tag{4.28}$$

where

$$\mathbf{v}_{x_0}(x)=\frac{x-x_0}{|x-x_0|},\quad x\in\Gamma \tag{4.29}$$

is a unit vector.

Proof. Since f is concave, therefore $-f$ is convex. The function h is also convex, because it is affine. Since the convexity property is held under addition of convex functions [73], $\Delta(x)=h(x)-f(x)$ is convex.

Since h is the linearization of f at x_0 and f is concave, we have $h\geq f$, according to Proposition 4.3.1. This always results in $\Delta(x)\geq 0$ according to the definition in (4.26) and (4.27). In addition, since $f(x_0)=h(x_0)$, $\Delta(x_0)=0$, and we can conclude that

$$x_0=\arg\min_{x\in\Gamma}\Delta(x)$$

as a point of global minimum of $\Delta(x)$. Using the first order necessary condition for the minimum points [73], we have

$$\nabla\Delta(x_0)=0. \tag{4.30}$$

Furthermore, noting that $\Delta(x)$ is convex, Lemma 4.3.1 allows us to conclude that $\Delta'(x)$ is either increasing or remains stationary as x is increased. This, in view of (4.30), leads to the conclusion that

$$\begin{aligned}\nabla\Delta(x)\leq&0,\quad \forall x<x_0,\\ \nabla\Delta(x)\geq&0,\quad \forall x>x_0,\end{aligned}$$

which, by using the definition of $\mathbf{v}_{x_0}$ in (4.29), can be rewritten in a more compact form as

$$\nabla\Delta(x)\cdot\mathbf{v}_{x_0}(x)\geq 0,\quad x\in\Gamma.$$

□

Using the results of Lemma 4.3.3 and Lemma 4.3.2, Theorem 4.3.2 is given below to find the points of maximum error in Γ, defined as $e_{max} = \sup_{x\in\Gamma}\Delta(x)$. Before giving the theorem, the following definition is necessary.

Definition 4.3.3. *[75] The convex hull of the set of k points $P_1, P_2, \ldots, P_k \in \Omega$ is denoted by* $\text{conv}(P_1, P_2, \ldots, P_k)$ *and is defined as*

$$\text{conv}(P_1, P_2, \ldots, P_k) = \{x \in \Omega \mid x = \sum_{i=1}^{k} t_i P_i,\ t_i \geq 0,\ \sum_{i=1}^{k} t_i = 1\},$$

Theorem 4.3.2. *Consider a class C^1 concave function $f : \Gamma \to \mathbb{R}$, over a convex set $\Gamma \subset \mathbb{R}$. Let the function be linearized around two points $x_{11}, x_{12} \in \Gamma$, with equations $y = h_1(x)$ and $y = h_2(x)$, respectively. Furthermore, consider the point $P_{int} = (x_{int}, y_{int}) = \{(x,y) \mid y = h_1(x),\ y = h_2(x)\}$. The solution to the following maximization problem*

$$\arg\sup_{x\in\Gamma} \Delta(x) \tag{4.31}$$

lies either on x_{int} or at the boundary, with boundary $\partial\Gamma = \{q_1, q_2\}$.

Proof. It can be recognized by Lemma 4.3.2 that $x_{11} \leq x_{int} \leq x_{12}$. Furthermore $x_{11}, x_{12} \in \Gamma$, which implies that x_{int} divides Γ into two sub-domains, each of which contains one of $\{x_{11}, x_{12}\}$. Let us denote the sub-domain containing x_{11} by $\Gamma_{x_{11}}$ and the sub-domain containing x_{12} by $\Gamma_{x_{12}}$. In order to prove this theorem, Γ will be split into 4 different sub-domains, namely Γ_2, Γ_1, Γ_3 and Γ_4, as follows

$$\begin{aligned} \Gamma_2 &= \text{conv}(x_{11}, x_{int}), \quad \Gamma_1 = \Gamma_{x_{11}} \setminus \Gamma_2 \\ \Gamma_3 &= \text{conv}(x_{int}, x_{12}), \quad \Gamma_4 = \Gamma_{x_{12}} \setminus \Gamma_3 \end{aligned} \tag{4.32}$$

By condition of Lemma 4.3.3, the distance function $\Delta(x)$, from equations (4.26) and (4.27), can be represented as

$$\Delta(x) = \begin{cases} \Delta_1(x) = h_1(x) - f(x) & , \quad x \in \Gamma_{x_{11}} \\ \Delta_2(x) = h_2(x) - f(x) & , \quad x \in \Gamma_{x_{12}} \end{cases} \tag{4.33}$$

In view of the fact that $\mathbf{v}_{x_{11}}$ and $\mathbf{v}_{x_{12}}$, as shown in Figure 4.2, are determined by using

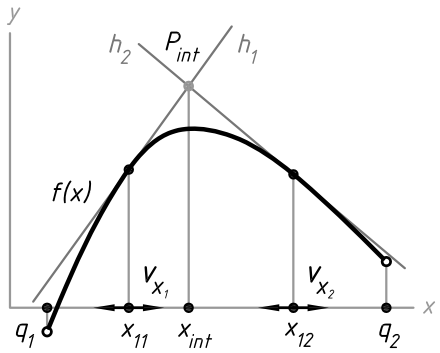

Figure 4.2: The intersection of H_1 and H_2 at P_{int}.

(4.29), as unit direction vectors at x_{11} and x_{12}, respectively, the following two cases are investigated.

CASE 1. $x \in \Gamma_2 \bigcup \Gamma_3$

CASE 2. $x \in \Gamma_1 \bigcup \Gamma_4$

CASE 1. First, we consider $x \in \Gamma_2$. Let $x_{\Gamma_2}(r) = x_{11} + \varepsilon r$, where $r \in \{r \in \mathbb{Z} > 0 \mid r < r_{max^2}\}$ with r_{max^2} denoting a relatively large integer and $\varepsilon > 0$ is a small constant determined in Γ_2 as $\varepsilon = (x_{int} - x_{11})/r_{max^2}$. Using $\mathbf{v}_{x_{11}}$ as a function of x, we have $\nabla\Delta_1(x_{\Gamma_2}) \cdot \mathbf{v}_{x_{11}}(x_{\Gamma_2}) \geq 0$ by Lemma 4.3.3. Therefore, for sufficiently small ε, $\Delta_1(x_{11}) \leq \Delta_1(x_{11} + \varepsilon)$, which is equivalent to $\Delta_1(x_{\Gamma_2}(0)) \leq \Delta_1(x_{\Gamma_2}(1))$. Similarly, we have $\Delta_1(x_{\Gamma_2}(1)) \leq \Delta_1(x_{\Gamma_2}(2))$, which using a sequence including $0 \leq r \leq r_{max^2}$ will reach the conclusion that $\Delta_1(x_{\Gamma_2}(r)) \leq \Delta_1(x_{\Gamma_2}(r_{max^2}))$. In other words we have

$$\Delta_1(x) \leq \Delta_1(x_{int}), \quad \forall x \in \Gamma_1. \tag{4.34}$$

Using the same reasoning, when we consider $x \in \Gamma_3$, let us define $x_{\Gamma_3}(r) = x_{12} - \varepsilon r$, where $r \in \{r \in \mathbb{Z} > 0 \mid r < r_{max^3}\}$ with r_{max^3} being a large integer, and ε is obtained in Γ_3 as $\varepsilon = (x_{12} - x_{int})/r_{max^3}$. Along the same lines, one can conclude that

$$\Delta_2(x) \leq \Delta_2(x_{int}), \quad \forall x \in \Gamma_2. \tag{4.35}$$

CASE 2. In the second place, let $x \in \Gamma_1$. using Lemma 4.3.3 we have $\nabla\Delta_1(x) \cdot \mathbf{v}_{x_{11}}(x_{\Gamma_1}) \geq 0$. Considering $x_{\Gamma_1}(r) = x_{11} - \varepsilon r$, where $r \in \{r \in \mathbb{Z} > 0 \mid r < r_{max^1}\}$ with r_{max^1} being a large integer and ε is determined in Γ_1 as $\varepsilon = (x_{11} - q_1)/r_{max^1}$, we may write $\Delta_1(x_{\Gamma_1}(0)) \leq \Delta_1(x_{\Gamma_1}(1))$. Note that $q_1, q_2 \in \partial\Gamma$ as stated in the theorem. Using a sequence, similar to the argument in Case 1, we have

$$\Delta_1(x) \leq \Delta_1(q_1), \quad \forall x \in \Gamma_3. \tag{4.36}$$

For $x \in \Gamma_4$, one can easily use the same reasoning to check that

$$\Delta_2(x) \leq \Delta_2(q_2), \quad \forall x \in \Gamma_4. \tag{4.37}$$

Equations (4.34), (4.35), (4.36) and (4.37) guarantee that an element from the set $\{x_{int}, q_1, q_2\}$ is indeed a solution to (4.31). This completes the proof of the theorem. □

The objective of the approximation algorithm at each stage is to linearize the function at points of maximum error occurring during the previous linearization. Theorem 4.3.2 ensures that after the first stage of approximation, the solution to (4.31) lies either at x_{int}, or q_1, or q_2. If the first two linearization hyperplanes H_1 and H_2 are based on the linearization of f at some points in the domain very close to q_1 and q_2 such that $\Delta(q_1) \leq e_{des}$ and $\Delta(q_2) \leq e_{des}$, the solution to (4.31) will be x_{int}, referring to Theorem 4.3.2. Therefore, x_{int} is the next point at which f should be linearized (see the upper plot in Figure 4.3). Denoting the linearization hyperplane around x_{int} by H_3, the second approximation stage starts as the point x_{int} adopts a new notation x_{13} (see the lower plot in Figure 4.3). Updating the distance function $\Delta(x)$ using (4.26), the problem of approximating f is to find

$$1) \ \arg\sup_{x_{11} \leq x \leq x_{13}} \Delta(x) \tag{4.38}$$

$$2) \ \arg\sup_{x_{13} \leq x \leq x_{12}} \Delta(x), \tag{4.39}$$

which are the new points of maximum error. Since f is concave within $x_{11} \leq x \leq x_{13}$ and $x_{13} \leq x \leq x_{12}$, Theorem 4.3.2 is then used to find the solution to (4.38) and (4.39). This process is continued as long as $\sup_{x\in\Gamma} \Delta(x) > e_{des}$.

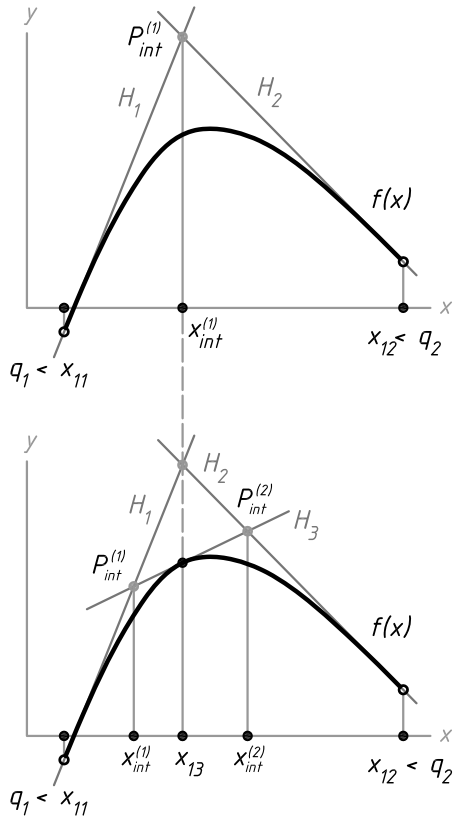

Figure 4.3: The upper plot shows the first stage of the approximation while the lower plot provides the second stage. Note that the superscripts reset at each stage.

With all the theoretical background that has been provided in this subsection, the algorithms for the intersection-based PWA approximation can be described in the next subsection. The flow diagram of the lemmas and the theorems that result in this algorithm is illustrated in Figure 4.4

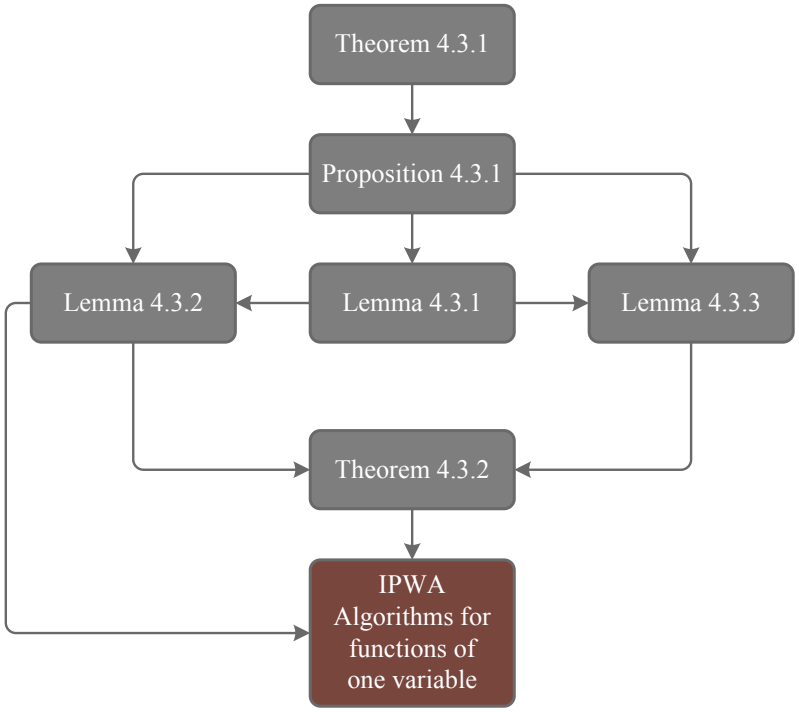

Figure 4.4: The flow of the theory for the proposed algorithms in Subsection 4.3.1 for functions of one variable.

4.3.1 The IPWA Algorithms

In this subsection, the algorithms implementing the intersection-based PWA (IPWA) approximation for both concave/convex and continuous functions are introduced.

Concave/Convex Functions

This algorithm is proposed for a concave function. If f is convex, $-f$ is then considered.

Problem 4.3.1. *Consider a concave function* $f : \Gamma \to \mathbb{R}$*, where* $\Gamma \subset \mathbb{R}$*. Find* $\bar{f}$ *over the domain of* f*.*

Algorithm 4.3.1.

1. The primary linearization points are determined first. The points are chosen to coincide with the points for which the user needs zero error. As mentioned above,

the primary linearization points are selected in accordance with the nature of the problem for which the IPWA is being obtained.

2. Using Taylor series, the function f is linearized around all the points that are obtained in step 1. The linearization hyperplanes and the functions representing them are denoted by H_i and $h_i(x)$, respectively, where $i \in \mathscr{I} = \{1,2,...,N_u\}$ and N_u is the number of linearization points at the u^{th} iteration.

3. Each two neighboring hyperplanes H_i will intersect with each other, resulting in a point under consideration of Lemma 4.3.2. These points are designated by $P_{int}^{(k)}(x)$, where $k \in \mathscr{K} = \{1,2,...,N_u-1\}$. Note that since each two neighboring hyperplanes intersect with each other, the number of intersection points is always equal to $N_u - 1$.

4. The projection of all intersection points $P_{int}^{(k)}$ on Γ is denoted by $x_{int}^{(k)}$.

5. Using Theorem 4.3.2 the points at which the local maximum error occurs are determined. According to this theorem, these points belong to the set $M = \{x_{11}, x_{int}^{(1)}, ..., x_{int}^{(k)}, x_{12}\}$. The global maximum is then obtained by updating $\Delta(x)$ using (4.26), and then evaluating $\Delta(x)$ for all the elements of M. Comparing the results, the value at which the global maximum error occurs and the error itself are found as

$$x_{e_{max}} = \arg\max_{x \in M} \Delta(x)$$

$$e_{max} = \max_{x \in M} \Delta(x)$$

6. The stopping criterion is defined as

$$e_{max} \leq e_{des} \tag{4.40}$$

where e_{des} is called *desired error* and is defined to be the maximum allowable error determined by the user. If the stopping criterion is met, the IPWA approximation

is returned. Otherwise, the point of maximum error is given to Step 3 for the next linearization stage. This iteration is continued until the stopping criterion is satisfied.

Remark 4.3.2. *One can still add other initial points heuristically to Step 1, such as the points of zero curvature. This idea was originally suggested by Casselman and Rodrigues in reference [76], as the essential idea of the SLP method.*

Continuous Functions

In this subsection, the function f is considered to be only continuous but not necessarily concave. Despite the fact that such a function is rather difficult to tackle, in many applications the nonlinear function is neither concave nor convex. For this purpose, the IPWA algorithm for approximating continuous functions is given in this subsection. In this algorithm, the inflection points of $f(x)$ are first found. The curvature of f at these points attains zero and the convexity of f changes. The set of inflection points is denoted by $K = \{x_K^1, x_K^2, \cdots, x_K^q\}$. Therefore, the function f can be split into $q+1$ functions, as $f_1(x), f_2(x), \cdots, f_{q+1}(x)$, each being either convex or concave. For this purpose, the initial linearization points are chosen to be the elements of K. The equations expressing the initial linearization hyperplanes $h_K^1, h_K^2, \cdots, h_K^q$ are then constructed by using the Taylor series. Since each $f_i(x)$ possesses either the concavity/convexity property, the IPWA algorithm for concave/convex functions is therefore used to compute the IPWA approximation for each $f_i(x)$.

The details of this method are summarized in the following algorithm.

Problem 4.3.2. *Consider a continuous function $f : \Gamma \to \mathbb{R}$, where $\Gamma \subset \mathbb{R}$. Find $\bar{f}$.*

Algorithm 4.3.2.

1. In the initial linearization stage, select the points from both categories:

(a) the initial point, as chosen in Step 1, and

(b) elements of set K.

2. Repeat Steps 3 to 6 from the Algorithm 4.3.1 for f.

Remark 4.3.3. *The regions produced by both proposed Algorithms 4.3.1 and 4.3.2 are convex and have been defined in equation* (4.6).

In this section, the approximation methodology for functions of one variable has been studied. The next section, deals with the same problem for functions of n-variables.

4.4 Approximation Theory For Functions of n-Variables

In Lemma 4.3.2 an intersection property of concave functions was derived. Lemma 4.4.5 will extend the results of Lemma 4.3.2 to n dimensions, but before going further, the following results are essential.

Definition 4.4.1. *[75] A set D is convex if a segment d between any two points $V_1, V_2 \in D$, lies in D, i.e.*

$$d = \{V_1 + (V_2 - V_1)t, \;\; t \in [0,1]\} \in D. \tag{4.41}$$

Definition 4.4.2. *The hypograph of function $f : \Omega \to \mathbb{R}$ is denoted by $\mathcal{H}(f)$ and is defined as*

$$\mathcal{H}(f) = \{(x,y) \in \Omega \mid y \leq f(x)\}. \tag{4.42}$$

Definition 4.4.3. *The epigraph of f is denoted by $\mathcal{E}(f)$ and is defined as*

$$\mathcal{E}(f) = \{(x,y) \in \Omega \mid y \geq f(x)\}. \tag{4.43}$$

Lemma 4.4.1. *Let $f : \Omega \to \mathbb{R}$ be a concave function over a convex set $\Omega \subset \mathbb{R}^n$. The axes $\{x,y\}$ are defined such that $x \in \Omega$ and $y \in \mathbb{R}$ is the image of x under f. Assume that $H = \{(x,y) \mid y = h(x)\}$ is a hyperplane. Define the parameterized curve $c(t) = (x_c(t), y_c(t))$*

such that $\{(x_c(t), y_c(t))\} = \{(x,y) \mid y = h(x) = f(x)\}$*, where* $t \in \mathbb{R}$*. Then there always exists a unique convex set D such that* $\{(x_c(t), y_c(t)) \in \Omega\} \subseteq \partial D$*.*

Proof. A hyperplane defined in the space $\Omega \times \mathbb{R}$ is an affine manifold which is a convex set of points. Since $f(x)$ is concave, its hypograph $\mathcal{H}(f) = \{(x,y) \mid y \leq f(x)\}$ is then a convex set. Moreover, the intersection of two convex sets is a convex set. Therefore, $D = \{(x,y) \mid y = h(x)\} \cap \{(x,y) \mid y \leq f(x)\}$ is a convex set. Furthermore, we have $\{(x,y) \mid y = h(x) = f(x)\} \subseteq \{(x,y) \mid y = h(x)\} \cap \{(x,y) \mid y \leq f(x)\}$. Therefore, according to the definitions of $c(t)$ and D, we have $\{(x_c(t), y_c(t))\} \subseteq \partial D$. □

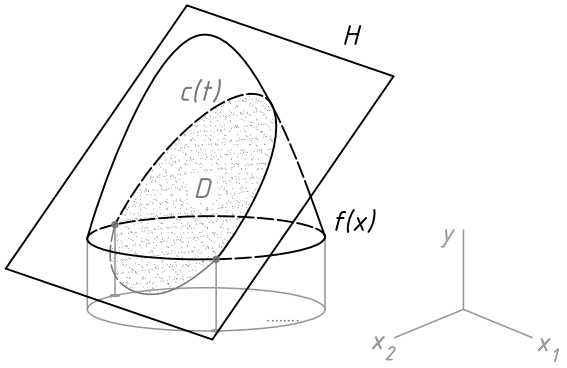

Figure 4.5: The intersection of H with $\{(x,y) \mid y = f(x)\}$ in three dimensional space.

For more clarification of the proof, see Figure 4.5 for the case $\Omega \subset \mathbb{R}^2$. Note that $c(t)$ is later produced by intersecting the graphs of f and h at a certain point as $(P_1, f(P_1))$, where $P_1 \in \Omega$, and therefore the existence of c is guaranteed.

Definition 4.4.4. *[77] An r-flat denoted by* $\mathcal{F}_r$ *is the set of points in the space* $\mathbb{R}^m$*, where* $r \leq m$*, and is defined as*

$$\mathcal{F}_r = \{\nu = \nu_0 + \sum_{i=1}^{r} t_i \theta_i, \;\; t_i \in \mathbb{R}\}, \tag{4.44}$$

where $\theta_1, \theta_2, \ldots, \theta_r$*, are r linearly independent vectors in* $\mathbb{R}^m$ *and* ν_0 *is a constant vector.*

Remark 4.4.1. *From Definition 4.4.4, the hyperplanes in* $\mathbb{R}^m$ *can be defined as* $\mathcal{F}_{m-1}$*. Furthermore, points, lines and planes are* $\mathcal{F}_0$*,* $\mathcal{F}_1$*, and* $\mathcal{F}_2$*, respectively.*

Definition 4.4.5. *Consider a hyperplane in the $\Omega \times \mathbb{R}$ space, where $\Omega \subset \mathbb{R}^n$. The coordinate system $(\hat{x},\hat{y})$, where $\hat{x} = [\hat{x}_1,\hat{x}_2,\ldots,\hat{x}_n]^T$ and $\hat{y} \in \mathbb{R}$ is defined such that axes $\{\hat{x}_1,\hat{x}_2,\ldots,\hat{x}_n\}$ lie in H and $\hat{y}$ is normal to H.*

Definition 4.4.6. *The operator $T : (x,y) \to (\hat{x},\hat{y})$ is defined to be the coordinate transformation between (x,y) and $(\hat{x},\hat{y})$.*

Note that the $(\hat{x},\hat{y})$ coordinate system is depicted in Figure 4.6 for the case of $n = 2$.

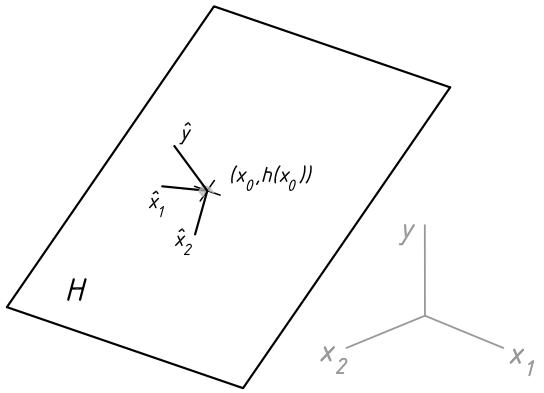

Figure 4.6: Hyperplane $H = \{(x,y) \mid y = h(x)\}$ and the coordinate system $(\hat{x},\hat{y})$ that is embedded in H such that $\{\hat{y}\} \perp H$. Note that $(x_0,h(x_0))$ is the origin of the coordinate system $(\hat{x},\hat{y})$.

Remark 4.4.2. *Coordinates $(\hat{x},\hat{y})$ can be obtained from (x,y) by $n+1$ consecutive rotations about $x_1,x_2,\ldots,x_n$ and y axes by angles $\phi^{(1)},\phi^{(2)},\ldots,\phi^{(n)}$ and ψ, respectively. The rotation matrix is computed as [78]*

$$\Lambda(\phi^{(1)},\phi^{(2)},\ldots,\phi^{(n)},\psi) = \Lambda_{\psi} \times \Lambda_{\phi^{(n)}} \times \Lambda_{\phi^{(n-1)}} \times \ldots \times \Lambda_{\phi^{(1)}}, \tag{4.45}$$

where $\Lambda_{(\cdot)}$ is the rotation matrix associated with each elementary rotation angles $\phi^{(1)}$, $\phi^{(2)},\ldots,\phi^{(n)}$ and ψ.

The system of coordinates $(\hat{x},\hat{y})$ lies on H and its origin is considered to be fixed at an arbitrary point $(x_0,h(x_0))$ (refer to Figure 4.6 for the case of $n = 2$). In view of this

fact and (4.45)*, the mapping function T from* (x,y) *to* $(\hat{x},\hat{y})$ *coordinates and its inverse are constructed as*

$$\begin{bmatrix} \hat{x}_1 \\ \hat{x}_2 \\ \vdots \\ \hat{x}_n \\ \hat{y} \end{bmatrix} = T\left(\begin{bmatrix} x_1 \\ x_2 \\ \vdots \\ x_n \\ y \end{bmatrix}\right) = \Lambda \begin{bmatrix} x_1 - x_{1_0} \\ x_2 - x_{2_0} \\ \vdots \\ x_n - x_{n_0} \\ y - h(x_0) \end{bmatrix}, \tag{4.46}$$

$$\begin{bmatrix} x_1 \\ x_2 \\ \vdots \\ x_n \\ y \end{bmatrix} = T^{-1}\left(\begin{bmatrix} \hat{x}_1 \\ \hat{x}_2 \\ \vdots \\ \hat{x}_n \\ \hat{y} \end{bmatrix}\right) = \Lambda^T \begin{bmatrix} \hat{x}_1 \\ \hat{x}_2 \\ \vdots \\ \hat{x}_n \\ \hat{y} \end{bmatrix} + \begin{bmatrix} x_{1_0} \\ x_{2_0} \\ \vdots \\ x_{n_0} \\ h(x_0) \end{bmatrix}. \tag{4.47}$$

In order to locate the axes $\{\hat{x}_1,\hat{x}_2,\ldots,\hat{x}_n\}$ *on H, n consecutive rotations about axes* $x_1, x_2^{\phi_0(1)},\ldots,x_n^{\phi_0(n-1)}$ *by given angles* $\phi^{(i)} = \phi_0^{(i)}$*, with* $i \in \{1,2,\ldots,n\}$ *are used. Note that* $x_2^{\phi_0(1)}$ *is the updated orientation of* x_2 *after the rotation about* x_1 *by* $\phi_0^{(1)}$ *is made, and for* $j \in \{2,3,\ldots,n\}$*,* $x_j^{\phi_0(j-1)}$ *is the updated orientation of* x_j *after the rotation about* $x_{j-1}^{\phi_0(j-2)}$ *is made. Accordingly,* $\bar{\Lambda}$ *is defined to be*

$$\bar{\Lambda} = \Lambda(\phi_0^{(1)}, \phi_0^{(2)}, \ldots, \phi_0^{(n)}, \psi). \tag{4.48}$$

The composed rotation that is based on the rotation matrix $\bar{\Lambda}$ *will automatically position the axis* $\hat{y}$ *normal to H.*

Remark 4.4.3. *The role of* ψ *in* (4.48) *is to rotate the axes* $(\hat{x}_1,\hat{x}_2,\ldots,\hat{x}_n)$ *in* $h(x)$ *about* $\hat{y}$ *while* $\hat{y}$ *is maintained normal to H. Once the values of* $\phi_0^{(i)}$ *are given,* $T : (x,y) \to (\hat{x},\hat{y})$ *is used as a function of* ψ*.*

Lemma 4.4.2. *Consider f, H and* $c(t)$ *from Lemma 4.4.1, and define* $x = [x_1,x_2,\ldots,x_n]^T$*. Assume the coordinate* $(\hat{x},\hat{y})$*, as considered in Definition 4.4.5, is located at an arbitrary*

point $(x_0, h(x_0))$*, where* $x_0 = [x_{1_0}, x_{2_0}, \ldots, x_{n_0}]^T$*. Then* $c(t)$ *can be implicitly represented by equation* $C(\hat{x}_1, \hat{x}_2, \ldots, \hat{x}_n) = 0$ *in* $(\hat{x}_1, \hat{x}_2, \ldots \hat{x}_n)$ *coordinates. Furthermore, if* $f \in \mathcal{C}^k$*, then* $\nabla^k C(\hat{x})$ *exists.*

Proof. Since $\{(x_c(t), y_c(t))\} \subset H$ and $(\hat{x}_1, \hat{x}_2, \ldots \hat{x}_n)$ coordinates are defined in H, $c(t)$ can be implicitly represented by an equation as $C(\hat{x}_1, \hat{x}_2, \ldots, \hat{x}_n) = 0$ in $(\hat{x}_1, \hat{x}_2, \ldots \hat{x}_n)$ coordinates. In order to determine $C(\hat{x})$, one needs to compute the equation $\hat{F}(\hat{x}, \hat{y}) = 0$ as the implicit representation of $f(x)$ in the $(\hat{x}, \hat{y})$ frame. Since $\{(x_c(t), y_c(t))\} = \{(x, y) \mid y = f(x)\} \cap \{(x, y) \mid y = h(x)\}$ and the fact that the origin of $(\hat{x}, \hat{y})$ coordinate system is located on H, we can conclude

$$C(\hat{x}) = \hat{F}(\hat{x}, 0). \tag{4.49}$$

For this purpose, Remark 4.4.2 and $\bar{\Lambda}$ defined in equation (4.48) are used. Substituting y with $f(x)$ in (4.46) and solving (4.46) for $\hat{y}$ gives

$$\hat{y} = \sum_{i=1}^{n} (x_i - x_{i_0}) \bar{\Lambda}_{n+1,i} + (f(x) - h(x_0)) \bar{\Lambda}_{n+1,n+1} \tag{4.50}$$

Using (4.47), x_i is expressed in terms of $\hat{x}_j$ and $\hat{y}$ as

$$x_i = \sum_{j=1}^{n} \hat{x}_j \bar{\Lambda}_{ji} + \hat{y} \bar{\Lambda}_{n+1,i} + x_{i_0}, \quad \forall i \in \{1, 2, \ldots, n\} \tag{4.51}$$

Replacing x_i by (4.51), f is equivalently denoted by

$$\begin{aligned} f(x) =& f(x_1(\hat{x}, \hat{y}), x_2(\hat{x}, \hat{y}), \ldots, x_n(\hat{x}, \hat{y})) \\ =& f\left(\sum_{j=1}^{n} \hat{x}_j \bar{\Lambda}_{j1} + \hat{y} \bar{\Lambda}_{n+1,1} + x_{1_0}, \ldots, \sum_{j=1}^{n} \hat{x}_j \bar{\Lambda}_{jn} + \hat{y} \bar{\Lambda}_{n+1,n} + x_{n_0} \right) \\ =& \hat{f}(\hat{x}, \hat{y}). \end{aligned} \tag{4.52}$$

Substituting x_i from (4.51) into (4.50) and using of the notation (4.52) results in

$$0 = \sum_{i=1}^{n} \left(\sum_{j=1}^{n} \hat{x}_j \bar{\Lambda}_{ji} + \hat{y} \bar{\Lambda}_{n+1,i} \right) \bar{\Lambda}_{n+1,i} - \hat{y} + \left(\hat{f}(\hat{x}, \hat{y}) - h(x_0) \right) \bar{\Lambda}_{n+1,n+1},$$

which is an implicit representation of function $f(x)$ in the $(\hat{x},\hat{y})$ coordinates. This implicit function is denoted by $\hat{F}(\hat{x},\hat{y})=0$, and is defined as

$$\begin{aligned}\hat{F}(\hat{x},\hat{y}) = &\sum_{i=1}^{n}\left(\sum_{j=1}^{n}\hat{x}_j\bar{\Lambda}_{ji}+\hat{y}\bar{\Lambda}_{n+1,i}\right)\bar{\Lambda}_{n+1,i}-\hat{y}\\ &+(\hat{f}(\hat{x},\hat{y})-h(x_0))\bar{\Lambda}_{n+1,n+1}.\end{aligned} \tag{4.53}$$

The mapping function $\hat{F}$ can be recast as

$$\hat{F}(\hat{x},\hat{y}) = \sum_{j=1}^{n}\eta_j\hat{x}_j+\eta_{n+1}\hat{y}+\eta_{n+2}\hat{f}(\hat{x},\hat{y})+\eta_{n+3}=0, \tag{4.54}$$

where

$$\begin{aligned}\eta_j &= \sum_{i=1}^{n}\bar{\Lambda}_{ji}\bar{\Lambda}_{n+1,i}, \quad \forall j\in\{1,2,\ldots,n\},\\ \eta_{n+1} &= \sum_{i=1}^{n}\bar{\Lambda}_{n+1,i}^2-1,\\ \eta_{n+2} &= \bar{\Lambda}_{n+1,n+1},\\ \eta_{n+3} &= -\bar{\Lambda}_{n+1,n+1}h(x_0).\end{aligned}$$

Letting $\hat{y}=0$ in the equation $\hat{F}(\hat{x},\hat{y})=0$, the equation $C(\hat{x})=0$, representing the intersection of the graph of f with H can be obtained as

$$\begin{aligned}C(\hat{x}) =&\hat{F}(\hat{x},0)\\ =&\sum_{j=1}^{n}\eta_j\hat{x}_j+\eta_{n+2}\hat{f}(\hat{x},0)+\eta_{n+3}=0,\end{aligned} \tag{4.55}$$

which indeed is the representation of $c(t)$ in the $(\hat{x},\hat{y})$ frame.

In order to investigate the differentiability property of $C(\hat{x})$, it is sufficient to examine the same property for $\hat{f}(\hat{x},0)$ since the rest of the components are linear and thus of class $\mathcal{C}^\infty$. Regarding (4.52) with $q\in\{1,2,\ldots,n\}$ we have

$$\frac{\partial\hat{f}}{\partial\hat{x}_q} = \sum_{p=1}^{n}\left.\frac{\partial f}{\partial x_p}\right|_{x=x(\hat{x},\hat{y})}\frac{\partial x_p}{\partial\hat{x}_q}. \tag{4.56}$$

Note that x_p is a linear function of $\hat{x}_q$, and thus the last term in (4.56) is constant. Taking the k^{th} derivative with respect to $\hat{x}_{q_i}$, where $q_i \in \{1,2,\ldots,n\}$ with $i \in \{1,2,\ldots,k\}$, yields

$$\frac{\partial^k \hat{f}}{\partial \hat{x}_{q_1} \partial \hat{x}_{q_2} \ldots \partial \hat{x}_{q_k}} = \sum_{p_1=1}^{n} \left[\sum_{p_2=1}^{n} \cdots \left[\sum_{p_k=1}^{n} \left[\frac{\partial^k f}{\partial x_{p_1} \partial x_{p_2} \ldots \partial x_{p_k}} \bigg|_{x=x(\hat{x},\hat{y})} \frac{\partial x_{p_k}}{\partial \hat{x}_{q_k}} \right] \cdots \frac{\partial x_{p_2}}{\partial \hat{x}_{q_2}} \right] \frac{\partial x_{p_1}}{\partial \hat{x}_{q_1}} \right]. \tag{4.57}$$

Since $f \in \mathcal{C}^k$ as well as x_i is a linear combination of $(\hat{x}_1, \hat{x}_2, \ldots, \hat{x}_n, \hat{y})$, one concludes that all components in the right hand side of (4.57) exist and thus $\nabla^k \hat{f}(\hat{x}, 0)$ exits. As remarked before, the existence of $\nabla^k \hat{f}(\hat{x}, 0)$ together with (4.55) implies the existence of $\nabla^k C(\hat{x})$. This completes the proof of this lemma. □

Corollary 4.4.1. *Based on the assumptions and the results of Lemma 4.4.1, if $H \perp \Omega$, then $c(t)$ can be represented as a concave function in the $(\hat{x}, \hat{y})$ coordinates.*

Proof. Consider the coordinate transformation T that maps (x, y) to $(\hat{x}, \hat{y})$, as defined in Definition 4.4.6. The transformation function T positions the axes $\{\hat{x}_1, \hat{x}_2, \ldots, \hat{x}_n\}$ in the n-dimensional space of the hyperplane H such that $\{\hat{y}\} \perp H$. Regarding Remark 4.4.3, T is a function of ψ, by which the axes $\{\hat{x}_1, \hat{x}_2, \ldots, \hat{x}_n\}$ can freely rotate about $\hat{y}$ axis. Since $H \perp \Omega$, with a proper choice of $\psi = \psi_0$, the orientation of the $\{\hat{x}, \hat{y}\}$ frame is adjusted such that $\{\hat{x}_n\} \parallel \{y\}$. This is schematically shown in Figure 4.7 for $n = 2$.

Let $\{c(t) = (x_c(t), y_c(t))\} = H \cap \{(x, y) \mid y = f(x)\}$, according to Lemma 4.4.1. As long as $H \perp \Omega$, and therefore $H \parallel \{y\}$, the set D defined as

$$D = \mathcal{H}(f) \cap H \tag{4.58}$$

can serve as the hypograph of c, i.e. $D = \mathcal{H}(c)$. Because $f(x)$ is concave, by Lemma 4.4.1, D is a convex set too. Furthermore, a function is concave if its hypograph is convex [73]. Therefore, the fact that $D = \mathcal{H}(c)$ is convex implies that $c(t)$ can be represented by a concave function. This function is defined by using the explicit representation of c by $C(\hat{x})$, as provided in Lemma 4.4.2. We thus can define $g : \Omega' \to \mathbb{R}$, where $\Omega' \subset \mathbb{R}^{n-1}$ is a

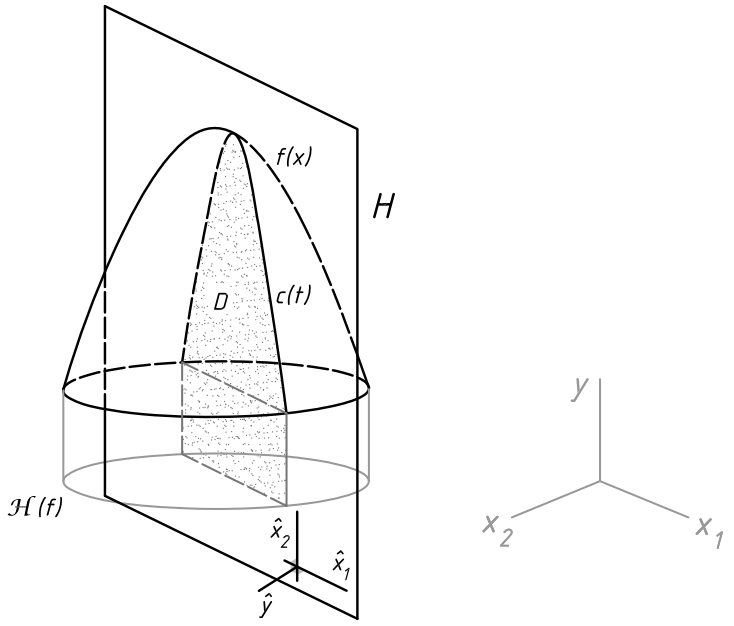

Figure 4.7: The hyperplane $H \perp \Omega$ is cutting the graph of f at c. The frame $\{\hat{x},\hat{y}\}$ is oriented on H such that $\{\hat{y}\} \perp \Omega$ and $\{\hat{x}_n\} \parallel \{y\}$, with $n = 2$. Note that $\mathcal{H}(f)$ denotes the hypograph of f.

concave function such that

$$\{\hat{x} \mid \hat{x}_n = g(\hat{x}_1, \hat{x}_2, \ldots, \hat{x}_{n-1})\} = \{\hat{x} \mid C(\hat{x}) = 0\}. \tag{4.59}$$

□

Corollary 4.4.2. *Under the assumptions and the results of Corollary 4.4.1, if $f : \Omega \to \mathbb{R}$ is a convex function, then $c(t)$ can be represented by a convex function in $(\hat{x},\hat{y})$ coordinates denoted by g as in equation* (4.59).

Proof. This can be trivially shown by using the fact that for f being convex, $-f$ is concave.

□

Lemma 4.4.3. *Let $f : \Omega \to \mathbb{R}$ be a concave function, where $\Omega \subset \mathbb{R}^n$ is a convex set. Suppose that $f \in \mathcal{C}^1$ in the neighborhood of arbitrary distinct points $P_i \in \Omega$, with $i = 1,2$. Let $H_{aux} = \{(x,y) \mid y = h_{aux}(x)\}$ represent a hyperplane passing through $(P_1, f(P_1))$ and $(P_2, f(P_2))$. Assume that h_1 and h_2 are linearizations of f at P_1 and P_2, respectively, and*

$h_1 - h_2$ is not identically zero everywhere. We now have $l_i = H_i \cap H_{aux}$, and by considering c from the result of Lemma 4.4.1, l_i is tangent to c at $(P_i, f(P_i))$, where $i = 1,2$.

Proof. In order to avoid potential confusion, let us define the dimension of the space, where the graph of f is embedded as $m = \dim\Omega + \dim f = n+1$. Per the assumption that H_{aux} is an arbitrary hyperplane passing through $(P_i, f(P_i))$, one has

$$(P_i, f(P_i)) \in \{(x,y) \mid y = h_{aux}(x)\} \cap \{(x,y) \mid y = h_i(x)\}. \tag{4.60}$$

Therefore $H_i \cap H_{aux}$ exists and is denoted by

$$l_i = \{(x,y) \mid y = h_i(x) = h_{aux}(x)\}, \tag{4.61}$$

Equations (4.60) and (4.61) imply that $(P_i, f(P_i))$ and l_i are a common point and a common flat $\mathcal{F}_{m-2}$, respectively for H_i and H_{aux}. Moreover $h_i - h_{aux}$ is not identically zero everywhere since $(P_1, f(P_1)) \notin H_2$ and $(P_2, f(P_2)) \notin H_1$ but $(P_i, f(P_i)) \in H_{aux}$, where $i = 1,2$. It is therefore understood that l_i passes through $(P_i, f(P_i))$. By Lemma 4.4.1, because f is a concave function, c as the boundary of the convex set $D = \{(x,y) \mid y = h_{aux}(x)\} \cap \{(x,y) \mid y \leq f(x)\}$ can be determined as

$$\{(x_c(t), y_c(t))\} = \{(x,y) \mid y = h_{aux}(x)\} \cap \{(x,y) \mid y = f(x)\}. \tag{4.62}$$

Considering the facts that $(P_i, f(P_i)) \in \{(x,y) \mid y = f(x)\}$ and $(P_i, f(P_i)) \in \{(x,y) \mid y = h_{aux}(x)\}$, where $i \in \{1,2\}$, one can say that $(P_i, f(P_i)) \in \{(x,y) \mid y = h_{aux}(x) \cap f(x)\}$. Therefore, per equation (4.62) it can be realized that

$$\{(P_1, f(P_1)), (P_2, f(P_2))\} \subset \{(x_c(t), y_c(t))\}. \tag{4.63}$$

Note that

1. $(P_1, f(P_1)) \in l_1$ and $(P_2, f(P_2)) \in l_2$,
2. equation (4.61) implies that $l_i \subset \{(x,y) \mid y = h_i(x)\},\ i = 1,2$,

3. H_1 and H_2 are tangent to f at $(P_1, f(P_1))$ and $(P_2, f(P_2))$, respectively,

so that one can conclude that l_1 and l_2 are tangent to f at $(P_1, f(P_1))$ and $(P_2, f(P_2))$, respectively. Furthermore, since

1. l_1 and l_2 are tangent to f at $(P_1, f(P_1))$ and $(P_2, f(P_2))$, respectively,

2. $l_i \subset \{(x,y) \mid y = h_{aux}(x)\},\ i = 1,2,$

3. equation (4.62) implies $\{(x_c(t), y_c(t))\} \subset \{(x,y) \mid y = h_{aux}(x)\}$,

4. given the relation (4.63),

5. c is contained in f,

one can then state that l_1 and l_2 are tangent to c at $(P_1, f(P_1))$ and $(P_2, f(P_2))$ respectively. See Figure 4.8 for the case of $\Omega \subset \mathbb{R}^2$. □

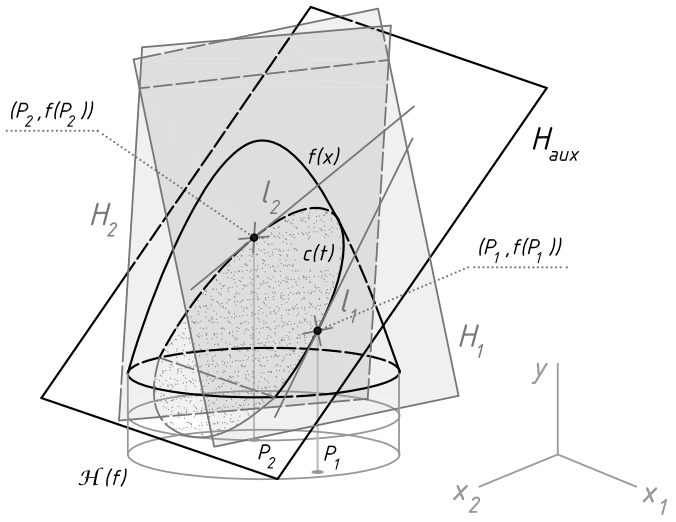

Figure 4.8: The tangent hyperplanes H_1 and H_2 to f at $(P_1, f(P_1))$ and $(P_2, f(P_2))$ are shown. The auxiliary hyperplane is positioned arbitrarily while holding the condition of Lemma 4.4.4.

Lemma 4.4.4. *Consider the function f, the points $\{P_1, P_2\}$ as well as the assumptions and the result of Lemma 4.4.3, there exits a hyperplane H_{aux} such that l_1 is not parallel to l_2.*

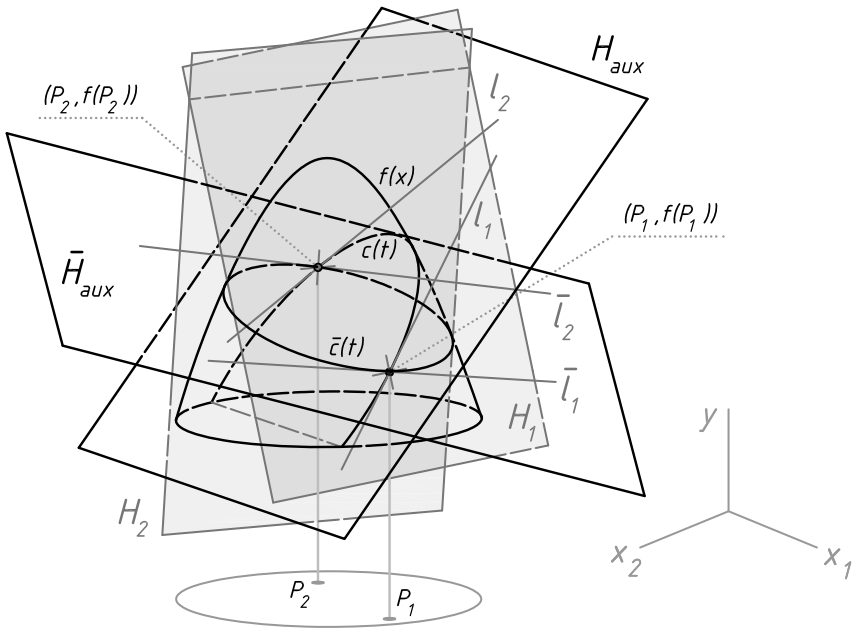

Figure 4.9: Hyperplanes H_1 and H_2, shown in grey, are tangent to f at $(P_1, f(P_1))$ and $(P_2, f(P_2))$. H_{aux} and $\bar{H}_{aux}$ are two distinct auxiliary hyperplanes both passing through $(P_1, f(P_1))$ and $(P_2, f(P_2))$. Note that $\{c(t) = (x_c(t), y_c(t))\} = \{(x,y) \mid y = h_{aux}(x)\} \cap \{(x,y) \mid y = f(x)\}$ and $\{\bar{c}(t) = (x_{\bar{c}}(t), y_{\bar{c}}(t))\} = \{(x,y) \mid y = \bar{h}_{aux}(x)\} \cap \{(x,y) \mid y = f(x)\}$. It is assumed that $\bar{l}_1 \parallel \bar{l}_2$.

Proof. Consider two arbitrary distinct auxiliary hyperplanes, as H_{aux} and $\bar{H}_{aux}$, both passing through $(P_i, f(P_i))$, with $i = 1,2$. These hyperplanes are shown in Figure 4.9 for $n = 2$. Hyperplanes H_{aux} and $\bar{H}_{aux}$, therefore cut the graph of f and H_i. The reason is that H_i is tangent to f at $(P_i, f(P_i))$, and H_{aux} and $\bar{H}_{aux}$ each pass through $(P_i, f(P_i))$. Let

$$l_i = H_{aux} \cap H_i, \tag{4.64a}$$

$$\bar{l}_i = \bar{H}_{aux} \cap H_i. \tag{4.64b}$$

Assume that $\bar{l}_1 \parallel \bar{l}_2$ and $l_1 \parallel l_2$. The following facts can then be concluded

1. Hyperplanes H_{aux} and $\bar{H}_{aux}$ are distinct and intersecting with each other at $(P_i, f(P_i))$, for $i = 1,2$, implying that $l_i \subset H_{aux}$ is not parallel to $\bar{l}_i \subset \bar{H}_{aux}$. This implies that l_i and $\bar{l}_i$ intersect with each other.

2. The equations in (4.64) imply that $l_i, \bar{l}_i \subset H_i$.

3. $l_1 \parallel l_2$ and $\bar{l}_1 \parallel \bar{l}_2$ are assumed to hold.

By Item 1, l_i and $\bar{l}_i$ intersect with each other. Therefore, a unique hyperplane can be passed through l_1 and $\bar{l}_1$, and a unique hyperplane can be passed through l_2 and $\bar{l}_2$. The combination of this result with the result of Item 2 shows that the unique hyperplane that can be represented by l_i and $\bar{l}_i$ is H_i, for $i = 1,2$. Note that $m = n+1$, and Item 3 on the other hand shows that l_1 and $\bar{l}_1$ that are in H_1 are respectively parallel to two l_2 and $\bar{l}_2$ that are in H_2. This yields the following result

$$H_1 \parallel H_2. \tag{4.65}$$

Since h_i is the linearization of f at P_i, we have $\nabla f(P_i) = \nabla h_i$, which together with (4.65) results in

$$\nabla f(P_1) = \nabla f(P_2). \tag{4.66}$$

Equation (4.66) with the assumption of $h_1 - h_2$ not being identically everywhere violates the fact that f is a concave function of class $\mathcal{C}^1$ in the neighborhood of P_1 and P_2. Hence, if there exists the hyperplane $\bar{H}_{aux}$ for which the assumption $\bar{l}_1 \parallel \bar{l}_2$ is held, then for any other hyperplane, such as the H_{aux} that passes through $(P_1, f(P_1))$ and $(P_2, f(P_2))$, we have l_1 not parallel to l_2. This completes the proof of the lemma. □

Lemma 4.4.5. *Consider a concave function $f : \Omega \to \mathbb{R}$, over a convex set $\Omega \subset \mathbb{R}^n$ with $x \in \Omega$ and $y \in \mathbb{R}$ as the image of f over Ω. Suppose f is of class $\mathcal{C}^1$ in a neighborhood of two distinct points $P_1, P_2 \in \Omega$. Let f be linearized at P_1 and P_2 with hyperplanes $H_1 = \{(x,y) \mid y = h_1(x)\}$ and $H_2 = \{(x,y) \mid y = h_2(x)\}$, respectively. Assume $\nabla f(P_1) \neq \nabla f(P_2)$, and the intersection of H_1 and H_2 is a singleton*

$$L_{int} = \{(x,y) \mid y = h_1(x), y = h_2(x)\} \tag{4.67}$$

and its projection onto Ω, denoted by $L_{pj} = \text{proj}_{\Omega} L_{int}$, lies between P_1 and P_2. In addition, L_{int} is a $\mathcal{F}_{m-2}$, where $m = n+1$.

Proof. Lemma 4.3.2 tackles the similar problem for f being a function of only one variable. Assume the result of Lemma 4.4.5 is true for a function of $(n-1)$-variables such as $g : \Omega' \to \mathbb{R}$, where $\Omega' \subset \mathbb{R}^{n-1}$, the proof is given using induction as follows.

The functions $h_1(x)$ and $h_2(x)$ representing the two hyperplanes are defined as

$$h_i(x) = f(P_i) + \nabla f(P_i)(x - P_i), \quad i \in \{1,2\}. \tag{4.68}$$

Since from the assumption $f \in \mathcal{C}^1$ for $x \in \{x \mid \|x - P_i\| < \varepsilon\}$, where ε is sufficiently small, and $\nabla f(P_1) \neq \nabla f(P_2)$, one concludes that

$$\nabla h_1(x) \neq \nabla h_2(x). \tag{4.69}$$

Therefore, H_1 in not parallel to H_2, implying that H_1 and H_2 intersect with each other. In order to determine $L_{int} = H_1 \cap H_2$, one must set $y = h_1(x)$ and $y = h_2(x)$, and solve the following set. Invoking the definition of h_1 and h_2 from equation (4.68) one may write

$$\mathcal{A}[x,\ y]^T = \mathcal{b} \tag{4.70}$$

where

$$\mathcal{A} = \begin{bmatrix} \nabla f(P_1) & -1 \\ \nabla f(P_2) & -1 \end{bmatrix}, \quad \mathcal{b} = \begin{bmatrix} \nabla f(P_1)P_1 - f(P_1) \\ \nabla f(P_2)P_2 - f(P_2) \end{bmatrix}, \tag{4.71}$$

and $\nabla f(P_i)$, with $i = 1,2$ is considered to be a row vector. Since $\nabla f(P_1) \neq \nabla f(P_2)$, according to the assumptions, the row vectors of matrix $\mathcal{A}$, i.e.

$$\mathcal{A}_1 = [\nabla f(P_1) \quad -1],$$
$$\mathcal{A}_2 = [\nabla f(P_2) \quad -1],$$

are linearly independent. Consider the following set of equations representing L_{int}

$$\sum_{i=1}^{n} \alpha_{ji} x_i + \alpha_{j,n+1} y + \alpha_{j0} = 0, \quad \forall j = \{1,2,\ldots,n+1\}, \tag{4.72}$$

where α_{j0} and α_{ji} are constants and $\alpha_{jj} = 0$. This together with the fact that $\mathcal{A}_1$ and $\mathcal{A}_2$ are linearly independent implies that the solution to equation (4.70) is unique [79], and therefore L_{int} is a singleton. Recall from the proof of Lemma 4.4.3, $m = \dim(\Omega) + \dim(y) =$

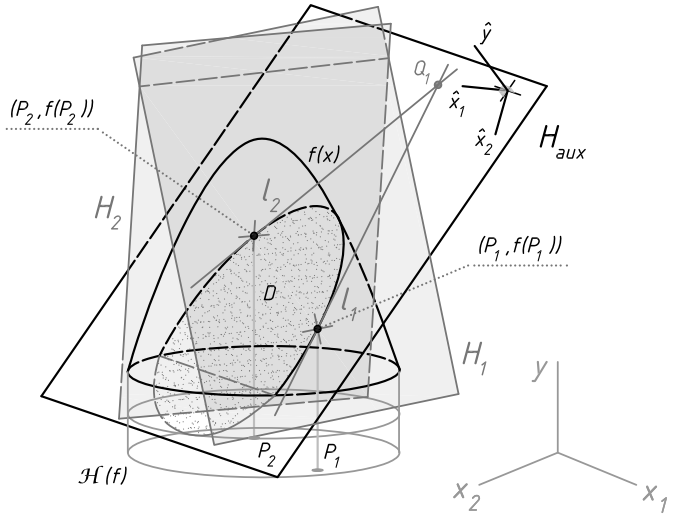

Figure 4.10: The tangent hyperplanes H_1 and H_2 to f at $(P_1, f(P_1))$ and $(P_2, f(P_2))$. The auxiliary hyperplane H_{aux} is positioned arbitrarily while the condition of Lemma 4.4.4 is satisfied.

$n+1$ is defined as the dimension of the space where the graph of $f(x)$ is embedded. Note that by Proposition 1-13 in [77], since H_1 and H_2 are two non-parallel $\mathcal{F}_{m-1}$, the intersection of H_1 and H_2 in $\mathbb{R}^m$, denoted by L_{int} and represented by equation (4.72), is a $\mathcal{F}_{m-2}$.

Although the existence of this intersection may seem to be trivial, the more important result of this lemma lies in the fact that L_{pj} is located between P_1 and P_2, i.e.

$$\exists M \in L_{pj} : \|P_1M\| + \|P_2M\| = \|P_1P_2\|, \tag{4.73}$$

where $M \in \Omega$ is a point, P_1M, P_2M and P_1P_2 are segments. First we address that H_1 and H_2 have two distinct common flats of dimension $(m-3)$ denoted by $\{Q_1, Q_2\} \in \Omega \times \mathbb{R}$, i.e.

$$Q_1 \neq Q_2 \tag{4.74a}$$

$$Q_1, Q_2 \subset \{(x,y) \mid y = h_1(x)\} \tag{4.74b}$$

$$Q_1, Q_2 \subset \{(x,y) \mid y = h_2(x)\} \tag{4.74c}$$

In order to find Q_1 and Q_2, two auxiliary hyperplanes H_{aux} and $\tilde{H}_{aux}$, are used. The hyperplane H_{aux} is produced by passing an arbitrary $\mathcal{F}_{m-1}$ through the two points

$(P_1, f(P_1))$ and $(P_2, f(P_2))$. Note that H_{aux} should not be perpendicular to Ω. This is schematically shown in Figure 4.10 for $m = 3$, as the highest tangible space.

Since the conditions of Lemma 4.4.3 are satisfied, we have

$$l_i = H_i \cap H_{aux}. \tag{4.75}$$

such that l_i is tangent to c at $(P_i, f(P_i))$. According to Lemma 4.4.4, the arbitrary hyperplane H_{aux} can be chosen such that l_1 is not parallel to l_2. According to Proposition 1-13 [77], since H_{aux} and l_i are not parallel in $\mathbb{R}^m$, l_i is an $\mathcal{F}_{m-2}$. Moreover, by the same proposition l_1 and l_2 are two non-parallel $\mathcal{F}_{m-2}$ in H, and we have Q_1, which is defined as

$$Q_1 = l_1 \cap l_2, \tag{4.76}$$

and represents an $\mathcal{F}_{m-3}$.

In the next step, the auxiliary hyperplane $\tilde{H}_{aux}$ is constructed by using the points $(P_1, f(P_1))$ and $(P_2, f(P_2))$, not arbitrarily but such that $\tilde{H}_{aux} \perp \Omega$ (refer to Figure 4.11 for $n = 2$). By choosing the right angle, we have

$$\{P_1, P_2\} \subset \{x \mid \tilde{H}_{aux} \cap \Omega\}. \tag{4.77}$$

The hyperplane $\tilde{H}_{aux}$ intersects with f at $\tilde{c}$, satisfying the conditions of Corollary 4.4.1. Therefore, $\tilde{c}$ can be represented by a concave function, as $g : \Omega' \to \mathbb{R}$, where $\Omega' \subset \mathbb{R}^{n-1}$ defined as

$$\hat{x}_n = g(\hat{x}_1, \hat{x}_2, \ldots, \hat{x}_{n-1}). \tag{4.78}$$

Note that H_1 and H_2 are tangent to f at $(P_1, f(P_1))$ and $(P_2, f(P_2))$. The two flats of dimension $(m-2)$ as $\tilde{l}_1$ and $\tilde{l}_2$ are therefore determined to be

$$\tilde{l}_i = H_i \cap \tilde{H}_{aux}. \tag{4.79}$$

By Lemma 4.4.3 and the fact that the function g is a representation for $\tilde{c}$, we have $\tilde{l}_1$ and $\tilde{l}_2$ tangent to g at $(P_1, f(P_1))$ and $(P_2, f(P_2))$. As stated in the beginning of the proof, we assumed that the results of this lemma are true for a function of $n-1$-variables. Note

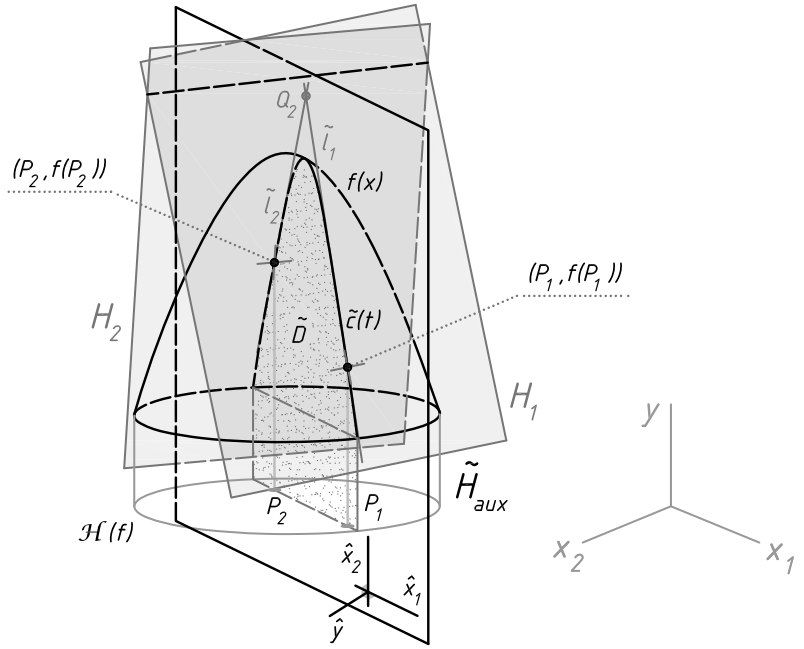

Figure 4.11: The tangent hyperplanes H_1 and H_2 to f at $(P_1, f(P_1))$ and $(P_2, f(P_2))$. The auxiliary hyperplane $\tilde{H}_{aux} \perp \Omega$, cutting the graph of f at $\tilde{c}$. Note that $\tilde{D} = \tilde{H}_{aux} \cap \mathcal{S}[f]$. The frame $\{\hat{x}, \hat{y}\}$ is oriented on $\tilde{H}_{aux}$ such that $\{\hat{y}\} \perp \Omega$ and $\{\hat{x}_n\} \parallel \{y\}$, with $n = 2$ as an special case.

that by equation (4.77) we have $P_1, P_2 \in \tilde{H}_{aux}$. Hence, letting $\hat{P}_i = T(P_i)$, with $i = 1, 2$, and noting that $g(\hat{P}_i) = T(f(P_i))$, we can use the results of Lemma 4.4.5 to state that $\tilde{l}_1$ and $\tilde{l}_2$ intersect with each other at a flat of dimension $m-3$, as $\hat{Q}_2$, and in addition,

$$\exists M' \in \text{proj}_{\Omega'} \hat{Q}_2 \ : \ \|\hat{P}_1 M'\| + \|\hat{P}_2 M'\| = \|\hat{P}_1 \hat{P}_2\| \tag{4.80}$$

Denoting $Q_2 = T^{-1}(\hat{Q}_2)$, since $\tilde{H}_{aux} \perp \Omega$, conditions (4.77) and (4.80) imply that for $\text{proj}_{\Omega} Q_2$ there exists a point such as M where

$$\exists M \in \text{proj}_{\Omega} Q_2 \ : \ \|P_1 M\| + \|P_2 M\| = \|P_1 P_2\| \tag{4.81}$$

In order to show that $Q_1 \neq Q_2$ the following reasoning is used. Let $l_{aux} = H_{aux} \cap \tilde{H}_{aux}$. Since $(P_i, f(P_i)) \in H_{aux}$ and $(P_i, f(P_i)) \in \tilde{H}_{aux}$, with $i = 1, 2$, we have

$$\begin{cases} (P_1, f(P_1)) \in l_{aux}, \\ (P_2, f(P_2)) \in l_{aux}. \end{cases} \tag{4.82}$$

Moreover, since $\tilde{l}_1$ is tangent to f at $(P_1, f(P_1))$ by Lemma 4.4.3, and $(P_1, f(P_1)) \neq (P_2, f(P_2))$, we have $(P_2, f(P_2)) \notin \tilde{l}_1$. Similarly, we can write $(P_1, f(P_1)) \notin \tilde{l}_2$. Summarizing these results, we have

$$\begin{cases} (P_1, f(P_1)) \in \tilde{l}_1, \\ (P_2, f(P_2)) \notin \tilde{l}_1, \end{cases} \text{ and } \begin{cases} (P_1, f(P_1)) \notin \tilde{l}_2, \\ (P_2, f(P_2)) \in \tilde{l}_2, \end{cases} \tag{4.83}$$

Equations (4.82) and (4.83) imply that $\tilde{l}_1 \cap \tilde{l}_2 \not\subset l_{aux}$. Recall that $Q_2 = \tilde{l}_1 \cap \tilde{l}_2$ and $l_{aux} = H_{aux} \cap \tilde{H}_{aux}$, therefore we conclude that

$$Q_2 \not\subset H_{aux} \cap \tilde{H}_{aux}. \tag{4.84}$$

Using the same reasoning for Q_1 we have

$$Q_1 \not\subset H_{aux} \cap \tilde{H}_{aux}. \tag{4.85}$$

Therefore, noting that $Q_1 \subset H_{aux}$ and $Q_2 \subset \tilde{H}_{aux}$, equations (4.84) and (4.85) yield

$$Q_1 \neq Q_2. \tag{4.86}$$

So far, the following results are obtained

$$Q_1 \subset H_1 \text{ and } Q_1 \subset H_2, \tag{4.87a}$$

$$Q_2 \subset H_1 \text{ and } Q_2 \subset H_2, \tag{4.87b}$$

$$Q_1 \neq Q_2. \tag{4.87c}$$

With the results in (4.87), conditions in (4.74) are satisfied, implying that $L_{int} = H_1 \cap H_2$ exists and is constructed by using Q_1 and Q_2. Note that since $Q_2 \subset L_{int}$, we have $\text{proj}_\Omega Q_2 \subset L_{pj}$. This fact along with condition (4.81) yields $M \in L_{pj}$ guaranteeing (4.73) to be true. This completes the proof of the lemma. □

Before going further, the following lemma, which is essential in this context is presented.

Lemma 4.4.6. *Let $f : \Omega \to \mathbb{R}$ be a concave function, where $\Omega \subset \mathbb{R}^n$ is a convex set. Assume that f is class $\mathcal{C}^1$ in the neighborhood of point $P_0 \in \Omega$. Assume also that f is linearized with $h(x)$ by the Taylor series around P_0. Then for any direction vector pointing from P_0 in Ω defined as*

$$\mathbf{v}_{P_0}(x) = \frac{x - P_0}{\|x - P_0\|}, \tag{4.88}$$

the distance function $\Delta(x)$, defined in (4.26) *and* (4.27)*, is monotonically increasing, i.e. for two collinear points $x^I, x^{II} \in \Omega$ defined as*

$$\begin{cases} x^I = s_1 \mathbf{v}_{P_0} \\ x^{II} = s_2 \mathbf{v}_{P_0} \end{cases}, \quad s_1, s_2 \in \mathbb{R}^+, \text{ and } s_1 < s_2, \tag{4.89}$$

we have

$$\nabla\Delta(x^I) \cdot \mathbf{v}_{P_0}(x) \leq \nabla\Delta(x^{II}) \cdot \mathbf{v}_{P_0}(x), \quad x \in \Omega. \tag{4.90}$$

Proof. Since the convexity of two functions is held under their addition [73], and the fact that $-f$ and h are both convex, $\Delta(x) = h(x) - f(x)$ is convex too. Moreover, according to Proposition 4.3.1, $h \geq f$, which implies that $\Delta(x) \geq 0$. Since $f(P_0) = h(P_0)$, we have $\Delta(P_0) = 0$, as a global minimum of Δ in Ω, i.e.

$$P_0 = \arg\min_{x \in \Omega} \Delta(x). \tag{4.91}$$

Let $\mathcal{P}_\mathbf{v}$ be a plane specified as $\mathbf{v}_{P_0} \in \mathcal{P}_\mathbf{v}$ and $\mathcal{P}_\mathbf{v} \perp \Omega$, as plotted in Figure 4.12 for $n = 2$. Consequently we have $\mathcal{P}_\mathbf{v} \parallel \{y\}$. Consider two orthogonal axes $\{\xi, \zeta\}$ in the plane $\mathcal{P}_\mathbf{v}$ such that

$$\mathbf{v}_{P_0} \in \{\xi\} \text{ and } \{\zeta\} \parallel \{y\}. \tag{4.92}$$

Since $\Delta(x)$ is convex, $-\Delta(x)$ is concave, allowing us to use the results of Corollary 4.4.1. Note that the plane $\mathcal{P}_\mathbf{v}$ is an $\mathcal{F}_1$ being perpendicular to Ω, so that the intersection of the graph of $-\Delta(x)$ with plane $\mathcal{P}_\mathbf{v}$ can be represented by a concave function of one variable, as $g : \Omega \cap \mathcal{P}_\mathbf{v} \to \mathbb{R}$. Since g is concave, $-g$ is convex. Let us denote $-g$ by $\delta_\mathbf{v} : \Omega \cap \mathcal{P}_\mathbf{v} \to \mathbb{R}$. In this case we have $\xi \in \Omega \cap \mathcal{P}_\mathbf{v}$ and $\zeta \in \mathbb{R}$ as the image of $\delta_\mathbf{v}$ over $\Omega \cap \mathcal{P}_\mathbf{v}$. Accordingly,

we can write

$$\zeta = \delta_{\mathbf{v}}(\xi) \tag{4.93}$$

Note that the plot of $y = \Delta(x)$ and $\zeta = \delta_{\mathbf{v}}(\xi)$ for $n = 2$ is shown in Figure 4.12.

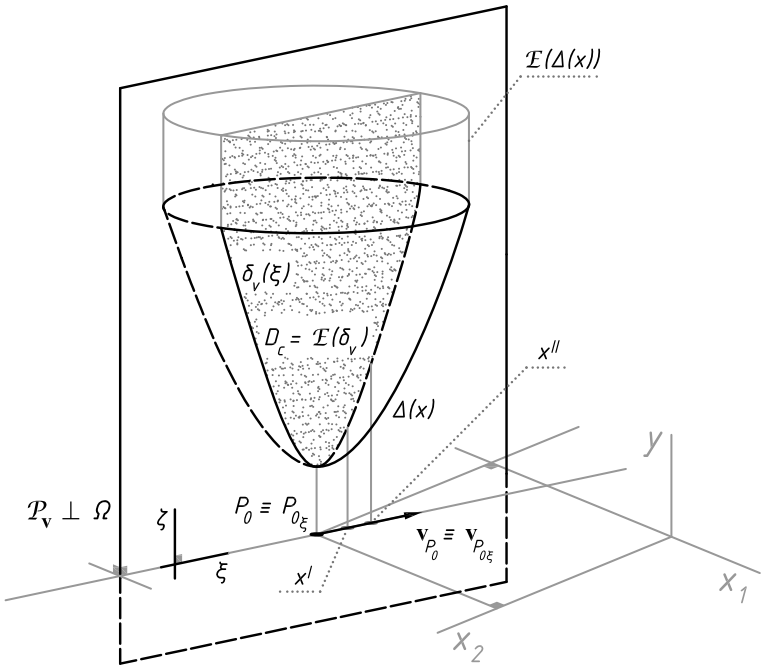

Figure 4.12: The plane $\mathcal{P}_{\mathbf{v}}$ intersecting the epigraph of $\Delta(x)$ at D_c generates the convex function $\delta_{\mathbf{v}}(\xi)$. Note that the triple-bar sign $(\equiv)$ indicates coincidence in this plot.

Let $T_{(\xi,\zeta)} : \{(x,y) \in \mathcal{P}_{\mathbf{v}}\} \to (\xi,\zeta)$ denote a transformation mapping from (x,y) to (ξ,ζ) coordinate system. Since P_0 lies in $\mathcal{P}_{\mathbf{v}}$ and by equation (4.92) the axis $\{\xi\}$ is along $\mathbf{v}_{P_0}$, one can define $(P_{0_\xi}, 0) = T_{(\xi,\zeta)}(P_0, 0)$ as the representation of P_0 in the (ξ,ζ) coordinate system. Using an alternative definition for $\delta_{\mathbf{v}}$ as $\{(\xi,\zeta) \mid \zeta = \delta_{\mathbf{v}}(\xi)\} = \{(x,y) \mid y = \Delta(x)\} \cap \mathcal{P}_{\mathbf{v}}$, we have

$$\{(\xi,\zeta) \mid \zeta = \delta_{\mathbf{v}}(\xi)\} \subset \{(x,y) \mid y = \Delta(x)\} \tag{4.94}$$

which implies

$$(P_{0_\xi}, \delta_{\mathbf{v}}(P_{0_\xi})) = T_{(\xi,\zeta)}(P_0, \Delta(P_0)) \tag{4.95}$$

From equations (4.91), (4.94) and (4.95) one concludes that

$$\left(\arg\inf_{\xi}\delta_{\mathbf{v}}(\xi),\inf_{\xi}\delta_{\mathbf{v}}(\xi)\right)=T_{(\xi,\zeta)}\left(\arg\inf_{x}\Delta(x),\inf_{x}\Delta(x)\right) \tag{4.96}$$

Now, we have $\delta_{\mathbf{v}}(\xi)$ that is a convex function of one variable defined in the (ξ,ζ) coordinate system, and P_{0_ξ} is its global minimum point. Moreover, from equation (4.92) the unit vector $\mathbf{v}_{P_0}$ is along ξ implying that one can use a replacement unit vector defined as

$$\mathbf{v}_{P_{0\xi}}(\xi)=\frac{\xi-P_{0_\xi}}{\|\xi-P_{0_\xi}\|}. \tag{4.97}$$

Using Lemma 4.4.2, the function $\delta_{\mathbf{v}}(\xi)$ is of class $\mathcal{C}^1$ since $\Delta(x)\in\mathcal{C}^1$. Consequently, the assumptions of Lemma 4.3.3 are satisfied, and thus we have

$$\nabla\delta_{\mathbf{v}}(\xi)\cdot\mathbf{v}_{P_{0\xi}}(\xi)\geq 0,\quad \xi\in\Omega\cap\mathcal{P}_{\mathbf{v}}. \tag{4.98}$$

Note that $\zeta=\delta_{\mathbf{v}}(\xi)$ yields the image of $x\in\{x\mid x\in\Omega\cap\mathcal{P}_{\mathbf{v}}\}=\{x\mid x=s\mathbf{v}_{P_0},s\in\mathbb{R}\}$ under $\Delta(x)$ in the ζ coordinate. This result together with equation (4.94) implies that equation (4.98) represents the *directional derivative* of $\Delta(x)$ along $\mathbf{v}_{P_0}$ in the (ξ,ζ) coordinates, which allows us to write

$$\nabla\Delta(x)\cdot\mathbf{v}_{P_0}(x)\geq 0, \tag{4.99}$$

for $x\in\{x\mid x\in\Omega\cap\mathcal{P}_{\mathbf{v}}\}$. Since $\mathcal{P}_{\mathbf{v}}$ is dependent on the direction of $\mathbf{v}_{P_0}(x)$, it is concluded that (4.99) holds for $x\in\Omega$. Consequently, equation (4.99) yields

$$\nabla\Delta(x^I)\cdot\mathbf{v}_{P_0}(x)\leq\nabla\Delta(x^{II})\cdot\mathbf{v}_{P_0}(x),\quad s_1<s_2. \tag{4.100}$$

□

The maximum error of approximation is defined as $e_{max}=\sup_{x\in\Omega}\Delta(x)$, where $\Delta(x)$ is defined in equations (4.26) and (4.27). Using the results of Lemmas 4.4.5 and 4.4.6, Theorem 4.4.1 is given to find the set of points in Ω where e_{max} lies.

Theorem 4.4.1. *Consider a class $\mathcal{C}^1$ concave function $f : \Omega \to \mathbb{R}$, $\Omega \subset \mathbb{R}^n$. Assume that Ω is bounded. Let the function be linearized around two distinct points $P_1, P_2 \in \Omega$ with hyperplanes $H_1 = \{(x,y) \mid y = h_1(x)\}$ and $H_2 = \{(x,y) \mid y = h_2(x)\}$, respectively. Furthermore, consider a flat of dimension $(n-1)$ as L_{int} defined in* (4.67)*. Also, let $L_{pj} = \text{proj}_{\Omega} L_{int}$. Then, the solution to the following maximization problem*

$$\arg\sup_{x \in \Omega} \Delta(x) \tag{4.101}$$

lies either on L_{pj}, or at the boundary of the domain $\partial\Omega$.

Proof. It can be recognized by Lemma 4.4.5 that L_{pj} is located between P_1 and P_2. Furthermore, L_{pj} which intersects Ω at $\{q_1, q_2\} = \partial\Omega \cap L_{pj}$, divides Ω into two regions $\mathscr{R}_i$ with $i = 1,2$, such that $P_i \in \mathscr{R}_i$. Therefore, $\partial\mathscr{R}_i$ consists of the discriminating line L_{pj} and a part of $\partial\Omega$. Define two unit vectors

$$\mathbf{v}_{P_i}(x) = \frac{x - P_i}{\|x - P_i\|}, \quad x \in \mathscr{R}_i, \quad i = 1,2. \tag{4.102}$$

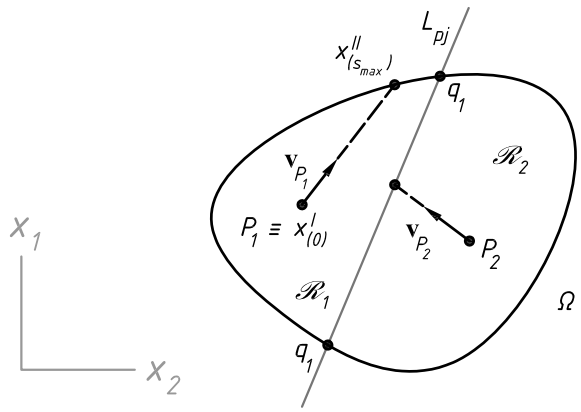

Figure 4.13: Two regions $\mathscr{R}_1$ and $\mathscr{R}_2$ that are produced as a result of the intersection of $\Omega \subset \mathbb{R}^2$ and L_{pj} are illustrated. Points $x^I_{(0)}$ and $x^{II}_{(s_{max})}$ are also shown for an arbitrary direction of vector $\mathbf{v}_{P_1}$ associated with region $\mathscr{R}_1$.

Note that the distance function in this case is a piecewise function defined by equation (4.26), that is repeated below as

$$\Delta(x) = \Delta_i(x), \;\; x \in \mathscr{R}_i, \;\; i = 1,2, \tag{4.103}$$

where

$$\Delta_i(x) = \begin{cases} |h_i(x) - f(x)| & , \quad h_i(x) < f(x), \\ h_i(x) - f(x) & , \quad h_i(x) \geq f(x). \end{cases} \tag{4.104}$$

According to Lemma 4.4.6, for any $x \in \mathscr{R}_i$ that specifies the direction of $\mathbf{v}_{P_i}$, there exists a set of pairs (x^I, x^{II}) which is produced for each of the regions by using $s_1, s_2 \in \mathbb{R}^+$, as

$$\left\{ (x^I, x^{II}) \mid x^I_{(s_1)} = s_1 \mathbf{v}_{P_i}, \;\; x^{II}_{(s_2)} = s_2 \mathbf{v}_{P_i}, \;\; s_1 < s_2 \leq s_{max} \right\}, \tag{4.105}$$

where the index (s_i) shows that x^I, and x^{II} are functions of s_1 and s_2, respectively. In addition, s_{max} is a limitation for s_2 such that $x^{II}_{(s_{max})} \in \partial\mathscr{R}_i$. Using the results of Lemma 4.4.6, we have

$$\nabla\Delta_i(x^I) \cdot \mathbf{v}_{P_i} \leq \nabla\Delta_i(x^{II}) \cdot \mathbf{v}_{P_i}, \quad s_1 < s_2, \tag{4.106}$$

which for $s_1 = 0$ and $s_2 = \varepsilon$, where ε is a sufficiently small positive real number, yields

$$\nabla\Delta_i(x^I_{(0)}) \cdot \mathbf{v}_{P_i} \leq \nabla\Delta_i(x^{II}_{(\varepsilon)}) \cdot \mathbf{v}_{P_i}, \quad 0 < \varepsilon, \tag{4.107}$$

By definition of x^I and x^{II} in (4.105) and the fact that $s_1, s_2 \geq 0$, it is realized that x^I and x^{II} are increased in the direction of $\mathbf{v}_{P_i}$. This conclusion together with the inequality (4.107) implies

$$\Delta(x^I_{(0)}) \leq \Delta(x^{II}_{(\varepsilon)}). \tag{4.108}$$

Inequality (4.108) in a sequence of (x^I, x^{II}) including $s_2 = s_1 + p\varepsilon$, with $s_1 = 0$ and $p \in \{p \in \mathbb{N} \mid p < p_{max}\}$, where p_{max} is defined such that $s_{max} = s_1 + p_{max}\varepsilon$, implies that

$$\Delta(x^I_{(0)}) \leq \Delta(x^{II}_{(s_{max})}). \tag{4.109}$$

As noted earlier, $x^{II}_{(s_{max})} \in \partial\mathscr{R}_i$, and according to inequality (4.109) one concludes that the value of $\Delta(x)$ is maximum for $x \in \partial\mathscr{R}_i$. On the other hand, $\mathscr{R}_i$ consists of the discriminating line L_{pj} and a part of $\partial\Omega$. Therefore, the solution to (4.101) lies either on L_{pj} or $\partial\Omega$. This completes the proof of the theorem. □

Referring to Definition 4.3.1 the piecewise affine hyperplanes for P_1 and P_2 as the nominal points is described by

$$H = \{(x,y) \mid y = h(x)\}, \quad h(x) = h_i(x), \quad x \in \mathscr{R}_i, , \quad i = 1,2, \tag{4.110}$$

where

$$h_i(x) = f(P_i) + \nabla f(P_i)(x - P_i). \tag{4.111}$$

Let us denote $h(x)$, defined in equation (4.110) and used in Theorem 4.4.1, the first stage of the intersection-based PWA approximation of the concave function f. This approximation can proceed to the next approximation stage if the function is linearized at the point of maximum error. Towards this end, the continuity of the approximated function is required.

Theorem 4.4.2. *The PWA approximation of a concave function $f : \Omega \to \mathbb{R}$ by $h(x)$ given in equations* (4.110) *and* (4.111) *is continuous, i.e.*

$$\lim_{\varepsilon \to 0} h_1(x^\star + \varepsilon \mathbf{v}_{x^\star}(x)) = \lim_{\varepsilon \to 0} h_2(x^\star + \varepsilon \mathbf{v}_{x^\star}(x)), \quad \forall x \in \Omega, \tag{4.112}$$

where $x^\star \in L_{pj} \cap \Omega$ and

$$\mathbf{v}_{x^\star}(x) = \frac{x - x^\star}{\|x - x^\star\|}. \tag{4.113}$$

Proof. The continuity property of h can be trivially shown by recalling that h is constructed as a result of the intersection of hyperplanes h_1 and h_2. The existence of these intersections are guaranteed by Lemma 4.4.5. Therefore, h defined by (4.110) is continuous. □

During any linearization stage, the PWA regions are produced by projecting L_{int} onto Ω. consequently, polytopic regions are produced in the domain. In order to accelerate each linearization stage, the procedure of finding the point of maximum error should be studied in detail. With the properties of $\Delta(x)$ provided in Lemma 4.4.6 and Theorem 4.4.1, Theorem 4.4.3 provides a straightforward tool for obtaining the points of maximum error. However, we need two preliminary definitions before presenting Theorem 4.4.3.

Definition 4.4.7. *[77] The convex hall of a set of finite number of points is called polytope.*

Definition 4.4.8. *The notation n-Polytope is used to denote the polytope of dimension n in space.*

As a remark to the definition of polytopes, a vertex is a 0-polytope, a segment is a 1-polytope, a polygon is a 2-polytope, and a polyhedron is a 3-polytope.

Theorem 4.4.3. *Given the assumption and results of Theorems 4.4.1 and 4.4.2, if f is linearized by h_i over an $n-$dimensional polytopic region $\mathscr{R}_i$, the solution to* (4.101) *lies at one of the vertices of $\mathscr{R}_i$.*

Proof. The proof of this theorem is given by using induction. Two steps are given here. Based on the arguments in each step, a conclusion is drawn for the Step n.

Step 1: Polytopic regions are convex, therefore by Theorem 4.4.1 the point $x_{max} = \arg\max_{x\in\mathscr{R}_i}\Delta(x)$ lies at the boundary of the $\mathscr{R}_i$. Let L_{pj} be the side of $\overline{\mathscr{R}}_i$, where x_{max} lies. By Lemma 4.4.5 we have

$$L_{pj} = \text{proj}_{\Omega} L_{int}. \tag{4.114}$$

Based on the fact that L_{int} is an $\mathcal{F}_{m-2}$, as stated in Lemma 4.4.5, the hyperplane H_{ort} as an $\mathcal{F}_{m-1}$ can be constructed such that $H_{ort} \perp \Omega$ and $L_{int} \subset H_{ort}$. Consequently, we have

$$L_{pj} \subset H_{orth} \cap \Omega. \tag{4.115}$$

The function $\Delta(x)$ is convex over Ω. Therefore, the result in equation (4.115) and Corollaries 4.4.2 and 4.4.1 are used to state that $\{(x,y) \mid y = \Delta(x)\} \cap H_{ort}$ can be represented by a convex function g, as

$$\begin{aligned}\{(\hat{x},\hat{y}) \mid \hat{y} = 0, \hat{x}_n = & g(\hat{x}_1,\hat{x}_2,\ldots,\hat{x}_{n-1}), \hat{x} \in H_{ort}\} = \\ & \{(\hat{x},\hat{y}) \mid (\hat{x},\hat{y}) = T(x,\Delta(x)), \quad x \in L_{pj}\},\end{aligned} \tag{4.116}$$

where the coordinates $(\hat{x},\hat{y})$ are defined in Definition 4.4.5 with $\{\hat{x}_n\} \parallel \{y\}$, and T is the coordinate transformation function defined in Definition 4.4.6.

Now, we have a convex function $g : L_{pj} \to \mathbb{R}$. Region $\overline{\mathscr{R}}_i$ is an n-polytope. Note that L_{pj} as a side of the polytopic region $\overline{\mathscr{R}}_i$ is an $(n-1)$-polytope. Define

$$\hat{x}_{max} = \underset{(\hat{x}_1,\hat{x}_2,\ldots,\hat{x}_{n-1})\in L_{pj}}{\arg\max} \; g(\hat{x}_1,\hat{x}_2,\ldots,\hat{x}_{n-1}). \tag{4.117}$$

Step 2: Based on the results of Step 1, Theorem 4.4.1 can be used for g to conclude that $\hat{x}_{max}$ lies in the ∂L_{pj}. Note that ∂L_{pj} consists of the sides of L_{pj}. Each side is an $(n-2)$-polytope. The point of $\hat{x}_{max}$ therefore lies in an $(n-2)$-polytope.

Continuing with the same reasoning to find the point of maximizing $\Delta(x)$ in $\mathscr{R}_i$, we arrive at the conclusion that in the Step n, the point of maximum error lies at the boundary of a 1-polytope. A 1-polytope is a segment and the sides of a segment are vertices. These vertices are the vertices of $\overline{\mathscr{R}}_i$. This completes the proof of the theorem. □

Definition 4.4.9. *Consider a set D. The cavity of D is denoted by* $\operatorname{cav}(D)$ *and is defined to be the set*

$$\operatorname{cav}(D) = \operatorname{conv}(D) \setminus D. \tag{4.118}$$

where $\operatorname{conv}(D)$ *denotes the convex hull of D as defined in Definition 4.3.3.*

Another important point which has to be considered in the new PWA approximation methodology is the convexity of the regions. If the produced regions are not convex, a wide range of theorems for analysis and synthesis cannot be applied to our PWA models. For this reason, the following theorem guarantees the convexity of such regions.

Theorem 4.4.4. *Consider a class* $\mathcal{C}^1$ *concave function* $f : \Omega \to \mathbb{R}$*, where* $\Omega \subset \mathbb{R}^n$ *is a convex set. The IPWA regions* $\mathscr{R}_i$ *produced as a result of the projection of* h_i *onto* Ω *are convex.*

Proof. The proof of this theorem is given by contradiction. Let $\mathscr{R}_i$ be a non-convex region as shown in Figure 4.14a for $n = 2$. Since the region $\mathscr{R}_i$ is non-convex and is produced by projecting H_i onto Ω, the hypograph of H_i is defined in $\mathscr{R}_i$ is non-convex. Accordingly,

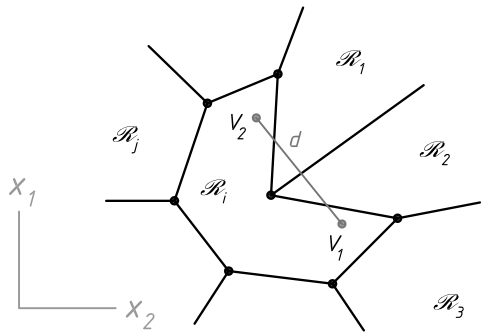

(a) A part of segment d lies out of $\mathscr{R}_i$.

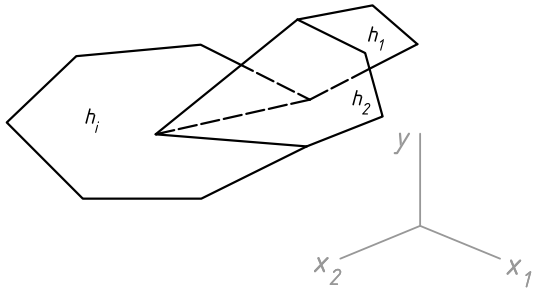

(b) As a result of non-convex region, the associated hyperplane becomes non-convex. The cavity of H_i is filled with H_1 and H_2.

Figure 4.14: By contradiction, $\mathscr{R}_i$ is assumed to be a non-convex region. This figure shows $\mathscr{R}_i$ and H_i for a two-dimensional domain ($n = 2$).

the set H_i over $\mathscr{R}_i$ is a non-convex subset of the hyperplane that serves as the linearization of f at P_i.

Using the violation of the definition of convex sets as given by Definition 4.4.1 for $\mathscr{R}_i$, there exists a segment d with $V \in d$, as

$$V(t) = V_1 + (V_2 - V_1)t, \quad \begin{cases} t \in [0,1], \\ V_1, V_2 \in \mathscr{R}_i, \end{cases} \tag{4.119}$$

such that we have

$$\mathcal{M} = d \setminus \{V \in \mathscr{R}_i\} \tag{4.120}$$

By Definition 4.4.9, we have $\mathcal{M} \in \text{cav}\,(\mathscr{R}_i)$. Since $\nabla h_i \neq \nabla h_j$, where j is the index for the neighboring region, and the fact that h is continuous, there must be more than one hyperplane filling the $\text{cav}\,(H_i)$. In other words, if there is only one hyperplane as H_j such that $\text{cav}\,(H_i) \in H_j$, then the fact that $\nabla h_i \neq \nabla h_j$ implies h defined in (4.110) and (4.111) is not continuous. Consequently, there are more than one region that fill the $\text{cav}\,(\mathscr{R}_i)$. This implies that there are more that one region where $\mathcal{M}$ lies. Let d, while connecting V_1 and V_2, intersects with at least two regions $\mathscr{R}_1$ and $\mathscr{R}_2$. These regions are shown for the case of $n = 2$ in Figure 4.14a for illustrative purposes. Define $t_1 < t_2 < t_3 < t_4 \in [0,1]$ such that

$V(t_1) \in \mathscr{R}_i$, $V(t_2) \in \mathscr{R}_2$, $V(t_3) \in \mathscr{R}_1$, and $V(t_4) \in \mathscr{R}_i$. Based on the continuity of h together with the assumption that $\nabla h_i \neq \nabla h_j$, we have either of the following conditions:

$$\nabla h_i(V(t_1)) \cdot \mathbf{v} < \nabla h_2(V(t_2)) \cdot \mathbf{v} > \nabla h_1(V(t_3)) \cdot \mathbf{v} < \nabla h_i(V(t_4)) \cdot \mathbf{v}, \tag{4.121a}$$

$$\nabla h_i(V(t_1)) \cdot \mathbf{v} > \nabla h_2(V(t_2)) \cdot \mathbf{v} < \nabla h_1(V(t_3)) \cdot \mathbf{v} > \nabla h_i(V(t_4)) \cdot \mathbf{v}, \tag{4.121b}$$

where $\mathbf{v}$ is a unit vector along the segment d. Let $\varphi(x)$ be defined as

$$\varphi(x) \triangleq f(x), \quad \forall x \in d. \tag{4.122}$$

Using definition of point V from equation (4.119), one can replace x by $V(t)$ in (4.122) to state $\varphi(V(t)) = f(V(t))$. It can be shown by Corollary 4.4.1 that $\varphi(V(t))$ is concave since $f(x)$ is concave. To avoid potential distraction, the details of the proof of this statement is omitted here. Moreover, the concavity of $\varphi(V(t))$ implies that $\varphi(V(t))$ is absolutely continuous [74]. Also $\varphi(V(t))$ is differentiable almost everywhere.

Since $t_1 < t_2 < t_3 < t_4$, according to Lemma 4.3.1 we have

$$\nabla\varphi(V(t_1)) < \nabla\varphi(V(t_2)) < \nabla\varphi(V(t_3)) < \nabla\varphi(V(t_4)) \tag{4.123}$$

Note that h_i, h_1, and h_2 are the linearization of the concave function f, therefore they serve as supporting hyperplanes for both $f(x)$ and $\varphi(V(t))$. On the other hand, condition (4.123) dictates the condition for the gradient of the supporting hyperplanes of function $\varphi(V(t))$, which is not consistent with condition (4.121a) nor with (4.121b), implying that $\mathscr{R}_i$ cannot be non-convex. □

Equipped with the theories that have been provided in this subsection, the algorithm for the intersection-based PWA approximation can be described in the next subsection. Figure 4.15 shows the flow diagram of the lemmas and the theorems that result in the IPWA algorithms provided in Subsection 4.4.1

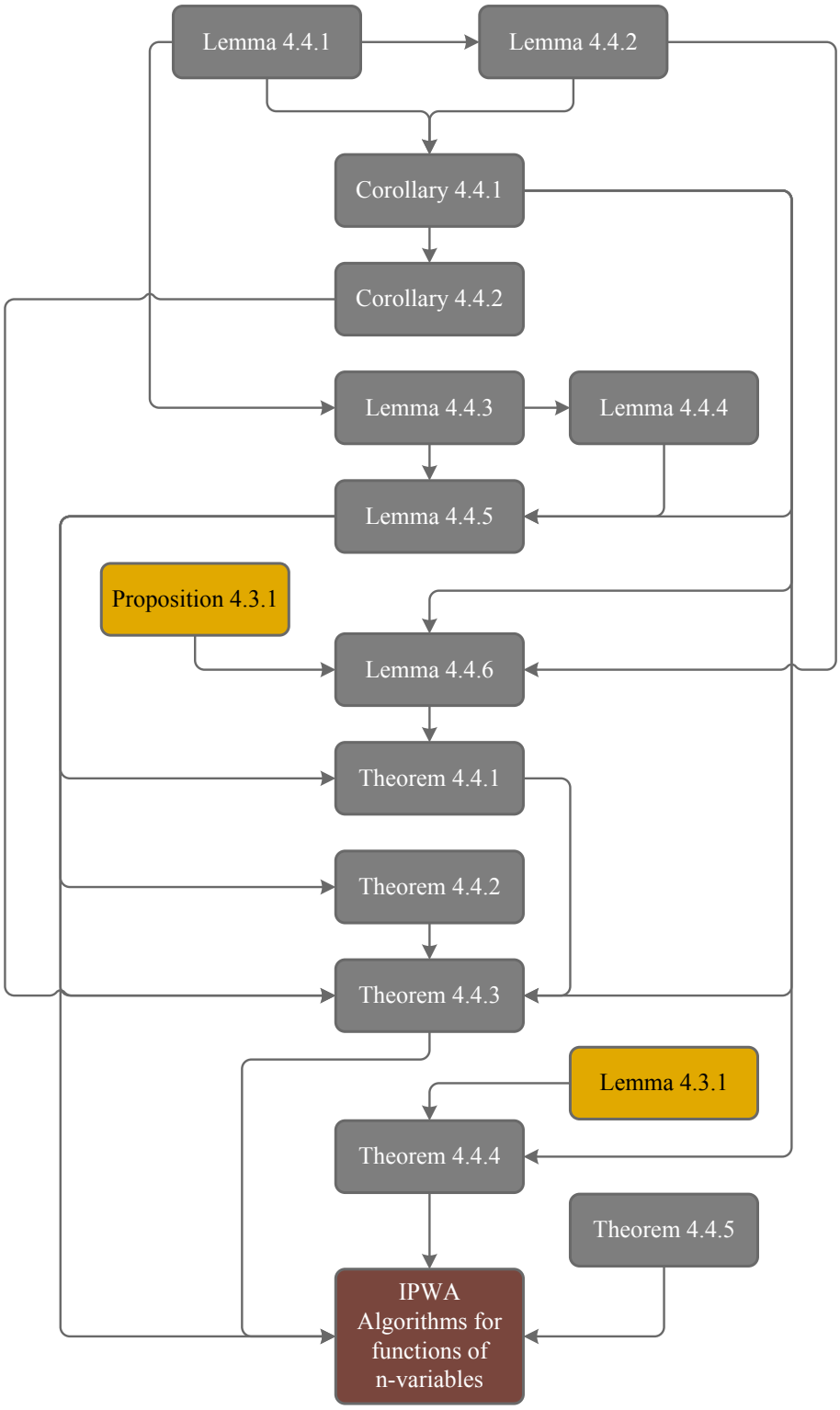

Figure 4.15: The flow diagram of the theory for the proposed algorithms in Subsection 4.4.1 for functions of $n-$variables. Note that the yellow blocks are from the IPWA approximation theory for functions of one variable.

4.4.1 The IPWA Algorithms

In this subsection, algorithms to perform the intersection-based PWA approximation for both concave/convex and continuous functions are introduced.

Concave/Convex Functions

This algorithm is proposed for a concave function. If f is convex, $-f$ is then considered.

Problem 4.4.1. *Consider a class $\mathcal{C}^1$ concave function $f : \Omega \to \mathbb{R}$, where $\Omega \subset \mathbb{R}^n$. Find $\bar{f}$ over the domain of f.*

Algorithm 4.4.1.

1. The primary linearization points are given.

2. Choose one of the linearization points from Step 1 and denote it by P_{N_u}, where N_u is the number of linearization points at the u^{th} iteration. At this stage $u = 1$ and N_u is determined by Step 1.

3. Using Taylor series, the function f is linearized around P_{N_u}. The produced linearization hyperplane is denoted by $H_i = \{(x,y) \mid y = h_i(x)\}$.

4. (a) If $N_u = 1$, go to Step 5.

   (b) If $N_u = 2$, H_1 and H_2 intersect with each other at $L^{1,2}_{int_u}$, according to Lemma 4.4.5. Projecting $L^{1,2}_{int_u}$ onto Ω results in $L^{1,2}_{pj_u}$.

   (c) If $N_u > 2$, find the intersections of h_{N_u} with h_i, where $i \in \{1,2,\ldots,N_u - 1\}$. Denote them by $L^{N_u,i}_{int_u}$, and their projection onto Ω by $L^{N_u,i}_{pj_u}$, where u is the linearization iteration number. Note that $L^{i,j}_{pj}$ is the projection of $L^{i,j}_{int}$ over Ω from the previous iteration. Note that the superscript j stands for the neighboring region of the i^{th} region.

The result of Sub-items 4b and 4c will be a set of convex regions denoted by $\mathscr{R}_k$, where $k \in \{1,2,\ldots N_u\}$, as guaranteed by Theorem 4.4.4. In case of the Sub-item 4a, we have $\mathscr{R}_1 = \Omega$.

5. Designate all vertices of regions $\mathscr{R}_k$ by $q_{k,\lambda}$, where $\lambda \in \{1,2,\ldots,\lambda_k^{max}\}$, with λ_k^{max} denote the number of vertices of region $\mathscr{R}_k$.

6. If f is already linearized around all the primary linearization points from Step 1, go to Step 7. Otherwise, choose the next primary linearization point, at which f is not linearized yet. Then let $u := u+1$, and go to Step 3.

7. By Theorem 4.4.3, the point at which the e_{max} occurs is determined as

$$e_{max} = \sup_{k,\lambda} \Delta(q_{k,\lambda}) \tag{4.124}$$

8. The stopping criterion is defined as

$$e_{max} \leq e_{des} \tag{4.125}$$

where e_{des} is called *the desired error* and is defined to be the maximum allowable error determined by the user. If the stopping condition is satisfied, the IPWA approximation is complete and, therefore exit the iteration. Otherwise, $u := u+1$ and

$$P_{N_u} = \arg\sup_{k,\lambda} \Delta(q_{k,\lambda}) \tag{4.126}$$

Then go to Step 3. This iteration is continued until the stopping condition is satisfied.

Remark 4.4.4. *The primary linearization points are suggested under two categories: First, in case of controller synthesis, the reference point where after applying the controller the system is expected to reach to the trajectories, and second, any point for which zero amount of error is required by the user.*

Continuous Functions

Despite the fact that non-concave functions are rather difficult to tackle, many applications have nonlinearities that are neither concave nor convex. For this purpose, two different algorithms which are successfully applied to the axial compression surge and stall problem are given in this subsection.

A. Fourth Order Concave Polynomial Approximation (FOCP)

The first algorithm proposed for approximating a non-concave function $f(x)$ by a PWA function is based on the mean curvature of the function graph. First the definition of Weingarten map is give for $n = 2$.

Definition 4.4.10. *[80] Let $\mathcal{S}(x, f(x))$ denote the smooth surface representing the graph of a smooth function $f : \Omega \to \mathbb{R}$. The Weingarten map of $\mathcal{S}$ is then defined as follows.*

$$W = -\nabla \mathbf{n}(x), \tag{4.127}$$

where $\mathbf{n}(x)$ is the unit normal vector field.

Definition 4.4.11. *Given the smooth surface $\mathcal{S}(x, f(x))$ and W denoting the Weingarten map of $\mathcal{S}$ from Definition 4.4.10, the mean curvature of $\mathcal{S}$ over Ω, is denoted by* $\text{curv}_\Omega \mathcal{S}$ *and is defined to be*

$$\text{curv}_\Omega \mathcal{S} = \frac{1}{2} \text{trace}\, W(\mathcal{S}). \tag{4.128}$$

For the definition of the mean curvature of higher dimensional surfaces the reader is referred to [81]. The idea is to approximate a function by a fourth order polynomial $p(x)$ with a specific structure such that:

1. The values of $f(x)$ and $p(x)$ are identical at the origin.

2. Although $f(x)$ is not a concave/convex function, it possesses either a negative or a

positive average value of its mean curvature over Ω. The second criterion is therefore,

$$\text{sign}[\text{curv}_\Omega \mathcal{S}(x, f(x))] = \text{sign}[\text{curv}_\Omega \mathcal{S}(x, p(x))] \tag{4.129}$$

3. $[p(x) - f(x)]^2$ is minimized over Ω.

With these specifications, the next theorem can be formulated to approximate f.

Theorem 4.4.5. *Let the function $f : \Omega \to \mathbb{R}^n$ be given over a convex set Ω. Assume that for $\mathcal{S}(x, f(x))$ defined in Definition 4.4.11 we have* $\text{sign}(\text{curv}_\Omega \mathcal{S}) = -1$. *Let $x_0 \in \Omega$ be a given point for the approximation of f. Then, by solving the system of algebraic equalities and inequalities* (4.131)*,* (4.132) *and* (4.133a)*, f can be approximated by a fourth order concave polynomial of the form*

$$p(x) = \sum_{i=1}^{n} \sum_{j=1}^{4} a_{ij} x_i^j + a_0 \tag{4.130}$$

Proof. Since x_0 is a given point for the approximation of $f(x)$, it is important to make $p(x)$ pass through x_0. We thus write

$$p(x)|_{x_0} = f(x)|_{x_0}$$

implying that

$$a_0 = f(x_0) \tag{4.131}$$

For p to be concave the negative-definiteness of its Hessian matrix is required. Since p comes from a specific class of fourth order polynomials (4.130), we have

$$\frac{\partial^2 p}{\partial x_i \partial x_j} = 0, \quad \forall i \neq j,$$

which significantly simplifies the structure of the Hessian matrix as

$$\nabla^2(p) = \begin{bmatrix} 12a_{14}x_1^2 + 6a_{13}x_1 + 2a_{12} & 0 & 0 \\ 0 & \ddots & 0 \\ 0 & 0 & 12a_{n4}x_n^2 + 6a_{n3}x_n + 2a_{n2} \end{bmatrix}$$

For the above matrix to be negative-definite, the eigenvalues which are the diagonal elements need to be negative, i.e.

$$12a_{i4}x_i^2 + 6a_{i3}x_i + 2a_{i2} = \begin{bmatrix} x_i \\ 1 \end{bmatrix}^T \begin{bmatrix} 12a_{i4} & 3a_{i3} \\ 3a_{i3} & 2a_{i2} \end{bmatrix} \begin{bmatrix} x_i \\ 1 \end{bmatrix} < 0,$$

where $i \in \{1,2,\ldots,n\}$. This condition in turn can be achieved by

$$\begin{cases} a_{i4} & < & 0 \\ 8a_{i4}a_{i2} - 3a_{i3}^2 & > & 0 \end{cases} \tag{4.132}$$

To optimally determine the other polynomial coefficients, the least squares technique is used [73]. Towards this end, the integral of squares of the errors $S(a)$ is minimized subject to the polynomial coefficients $a = [a_{11},...,a_{14},\ldots,a_{n1},...,a_{n4}]$ as

$$S(a) = \int_\Omega [f(x) - p(x,a)]^2 dx_1 dx_2 \ldots dx_n$$

$$\min S(a)$$

Since $S(a)$ is convex, the solution can be trivially found by applying the first order necessary condition [73], namely by finding the solution of the following set of linear algebraic equations

$$\frac{\partial S(a)}{\partial a_{ij}} = 0 \tag{4.133a}$$

where $i \in \{1,2,\ldots,n\}$ and $j \in \{1,2,3,4\}$. □

Remark 4.4.5. *In order to find the the polynomial coefficients, the following procedure is conducted.*

1. *The set of equations* (4.131)*,* (4.132) *and* (4.133a) *are applied to PENBMI [49] with YALMIP [82] interface.*

2. *If the polynomial coefficients are found satisfying* (4.132)*, exit the algorithm. Otherwise go to the Step 3.*

3. *one of the equations from* (4.133a) *will be eliminated as follows. The solution to* (4.131)*,* (4.132) *and* (4.133a) *for* a_{ij} *is computed, and* e_{max} *is determined* $4 \times n$ *times. Each time only one of the equations from* (4.133a) *is eliminated. At the end,* a_{ij} *associated with the trial that resulted in the minimum* e_{max} *is selected.*

Problem 4.4.2. *Consider a class* $\mathcal{C}^2$ *non-concave/non-convex function* $f : \Omega \to \mathbb{R}$*, where* $\Omega \subset \mathbb{R}^n$*. Assuming that the average value of the mean curvature of* f *is negative, find* $\bar{f}$*.*

Once the non-concave function $\bar{f}$ is approximated by a concave polynomial, the concave algorithm 4.4.1 can be applied to find the IPWA.

B. Conservative Heuristic Approach (CONS)

For a number of non-concave/non-convex functions, $\text{curv}_\Omega \mathcal{S}(x, f(x))$ attains a value close to zero, which forcibly prevents us to approximate it with a concave/convex function. For these types of non-concave/non-convex functions, the *Conservative Approach* is proposed. In this algorithm, the non-concave function f is approximated in a way similar to the concave approximation algorithm, with the main difference that the surface mean curvature of f is considered. This is due to the fact that the theorems provided in Subsection 4.4 are not valid for non-concave functions. Although the concept of the surface mean curvature does not demonstrate separation of concave and convex parts of a function, it can heuristically be used to find the initial linearization points that are not in the highly curved part of the surface $\mathcal{S}(x, f(x))$. Hence, every step of the approximation by the conservative heuristic approach has to be checked to determine if the results of the above theorems are not violated. The detail of this method is explained in what follows.

Problem 4.4.3. *Consider a non-concave/non-convex function* $f : \Omega \to \mathbb{R}$*, where* $\Omega \subset \mathbb{R}^n$*. Assuming* $\text{curv}_\Omega \mathcal{S}(x, f(x)) \approx 0$*, find* $\bar{f}$*.*

Algorithm 4.4.2.

1. In the initial linearization stage, select the points from the following categories:

   (a) the given points, and

   (b) the points at which the absolute value of the surface mean curvature attains a minimum value.

2. Repeat Steps 2 and 3 from Algorithm 4.4.1.

3. Do Step 4 from Algorithm 4.4.1, but with the following main differences. Check if $L_{int_u}^{N_u,i}$ associated with the intersection of h_{N_u} and h_i is located between P_{N_u} and P_i, with $i \in \{1,2,\ldots,N_u-1\}$. If this condition is not satisfied, the algorithm is stopped, and no IPWA approximation will be returned. Furthermore, the associated region with P_{N_u} is created as instructed in the Algorithm 4.4.3 (described next).

4. Using a numerical optimization method such as the steepest descent, or Newton's method, find the points of e_{max} over the entire domain.

5. The sopping criterion consists of two parts:

   (a) Either the condition (4.125) is satisfied or

   (b) $L_{pj_u}^{N_u,i}$ is not located between the two linearization points.

   If the stopping criterion is not met, the loop is repeated from Step 2 to the end of Step 5. Otherwise the PWA intersection-base approximation for f is returned.

Non-convex regions are difficult to define or to work with. Therefore, they need to be divided into several convex subregions. The procedure for dividing the non-convex regions is described next.

Algorithm 4.4.3.

1. Consider the u^{th} iteration of the linearization. Let the non-convex regions for linearization points P_i, where $i \in \{1,2,\ldots,N_u-1\}$ be already determined. Note that in these non-convex regions h_i are defined.

2. The function f is linearized by h_{N_u} around P_{N_u}. The part of $h_{N_u}(x)$ for which $h_{N_u}(x) > h_i(x)$ is then discarded.

3. The remaining part of h_{N_u} is projected onto Ω, creating region $\mathscr{R}_{N_u}$.

4. Since $\mathscr{R}_{N_u}$ is not guaranteed to be convex, it is split into as many regions as $L^{i,j}_{pj_u}$ intersects $\mathscr{R}_{N_u}$, where $i,j \in \{1,2,\ldots,N_u\}$.

5. The boundary of $\mathscr{R}_{N_u}$ consists of $L^{i,j}_{pj_u}$ that are $\mathcal{F}_{m-2}$. The half-spaces $HS^{i,j}$ are defined to be the either side of $L^{i,j}_{pj_u}$ in Ω. The half-spaces are convex, therefore their intersections are convex too. Denote any intersection of three half-spaces that belongs to $\mathscr{R}_{N_u}$ by $\mathscr{R}^{(r)}_{N_u}$ such that $\mathscr{R}_{N_u} = \bigcup_r \mathscr{R}^{(r)}_{N_u}$.

6. $\mathscr{R}_{N_u}$ is returned that is divided into a number of convex sub-regions $\mathscr{R}^{(r)}_{N_u}$.

4.5 Conclusions

In this chapter, a new methodology for producing a continuous PWA approximation of nonlinear functions was developed. Using this technique, the axial compressor stall and surge problem will be treated in the next chapter, which has not been addressed before in the literature. The proposed IPWA approximation has the following properties:

- Continuity of the vector fields,

- Optimality of the linearization of the nonlinear function relative to the maximum approximation error,

- Increased reduction of the approximation error for a fixed number of regions and vice versa (as compared to the Voronoi-based and the uniform grid PWA models for the motivating Moore-Greitzer system as discussed in Section 5.2),

- Consistency of the derivative of the nonlinear function with the derivative of its approximation at the linearization points.

In particular the reduction in the number of the PWA regions for a fixed approximation error is discussed here. With the current complexity in solving bilinear matrix inequalities, which occurs for many physical systems, number of PWA regions plays a significant role for finding the PWA state feedback gains. The more the number of the PWA regions, the harder is solving the set of BMIs.

Chapter 5

Axial Compressor Surge and Stall Suppression

This chapter addresses the control synthesis problem of the Moore-Greitzer axial compressor model describing the two major compressor instabilities − surge and rotating stall − using both pseudo Euler-Lagrange and piecewise affine methodologies. The compressor no-stall (surge) problem has already been addressed in Chapter 3. This chapter is organized as follows. Section 5.1 addresses the simulation of the closed-loop system associated with application of each nonlinear technique. In Section 5.2, the IPWA model of the third order stall and surge system is given. Finally, a PWA synthesis technique is used to control the system.

5.1 Pseudo Euler-Lagrange (PEL) Approach

5.1.1 Pseudo Euler-Lagrange Control Synthesis Problem

As given in Chapter 2, the third order Moore-Greitzer compressor model has the following form

$$\dot{x}_1 = -x_2 + \frac{3}{2}x_1 + \frac{1-(1+x_1)^3}{2} - 3x_3(1+x_1) \tag{5.1a}$$

$$\dot{x}_2 = \frac{1}{\beta^2}(x_1 - u) \tag{5.1b}$$

$$\dot{x}_3 = -\sigma x_3^2 - \sigma x_3\left(2x_1 + x_1^2\right) \tag{5.1c}$$

Furthermore, as shown in Chapter 2, the simplifying equations corresponding to (5.1) for obtaining the pure surge model is given by

$$\dot{x}_1 = -x_2 - \frac{3}{2}x_1^2 - \frac{1}{2}x_1^3 \tag{5.2a}$$

$$\dot{x}_2 = \frac{1}{\beta^2}(x_1 - u), \tag{5.2b}$$

As developed in Chapter 3, the pseudo Euler-Lagrange controller has the following form

$$u_2(x_1,x_2) = \beta^2(\alpha+\rho)(\frac{3}{2}x_1^2 + \frac{1}{2}x_1^3) - \beta^2(\gamma+\rho)x_1 - \beta^2\rho x_2. \tag{5.3}$$

By conditions (3.68), (3.78), (3.87a) and (3.87c), α and ρ are selected to be $\alpha = -4$ and $\rho = 3.0$. Since potential variations of $\bar{\beta}$ is considered, one needs to be careful in selecting γ. This is accomplished by using the allowable γ chart shown in Figure 3.1 as well as equation (3.87b). Accordingly, $\gamma = 3.5$ for $\alpha = -4$ is chosen. With this selection the closed-loop surge model is stabilized with a maximum variation of $\pm 8\%$ in the parameter $\bar{\beta}$. The simulation results are provided in Figure 5.1

Although the controller was successfully applied to the pure surge model (5.2), one needs to investigate the stability property of the full order closed-loop system (5.1) using this controller (5.3). For this purpose, it is important to know when the controller is to be applied to the surged model. The reason is that $x_3 = 0$ was assumed in the pure surge

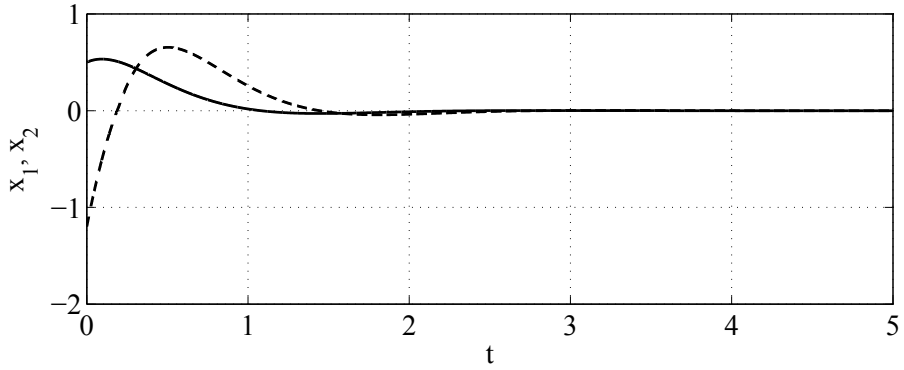

(a) States corresponding to the solid and dashed lines represent x_1 and x_2, respectively.

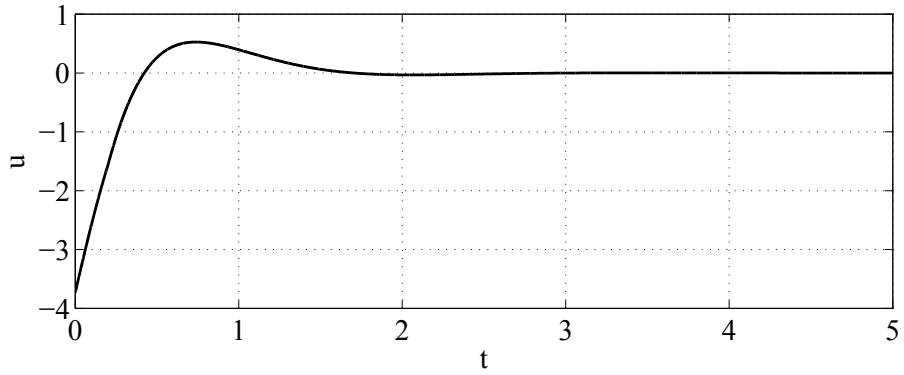

(b) Control input signal.

Figure 5.1: Simulation of the closed-loop system by the pseudo Euler-Lagrange with an 8% variation in $\bar{\beta}$ for the initial condition $x_0 = [0.5 \quad -1.2]$.

model, whereas $x_3 \neq 0$ corresponding to the initial time. The following two suggestions are proposed.

Suggestion 1: Sensors

Using hot wires, or velocity probes the circumferential velocity disturbance can be measured. According to equations (2.20) and (2.26), the disturbance is related to the stall amplitude A, which is related to x_3 as $x_3 = A^2$. Therefore, the inception and settling time of x_3 can be measured. Let us denote the settling time of x_3 by t_s. The controller (5.3) is then applied to the third order system (5.1) at t_s, which is the method that is used in practice. In order to implement the proposed controller in MATLAB, one either needs to

i	$x_{i_0}^{min}$	$x_{i_0}^{max}$	$\mathbb{N}_i^b$
1	-2.0	2.0	$\{1, 2, \ldots, 7\}$
2	-2.0	2.0	$\{1, 2, \ldots, 7\}$
3	0.0	1.0	$\{1, 2, \ldots, 7\}$

Table 5.1: Set of parameters that specify the initial conditions of the open-loop full order Moore-Greitzer model.

simulate sensors, or to follow the Suggestion 2.

Suggestion 2: Simulation Experiment

Using a relatively wide range of initial conditions, the open-loop system (5.1) is simulated for the stall amplitude. The set of initial conditions for each state has the form

$$x_{i_0} \in \left\{ x_i \mid x_i = x_{i_0}^{min} + \frac{n_i}{\max n_i}(x_{i_0}^{max} - x_{i_0}^{min}),\ n_i \in \mathbb{N}_i^b \right\}, \tag{5.4}$$

where $i = 1, 2, 3$ is the state index, $x_{i_0}^{min}$ and $x_{i_0}^{min}$ are the minimum and the maximum initial values considered for the state x_i, and $\mathbb{N}_i^b$ is a bounded subset of natural numbers. Figure 5.2 illustrates the open-loop simulation of (5.4) associated with more than 340 sets of initial conditions that are given in Table 5.1.

According to the simulation conducted for these initial conditions (refer to Figure 5.2), x_3 damps out very quickly as compared to the other two states and reaches zero. Note that the initial conditions for x_1 and x_2 are chosen from the sets $|x_{1_0}| \leq 2$ and $|x_{2_0}| \leq 2$. This is due to the fact that the settling time for x_3 was decreased while $|x_{1_0}|$ and $|x_{2_0}|$ were increased beyond 2, according to the simulation results.

As shown in Figure 5.2, the state x_3 settles down within less that 0.7 seconds, allowing one to apply the proposed PEL controller to the third order model. However, a modeled sensor in MATLAB is used to determine the settling time of x_3 in the following simulations.

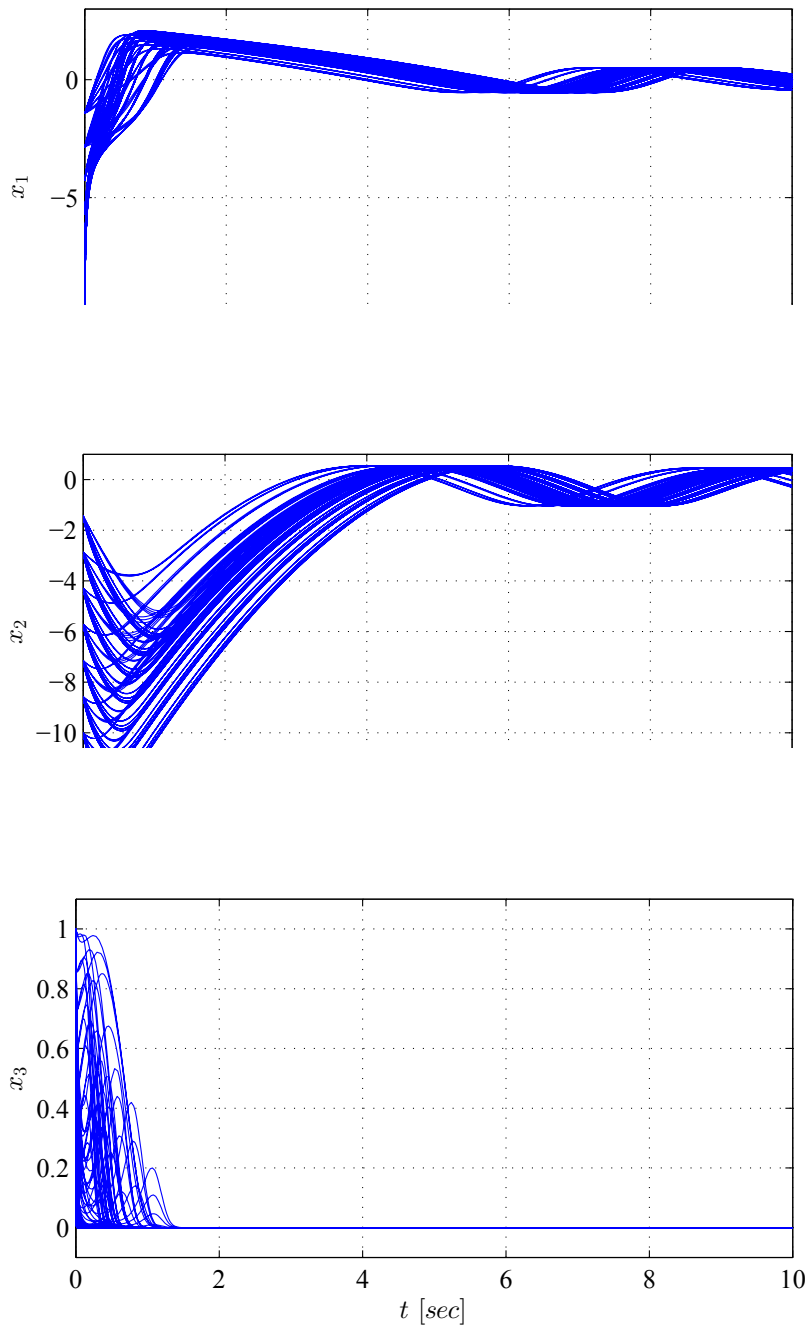

Figure 5.2: Simulation of the open-loop third order Moore-Greitzer model with more than 340 sets of initial condition.

5.1.2 Comparison

Pseudo Euler-Lagrange:

The proposed controller in equation (5.3) is used to control the third order Moore-Greitzer model (5.1). The results of the simulations are shown using the **solid lines** in Figures 5.4a, 5.4b, and 5.4c. The initial conditions used for the simulations are given as follows

$$x_0 = [-1.2 \;\; 1.0 \;\; 0.5]^T, \tag{5.5a}$$

$$x_0 = [0.6 \;\; -1.4 \;\; 0.2]^T, \tag{5.5b}$$

$$x_0 = [1.7 \;\; -0.4 \;\; 0.9]^T. \tag{5.5c}$$

Backstepping:

One of the best techniques that is used to control the system (5.2) is backstepping. The design procedure, as well as the solution to this problem is already addressed in Section 3.5.2. The backstepping control law that was obtained in Chapter 3 is repeated here

$$u_2 = (1-\beta^2)x_1 + \beta^2\gamma_b x_2 + \beta^2 \frac{9\gamma_b}{8\alpha_b}(x_2 - \gamma_b x_1) \tag{5.6}$$

The closed-loop system was given a disturbance of an 8% change in $\bar{\beta}$, for which the simulations are given in Figure 5.3.

Although the system does not become unstable, according to equation (3.59) the candidate Lyapunov function is not negative definite (for $(x_1, x_2) = (-2.1, 2.0)$ we have $\dot{V} = 0.85 > 0$). This implies that there is no guarantee that for a different initial condition the system is stable. However, we still take into the consideration that a Lyapunov function may be found for the closed-loop disturbed MG system by the controller (5.6). Therefore, using the initial conditions that are given in (5.5), the controller in (5.6) is applied to the third order MG model. The results of the simulations are shown using the **dashed lines** in Figures 5.4a, 5.4b, and 5.4c. Comparing the third order system (5.1) response using the

PEL and the *backstepping* controllers, as shown in Figure 5.4, the following observations are made.

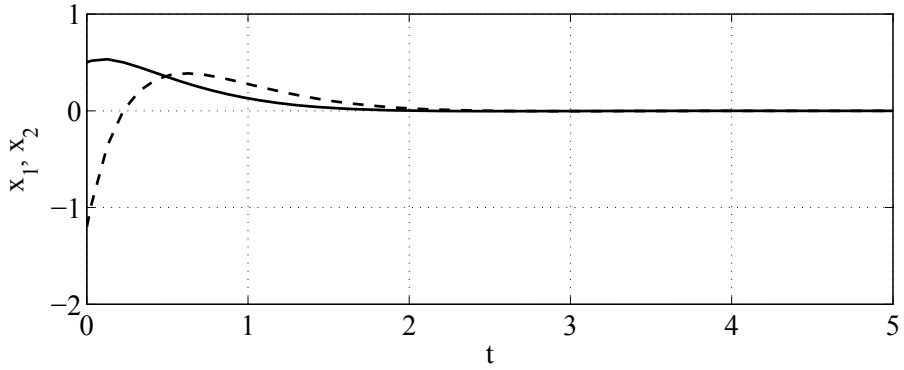

(a) States corresponding to the solid and dashed lines represent x_1 and x_2, respectively.

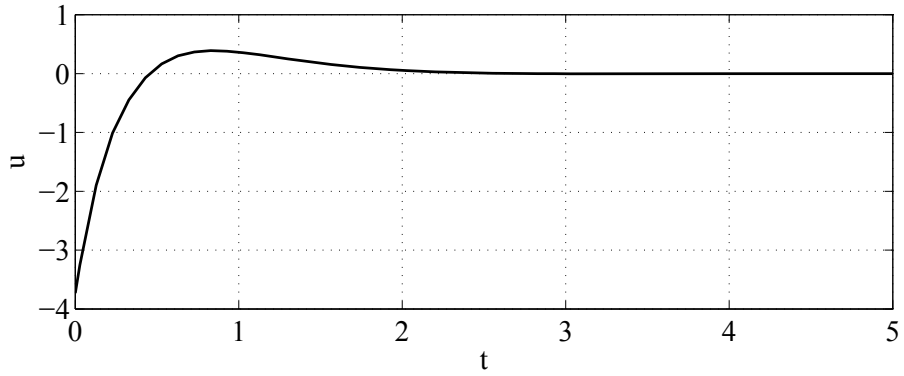

(b) Control input signal.

Figure 5.3: Simulation of the closed-loop system by the backstepping with an 8% variation in $\bar{\beta}$ for the initial condition $x_0 = [0.5 \quad -1.2]$.

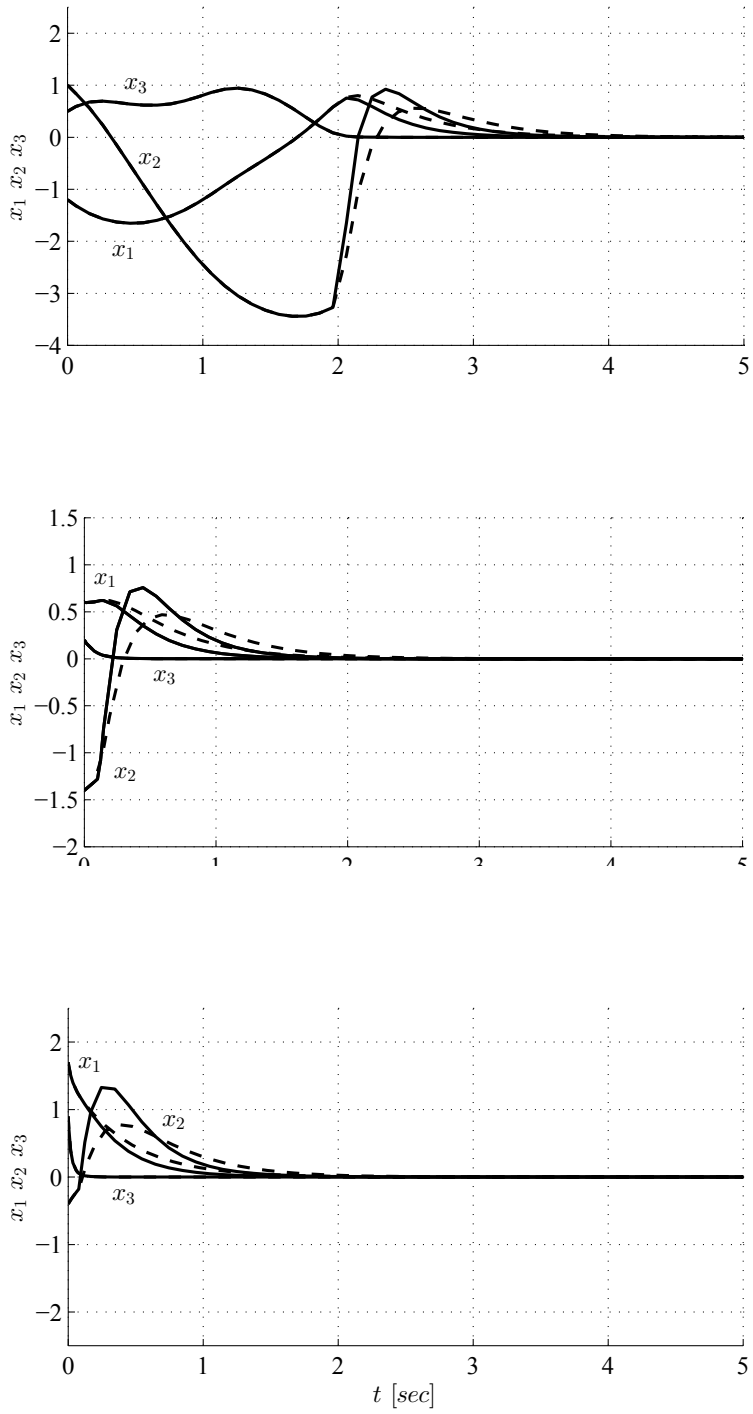

(c) The initial condition is $x_0 = [1.7 \quad -0.4 \quad 0.9]^T$.

Figure 5.4: States corresponding to the solid and dashed lines represent the closed-loop third order MG model by using *PEL* and *backstepping* techniques, respectively.

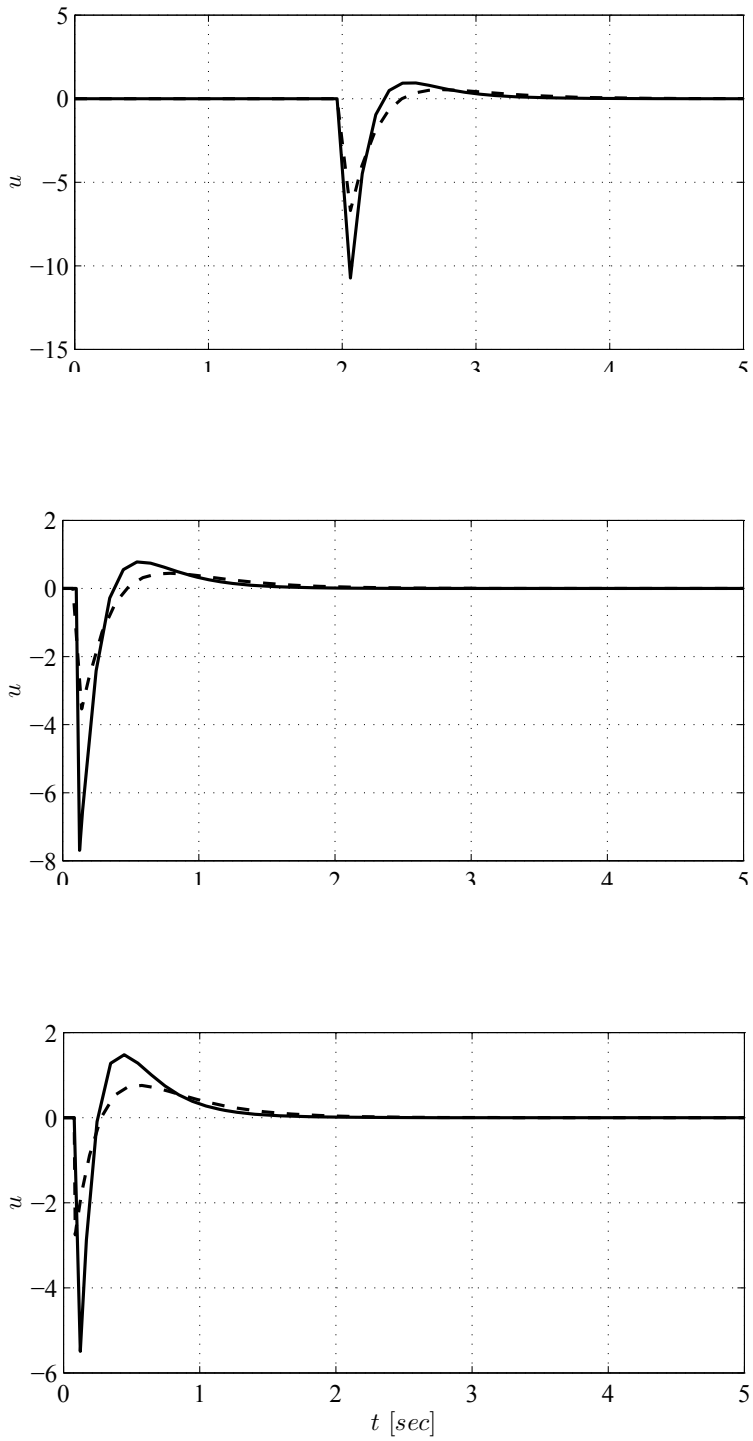

(c) The initial condition is $x_0 = [1.7 \quad -0.4 \quad 0.9]^T$.

Figure 5.5: The solid and dashed lines correspond to the *PEL* and *backstepping* control laws, respectively. Note that the kink point represents the first control signal after the delay.

1. The settling time of the states using the PEL controller is less than the settling time of the states using the backstepping controller.

2. Using the backstepping controller the maximum overshoot of the system response is less than the system response by using the PEL.

Figure 5.5 represents the *PEL* control action versus the *backstepping* control action. As it was discussed in Section 5.1.1, the stall amplitude is measured using sensors. As the stall amplitude is damped out, the control signal obtained by using the second order system (5.2) is applied to the third order system (5.1).

Feedback Linearization:

The control law that was driven based on the feedback linearization technique is given below

$$u_2 = -\beta^2 \left[\frac{3}{4}x_1^5 + \frac{15}{4}x_1^4 + \left(\frac{1}{2}k_1^f + \frac{9}{2}\right)x_1^3 + \frac{3}{2}x_1^2 x_2 + \frac{3}{2}k_1^f x_1^2 + 3x_1 x_2 - \left(\frac{1}{\beta^2} + k_2^f\right)x_1 + k_1^f x_2 \right]. \tag{5.7}$$

This controller for the surge model loses stability for an 8% of disturbance in the $\bar{\beta}$ (refer to Figure 5.6). The position of the closed-loop poles are chosen to yield

$$\zeta = 0.5$$

$$\omega_n = 0.5$$

so that $P_i = -\zeta\omega_n \pm \sqrt{1-\zeta^2}\omega_n j$. The simulations associated with this system are given in Figure 5.6. Note that the aircraft is considered as a safety-critical system. Figure 5.6 shows that the feedback linearization method does not provide a reliable and robust solution for the aerial engine surge problem due to instability.

5.1.3 Conclusions

In this section, the axial compressor surge problem was treated with three different non-linear control techniques. As shown, the pseudo Euler-Lagrange provided the third order

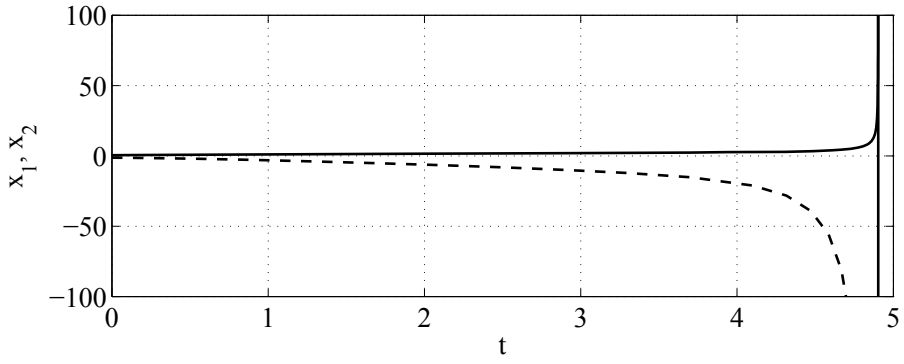

(a) States corresponding to the solid and dashed lines represent x_1 and x_2, respectively.

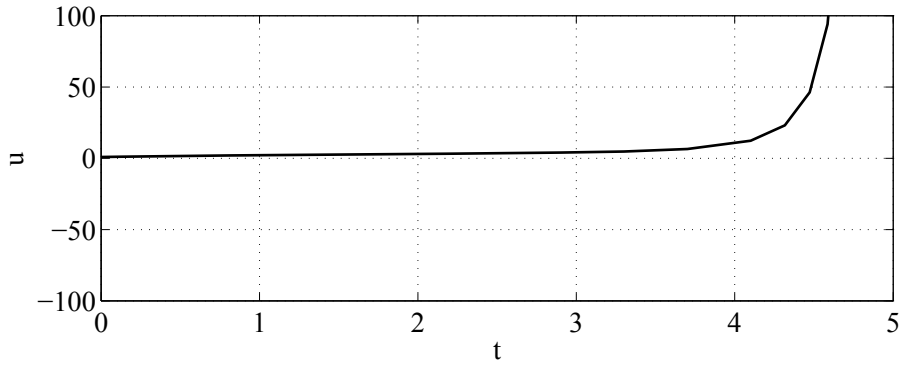

(b) Control input signal.

Figure 5.6: Simulation of the closed-loop system by the feedback linearization with an 8% variation in $\bar{\beta}$ for the initial condition $x_0 = [0.5 \quad -1.2]$.

Moore Greitzer model with robustness. Accordingly, for some system parameter variations the system was still guaranteed to be stable, which could not be accomplished by using the feedback linearization technique. The backstepping controller was also able to stabilize the disturbed system to the origin. Nevertheless, we did not obtain a formal mathematical proof that the backstepping method guarantees stability under parameter variations.

5.2 Piecewise Affine Approach

5.2.1 IPWA Approximation and the Modeling Problem

In this section the proposed IPWA approximation method will be compared to the uniform grid and the Voronoi-based PWA approximation techniques. Accordingly, a brief introduction of these methods and the general notion of the algorithms are given. However, the reader is encouraged to refer to the original literature, namely reference [39] for the uniform grid and reference [76] for the Voronoi-based techniques.

A. Uniform Grid PWA Approximation Technique

The uniform grid PWA approximation can be used to approximate a continuous function of $n-$variables. However, the following algorithm is given for a function of $2-$variables, since the nonlinear functions that are approximated in this section are functions of $2-$variables. Let $f : \Omega \to \mathbb{R}$ be a continuous nonlinear function, where $\Omega \subset \mathbb{R}^2$.

1. Axes $\{x_1\}$ and $\{x_2\}$ are uniformly partitioned into m_1 and m_2 regions, respectively.

2. By using a sized partitioning of each axis (i.e. $\{x_1, x_2\}$), the domain is uniformly partitioned into $m_1 \times m_2$ rectangular regions that are denoted by $\mathscr{R}_{ij}^R$, where R in the superscript stands for rectangular, and $i \in \{1,2,\ldots,m_1\}$ and $j \in \{1,2,\ldots,m_2\}$. Denote the vertices of $\mathscr{R}_{ij}^R$ by V_1, V_2, V_3 and V_4.

3. Using the main diagonal V_1V_3 each rectangular region $\mathscr{R}_{ij}^R$ is the subdivided into two simplices, which in this case are triangles. These simplicial regions are denoted by $\mathscr{R}_{ij}^U$ and $\mathscr{R}_{ij}^L$. Note that the vertices of $\mathscr{R}_{ij}^U$ are $\{V_1, V_2, V_3\}$ and the vertices of $\mathscr{R}_{ij}^L$ are $\{V_1, V_3, V_4\}$.

4. The nonlinear function f is then evaluated at each vertex of the regions $\mathscr{R}_{ij}^U$ and $\mathscr{R}_{ij}^L$. Accordingly, two hyperplanes $\{(x,y) \mid y = h_{ij}^U(x)\}$ and $\{(x,y) \mid y = h_{ij}^L(x)\}$

are constructed by using the sets of points $\{(V_1, f(V_1)), (V_2, f(V_2)), (V_3, f(V_3))\}$ and $\{(V_1, f(V_1)), (V_3, f(V_3)), (V_4, f(V_4))\}$, respectively.

5. The algorithm returns functions $h_{ij}^U : \mathscr{R}_{ij}^U \to \mathbb{R}$ and $h_{ij}^L : \mathscr{R}_{ij}^L \to \mathbb{R}$.

In order to reach a desirable maximum approximation error, the number of partitions corresponding to each axis is increased. Therefore, the algorithm is conducted starting Step 3.

B. Voronoi-based PWA Approximation Technique

The Voronoi-based PWA approximation technique was originally introduced for functions of $2-$variables [76]. In this section, a concise algorithm associated with this methodology is given.

Definition 5.2.1. *[76] Let $\Omega \subset \mathbb{R}^2$ denote a given domain, and $\Xi = \{X_1, X_2, \ldots, X_m\} \subset \Omega$ designate the set of generators or Voronoi centers. The Voronoi cell $\mathcal{V}(X_i)$ in Ω corresponding to the generator in X_i is then defined by*

$$\mathcal{V}(X_i) = \{x \in \Omega \mid \|x - X_i\| < \|x - X_j\|\}, \ \ \forall X_i, X_j \in \Xi \ \ with \ j \neq i. \tag{5.8}$$

Let $f : \Omega \to \mathbb{R}$ be a continuous nonlinear function, where $\Omega \subset \mathbb{R}^2$. The Voronoi-base PWA approximation of f is computed as follows:

1. A set of initial generators $\Xi = \{X_1, X_2, \ldots, X_m\}$ are given. The criterion to determine the generators is based on the points, where the surface of the function f has the minimum value of mean curvature, as defined in Definition 4.4.1.

2. The domain Ω is then partitioned into m Voronoi cells denoted by $\mathcal{V}(X_i)$ according to Definition 5.2.1.

3. For each generator, the hyperplane $\{(x, y) \mid y = h_i(x)\}$ is constructed by linearizing f around X_i. The functions $h_i : \mathcal{V}(X_i) \to \mathbb{R}$ are therefore produced.

4. The maximum error e_{max} is obtained numerically, as

$$e_{max} = \arg\max \left[\sup_{x \in \mathcal{V}(X_i)} (f(x) - h_i(x)) \right] \tag{5.9}$$

The argument of the above maximization is denoted by x^*.

5. Let e_{des} be the user-defined desirable maximum approximation error. Then if the criterion $e_{max} < e_{des}$ is satisfied, the algorithm is stopped and it returns functions h_i. Otherwise go to Step 6.

6. Let $X_{m+1} = x^*$ and $m := m+1$. Go to Step 2.

C. Application of PWA Approximation Methods to the Moore-Greitzer Model

With reference to equation (5.1), the MG model uses two nonlinear functions

$$f_1(x) = -\sigma x_3^2 - \sigma x_3 \left(2x_1 + x_1^2\right) \tag{5.10a}$$

$$f_2(x) = \frac{1-(1+x_1)^3}{2} - 3x_3 x_1 \tag{5.10b}$$

The approximation domain Ω for both of these functions is chosen as follows

$$\Omega = \{x \mid Dx + d \leq 0\} \tag{5.11}$$

$$D = \begin{bmatrix} -0.8894 & 0.45714 \\ 0.48678 & 0.87353 \\ 1 & 0 \\ -0.49103 & 0.87114 \\ -0.34182 & -0.93976 \\ -1 & 0 \end{bmatrix}, \quad d = \begin{bmatrix} 1.6467 \\ 1.6396 \\ 0 \\ 1.7946 \\ 1.0253 \\ 1.5 \end{bmatrix}$$

The above region is chosen as the domain of the nonlinearity because in the chosen Ω we have

- the operating point is contained, and

- f_1 is highly nonlinear,

By checking the Hessian matrix of f_1 and f_2, it can be shown that these functions are not concave nor convex, implying that the algorithm for concave functions cannot directly be applied to them.

Although f_1 is not concave over Ω, the average of its mean surface curvature is negative $\bar{H}_\Omega(f_1) = -0.67$. For this reason, we can apply the *FOCP* [1] algorithm to compute the concave approximant, for which the *intersection-based PWA approximation for concave functions* is applicable. Although $\bar{H}_\Omega(f_2) = -0.13$ is negative, the concave polynomial approximation is not suitable for f_2. For this reason, the *CONS* [2] algorithm is used to determine the intersection-based approximation of f_2. Since the regions are convex polytopes, they can be defined as

$$\mathscr{R}_i = \{x \mid E_i x + e_i \leq 0\} \tag{5.12}$$

where E_i is an $m \times 3$ and e_i is an $m \times 1$ matrices, and m is the number of edges associated with the i^{th} region.

The maximum error and the number of regions that are obtained for the approximation are listed in Table 5.2. As can be seen from Table 5.2, for a fixed number of regions the intersection-based PWA approximation for the MG model yields less amount of approximation error.

5.2.2 PWA Control Synthesis Problem

The synthesis method used in this section is the PWA state feedback method, primarily based on [28]. For this purpose, a common quadratic Lyapunov function $V = x^T P x$ is required such that $V > 0$ and $\dot{V} < -\alpha V$, where P is a 3×3 symmetric matrix and $\alpha > 0$. These conditions guarantee the exponential stability of the PWA system. The reader is

[1] FOCP is an acronym standing for *Fourth Order Concave Polynomial Approximation* introduced in Subsection 4.4.1.A.

[2] CONS is an acronym standing for *Conservative Approach* introduced in Subsection 4.4.1.B.

PWA Approximation of $\mathbf{f_1(x)}$ with 5 Regions		
APPROXIMATION METHOD	e_{max}	CONTINUITY
Intersection-based FOCP	**8.53**	**Continuous**
Voronoi-based	9.88	Discontinuous
Uniform Grid	10.65	**Continuous**
PWA Approximation of $\mathbf{f_2(x)}$ with 2 Regions		
Intersection-based CONS	**3.46**	**Continuous**
Voronoi-based	5.58	Discontinuous
Uniform Grid	4.89	**Continuous**

Table 5.2: A brief summary of the PWA approximation of $f_1(x)$ and $f_2(x)$ using different methods.

encouraged to refer to [28] for more detail. Following [28], the next BMI has to be solved for determining the state feedback gains

$$\begin{bmatrix} G_1 & G_2 \\ G_2^T & G_3 \end{bmatrix} < 0 \tag{5.13}$$

where $G_1 = (A_iQ + B_iY_i)^T + (A_iQ + B_iY_i) + \alpha Q + Q^T E_i^T \Lambda_i E_i Q$, $G_2 = (b_i + B_i m_i) + Q^T E_i^T \Lambda_i e_i$ and $G_3 = e_i^T \Lambda_i e_i$. In the above inequality $Q = P^{-1}$ and $Y_i = K_i Q$, where K_i is the state feedback gain for the i^{th} region, m_i is the state feedback affine term and Λ_i is an $m \times m$ matrix with non-negative elements. For more detail the reader is referred to [28].

Solving the inequality (5.13) by using PENBMI [49] with YALMIP [82] interface, the following Lyapunov matrix is obtained

$$P = \begin{bmatrix} 701.1853 & -265.5056 & 1.2700 \\ -265.5056 & 103.7864 & -0.5107 \\ 1.2700 & -0.5107 & 0.0039 \end{bmatrix} \tag{5.14}$$

The resulting state feedback gains are given by

$$K_1 = [\ 736.89 \quad -115.61 \quad 42.91\ ], \quad m_1 = 0$$
$$K_2 = [\ 786.65 \quad -125.01 \quad 47.05\ ], \quad m_2 = -2.8603$$
$$K_3 = [\ 720.50 \quad -112.82 \quad 42.03\ ], \quad m_3 = 3.1026$$
$$K_4 = [\ 1027.7 \quad -162.13 \quad 60.64\ ], \quad m_4 = -2.0473$$
$$K_5 = [\ 724.66 \quad -113.45 \quad 42.21\ ], \quad m_5 = -1.6368$$

By selecting $\beta = 1/\sqrt{2}$ and $\alpha = 7$ taken from [16], the simulation results for two different sets of initial conditions, namely $x_0 = [0.4,\ -1.4,\ 0.5]^T$ and $x_0 = [1.04,\ 0.55,\ 0.5]^T$, are shown in Figures 5.7a and 5.7b . In simulations, by applying the state feedback gains to the intersection-based PWA MG model, it follows that the oscillatory nonlinear model (5.1) is damped out within a short time period. As can be seen form Figures 5.7a and 5.7b, the settling times corresponding to $x_0 = [0.4,\ -1.4,\ 0.5]^T$ and $x_0 = [1.04,\ 0.55,\ 0.5]^T$ are 2.4 and 0.8 seconds, respectively.

5.2.3 Conclusions

In this section, the intersection-based PWA approximation method, as a new and powerful method in the PWA approximation of nonlinear systems was developed. Using the algorithms provided in Section 4.4.1, the PWA models can be constructed for a wide range of nonlinear functions. The method was successfully applied to the Moore-Greitzer axial compressor surge and stall dynamics, as a safety-critical system. This model had never been stabilized by using the PWA method in the literature before. However, due to the computational complexities involved solving the BMIs are difficult in certain cases. For instance, using PENBMI we were not be able to obtain the state feedback gains for the PWA model obtained by the Voronoi-based and the uniform grid PWA approximation methods.

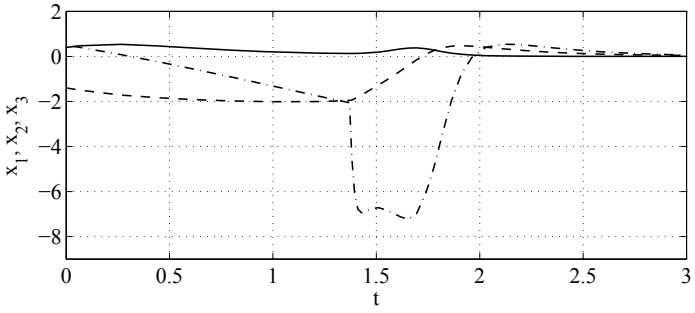

(a) The initial condition is $x_0 = [0.4,\ -1.4,\ 0.5]^T$.

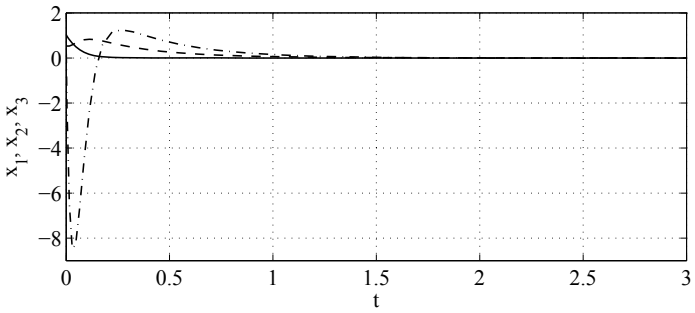

(b) The initial condition is $x_0 = [1.04,\ 0.55,\ 0.5]^T$.

Figure 5.7: Simulation results of the closed-loop MG model using the state feedback PWA controller. The dashed, dash-dot and the solid lines represent x_1, x_2 and x_3, respectively.

Chapter 6

Conclusions and Future Research

6.1 Conclusions

This chapter summarizes the main contributions of this research. In Chapter 2, the axial compressor that is used in gas turbines were introduced. Then rotating stall and surge were discussed. They are two important instabilities in a compressor that may cause severe mechanical damage and engine flame-out. Following the work done by Moore and Greitzer in [3], a second order surge and a third order surge and rotating stall dynamics were provided.

In Chapter 3, pseudo Euler-Lagrange systems that were introduced in [25] were extended to a system of the same order, but with additional nonlinear terms. The proposed method enables one to fit a more general class of second order systems for performing and solving Lyapunov-based control synthesis problems, such as the second order axial compression surge phenomenon in jet engines. Accordingly, the stability analysis of the extended pseudo Euler-Lagrange systems and the technique used to formulate a second order system as an extended pseudo Euler-Lagrange system were addressed. The proposed technique was applied to the stabilization problem of the no-stall Moore-Greitzer axial compressor model. In order to compare the stabilization properties of the proposed

method, a feedback linearization and a backstepping controllers were also designed as benchmark methods. The main advantages of the pseudo Euler-Lagrange method for the suppression of the Moore-Greitzer model oscillation were found to be the following:

- The pseudo Euler-Lagrange technique provides the designed controller with a broad margin for choosing the control law coefficients such that the stability of the closed-loop system is guaranteed for a range of disturbances.
- During the design process, nonlinearities that may enhance the stability quality of the system are not canceled out as it is done in the feedback linearization technique.

In Chapter 4, the Intersection-based Piecewise Affine (IPWA) approximation method was proposed. After a brief review on PWA systems, the approximation theory for functions of one variable was first addressed. The theory of the proposed methodology was then extended to functions of n-variables. Using the intersection-based Piecewise Affine (IPWA) models, the following properties can be achieved:

- Continuity of the vector fields,
- Optimality of the linearization of the nonlinear function relative to the maximum approximation error,
- Increased reduction of the approximation error for a fixed number of regions can be achieved for the motivating Moore-Greitzer system in Section 5.2 (as compared to the Voronoi-based and the uniform grid PWA models),
- Consistency of the derivative of the nonlinear function with the derivative of its approximation at the linearization points.

The obtained and derived IPWA approximation technique results were used to approximate a third order axial compressor stall and surge system. The PWA control synthesis tools [28] are then used to design controllers for the obtained IPWA model.

In Chapter 5, the control synthesis problem of the Moore-Greitzer axial compressor model describing the two major compressor instabilities − namely the rotating stall and surge − was addressed by using both the pseudo Euler-Lagrange and the piecewise affine methodologies. The associated closed-loop system simulations corresponding to each nonlinear technique were provided. The obtained IPWA model of the third order stall and surge system, and a PWA synthesis technique [28] is then used to control the closed-loop system.

6.1.1 Contributions

The contributions of this work consist of proposing the following:

1. A new controller synthesis formulation for pseudo Euler-Lagrange systems is proposed, giving a more general form of this class of second order systems. By adding a nonlinear term, in contrast to previous work, the dynamics of both states are nonlinear functions of both states. In this regard, a more general class of physical nonlinear systems can be analyzed. Moreover, since there are always modeling uncertainties of as well as potential parameter variations, the advantages of the PEL method enable one to have a safe margin of stability.

2. A new PWA approximation methodology for functions of n-variables is developed. It is shown that continuity of the vector field and increased reduction in the approximation error are two important properties that can be achieved by using this technique. These advantages help to reduce the computation complexity of the PWA controller synthesis method.

6.2 Future Research

Based on the proposed methodologies in this thesis, the following interesting extensions are suggested. In Chapter 3, pseudo Euler-Lagrange systems were extended to comprise

more complex nonlinearities. Accordingly, the potential extensions in this field may include:

- Exploring the opportunities of the PEL systems addressed in Theorem 3.3.1 for higher order systems. Most of the physical phenomena are described by higher order set of differential equations. Aircraft flight dynamics, car dynamics or gas turbine governing equations are cases in point. Therefore, extending the PEL systems to higher order ODEs may provide a systematic procedure for designing Lyapunov-based controllers.

In Chapter 4, a new methodology for generating a PWA approximation of functions of n-variables was addressed. However, one can still consider the following problems:

- Considering the PWA synthesis problem for a given plant, how many regions are sufficient for the IPWA approximation such that a PWA state feedback gains are guaranteed to be determined?

- Given the amount of error, what is the approximation algorithm that minimizes the number of regions?

- The robustness of the controller designed for the rotating stall and surge phenomena is an interesting problem. To investigate such a problem, the interested reader is referred to [83], where the uncertainty of parameters in piecewise affine systems are addressed.

- And last but not the least, one can explore the use of PWA differential inclusion for the stability analysis and the control synthesis problems of a given plant based on the following suggestion. The nonlinear function associated with plant dynamics can be bounded with two convex (or concave) functions as the upper and the lower bound of the differential inclusion. IPWA algorithm can then be applied to generate the IPWA approximation of the upper and the lower bounds.

Bibliography

[1] Academic dictionaries and encyclopedias. [Online]. Available: http://en.academic.ru/dic.nsf/enwiki/37101

[2] T. Giampaolo, *The gas turbine handbook: Principles and practices*. Marcel Dekker Incorporated, 2003.

[3] F. K. Moor and E. M. Greitzer, "A Theory of Post-stall Transients in Axial Compression Systems: Part I-Development of Equations," *Journal of Engineering for Gas Turbines and Power*, pp. 68–76, 1986.

[4] J. Chen and R. Patton, *Robust model-based fault diagnosis for dynamic systems, 1999*. Kluwer Academic Publishers, Dordrecht, 1999.

[5] H. Cohen, G. F. C. Rogers, and H. Saravanamuttoo, *Gas Turbine Theory*, 4th ed. Longman, 1996.

[6] N. Meskin, E. Naderi, and K. Khorasani, "Fault diagnosis of jet engines by using a multiple model-based approach," *ASME Conference Proceedings*, vol. 2010, no. 43987, pp. 319–329, 2010. [Online]. Available: http://link.aip.org/link/abstract/ASMECP/v2010/i43987/p319/s1

[7] N. Daroogheh, A. Vatani, M. Gholamhossein, and K. Khorasani, "Engine life evaluation based on a probabilistic approach," in *International Mechanical Engineering Congress & Exposition*. USA, Texas, Houston: ASME, November 2012.

[8] A. Epstein, F. Williams, and E. Greitzer, "Active suppression of aerodynamic instabilities in turbomachines," *Journal of Propulsion and Power*, vol. 5, no. 2, pp. 204–211, 1989.

[9] J. Paduano, L. Valavani, A. Epstein, E. Greitzer, and G. Guenette, "Modeling for control of rotating stall," *Automatica*, vol. 30, no. 9, pp. 1357–1373, 1994.

[10] M. Krstić, I. Kanellakopoulos, and P. Kokotović, *Nonlinear and Adaptive Control Design*, 1st ed. John Wiley & Sons, Inc., 1995.

[11] R. D'Andrea, R. Behnken, and R. Murray, "Active control of an axial flow compressor via pulsed air injection," *California Institute of Technology*, 1996.

[12] H. Weigl, J. Paduano, L. Frechette, A. Epstein, E. Greitzer, M. Bright, and A. Strazisar, "Active stabilization of rotating stall and surge in a transonic single stage axial compressor," Ph.D. dissertation, Massachusetts Institute of Technology, Dept. of Aeronautics and Astronautics, 1997.

[13] Y. Liang and D. Liaw, "Detection of surge and stall in compression systems: an example study," *Automatic Control, IEEE Transactions on*, vol. 46, no. 10, pp. 1609–1613, 2001.

[14] F. Blanchini and P. Giannattasio, "Adaptive control of compressor surge instability," *Automatica*, vol. 38, no. 8, pp. 1373–1380, 2002.

[15] M. Nayfeh and E. Abed, "High-gain feedback control of rotating stall in axial flow compressors," *Automatica*, vol. 38, no. 6, pp. 995–1001, 2002.

[16] A. Shiriaev, R. Johansson, A. Robertsson, and L. Freidovich, "Output Feedback Stabilization of the Moore-Greitzer Compressor Model," *Proceedings of the 44th IEEE Conference on Decision and Control, and the European Control Conference*, pp. 1102–1107, December 2005.

[17] A. Babbar and V. Syrmos, "Data driven approach for fault detection and identification using competitive learning techniques," in *European Control Conference, Kos, Greece*, 2007.

[18] E. Ortiz and V. Syrmos, "Support vector machines and wavelet packet analysis for fault detection and identification," in *Neural Networks, 2006. IJCNN'06. International Joint Conference on*. IEEE, 2006, pp. 3449–3456.

[19] R. Patton, P. Frank, and C. R., *Issues in Fault Diagnosis in Dynamic Systems*. Springer-Verlag, 2000.

[20] J. He, Z. Zhou, X. Yin, and S. Chen, "Using neural networks for fault diagnosis," in *Neural Networks, 2000. IJCNN'06. International Joint Conference on*. IEEE, 2000, pp. 217–220.

[21] G. Betta, C. Liguori, and A. Pietrosanto, "An advanced neural-network-based instrument fault detection and isolation scheme," *IEEE Transactions on Instrumentation and Measurement*, vol. 47, no. 2, pp. 507–512, 1998.

[22] J. Gertler, *Fault detection and diagnosis in engineering systems*. CRC, 1998.

[23] N. Daroogheh, A. Baniamerian, H. Nayyeri, and K. Khorasani, "Deterioration detection and health monitoring in aircraft jet engines," in *International Mechanical Engineering Congress & Exposition*. ASME, 2012.

[24] K. Ogata, *Modern Control Engineering*, 4th ed. Prentice Hall, 2002.

[25] L. Rodrigues, "Lyapunov stability of pseudo Euler-Lagrange systems," in *20^{th} Mediterranean Conference on Control and Automation*, July 2012, pp. 416–420.

[26] M. Johansson, *Piecewise Linear Control Systems*, 1st ed. Springer-Verlag, Berlin, 2003.

[27] L. Rodrigues and J. How, "Synthesis of piecewise-affine controllers for stabilization of nonlinear systems," vol. 3, Hawaii, Maui, dec. 2003, pp. 2071–2076.

[28] L. Rodrigues and S. Boyd, "Piecewise-affine state feedback for piecewise-affine slab systems using convex optimization," *Systems & Control Letters*, vol. 54, pp. 835–853, 2005.

[29] S. Casselman and L. Rodrigues, "Piecewise affine modeling of a micro air vehicle using voronoi partitions," in *Proceedings of the European Control Conference,*, Budapest, Hungary, 2009, pp. 3857–3862.

[30] A. Cantoni, "Optimal curve fitting with piecewise linear functions," *IEEE Transactions on Computers*, vol. C-20, pp. 59–67, January 1971.

[31] I. Tomek, "Two algorithms for piecewise-linear continuous approximation of functions of one variable," *IEEE Transactions on Computers*, vol. C-24, pp. 445–448, April 1974.

[32] P. Julian, A. Desages, and O. Agamennoni, "High-level canonical piecewise linear representation using a simplicial partition," *IEEE Transactions on Circuits and Systems I: Fundamental Theory and Applications*, vol. 46, pp. 1057–7122, April 1999.

[33] R. E. Groff, P. P. Khargonekar, and D. E. Koditschek, "A local convergence proof for the MINVAR algorithm for computing continuous piecewise linear approximations," *SIAM Journal of Numerical Analysis*, vol. 41, no. 3, pp. 983–1007, 2003.

[34] S. Azuma, J. Imura, and T. Sugie, "Lebesgue piecewise affine approximation of nonlinear systems," *Nonlinear Analysis: Hybrid Systems*, vol. 4, no. 1, pp. 92–102, 2010.

[35] M. Storace and O. D. Feo, "Piecewise-linear approximation of nonlinear dynamical systems," *IEEE Transactions on Circuits and Systems*, vol. Vol. 51, no. No. 4, pp. 830–842, 2004.

[36] J. M. Gonçalves, A. Megretski, and M. A. Dahleh, "Global analysis of piecewise linear systems using impact maps and surface lyapunov functions," *IEEE Transactions on Automatic Control*, vol. Vol. 48, no. No. 12, pp. 2089–2106, 2003.

[37] E. Asarin, T. Dang, and A. Girard, *Hybrid Systems: Computation and Control*. Springer, 2003, pp. 20–35.

[38] G. Feng, "Controller design and analysis of uncertain piecewise-linear systems," *IEEE Transactions on Circuits and Systems - I: Fundamental Theory and Applications*, vol. Vol. 49, no. No. 2, pp. 224–232, 2002.

[39] L. Rodrigues and J. P. How, "Automated Control Design for a Piecewise-Affine Approximation of a Class of Nonlinear Systems," in *Proceedings of the American Control Conference*, Virginia, Arlington, 2001, pp. 3189–3194.

[40] W. Yue, L. Rodrigues, and B. Gordon, "Piecewise-affine control of a three DOF helicopter," in *Proceedings of the 2006 American Control Conference*, Minnesota, Minneapolis, 2006, pp. 3924–3929.

[41] D. Corona and B. D. Schutter, "Adaptive cruise control for a SMART car: A comparison benchmark for MPC-PWA control methods," *IEEE Transactions on Control Systems Technology*, vol. Vol. 16, no. Number 2, pp. 365–372, 2008.

[42] G. Ferrari-Trecate, M. Muselli, D. Liberati, and M. Morari, "A clustering technique for the identification of piecewise affine systems," *Automatica*, vol. 39, no. 2, pp. 205–217, 2003.

[43] A. Bemporad and M. Morari, "Control of systems integrating logic, dynamics, and constraints," *AUTOMATICA-OXFORD-*, vol. 35, pp. 407–428, 1999.

[44] C. Tomlin, I. Mitchell, and R. Ghosh, "Safety verification of conflict resolution manoeuvres," *IEEE Transactions on Intelligent Transportation Systems*, vol. 2, no. 2, pp. 110–120, 2001.

[45] R. Ghosh, A. Tiwari, and C. Tomlin, "Automated symbolic reachability analysis; with application to delta-notch signaling automata," *Hybrid Systems: Computation and Control*, pp. 233–248, 2003.

[46] S. Azuma and J. Imura, "Polynomial-time probabilistic controllability analysis of discrete-time piecewise affine systems," *IEEE Transactions on Automatic Control*, vol. 52, no. 11, pp. 2029–2046, 2007.

[47] ——, "Polynomial-time probabilistic observability analysis of sampled-data piecewise affine systems," in *Decision and Control, 2005 and 2005 European Control Conference. CDC-ECC'05. 44th IEEE Conference on*. Spain, Seville: IEEE, 2005, pp. 6644–6649.

[48] B. Samadi and L. Rodrigues, "Extension of local linear controllers to global piecewise affine controllers for uncertain non-linear systems," *International Journal of Systems Science*, vol. 39, no. 9, pp. 867–879, 2008.

[49] M. Kočvara and M. Stingl, "PENBMI: An optimization software package (version 2.1)," 2008.

[50] J. Mattingly and H. von Ohain, *Elements of gas turbine propulsion*. McGraw-Hill New York, 1996.

[51] E. M. Greitzer, "The stability of pumping systems-the 1980 freeman scholar lecture," *ASME Transactions Journal of Fluids Engineering*, vol. 103, pp. 193–242, 1981.

[52] F. Willems and B. De Jager, "Modeling and control of compressor flow instabilities," *Control Systems, IEEE*, vol. 19, no. 5, pp. 8–18, 1999.

[53] B. de Jager, "Rotating stall and surge control: A survey," in *Decision and Control, 1995., Proceedings of the 34th IEEE Conference on*, vol. 2. Louisiana, New Orleans: IEEE, 1995, pp. 1857–1862.

[54] J. Ffowcs Williams, M. Harper, and D. Allwright, "Active stabilization of compressor instability and surge in a working engine," *Journal of turbomachinery*, vol. 115, no. 1, pp. 68–75, 1993.

[55] I. Day, "Active suppression of rotating stall and surge in axial compressors," *Journal of Turbomachinery;(United States)*, vol. 115, no. 1, 1993.

[56] S. Yeung and R. Murray, "Reduction of bleed valve rate requirements for control of rotating stall using continuous air injection," in *Control Applications, 1997., Proceedings of the 1997 IEEE International Conference on*. Connecticut, Hartford: IEEE, 1997, pp. 683–690.

[57] K. Nakagawa, M. Fujiwara, T. Nishioka, S. Tanaka, and Y. Kashiwabara, "Experimental and numerical analysis of active suppression of centrifugal compressor surge by suction-side valve control," *JSME international journal. Series B, fluids and thermal engineering*, vol. 37, no. 4, pp. 878–885, 1994.

[58] W. Jungowski, M. Weiss, and G. Price, "Pressure oscillations occurring in a centrifugal compressor system with and without passive and active surge control," *Journal of turbomachinery*, vol. 118, no. 1, pp. 29–40, 1996.

[59] P. Tijl, "Modeling, simulation and evaluation of a centrifugal compressor with surge avoidance control," *MD Thesis*, 2004.

[60] L. He, "Computational study of rotating-stall inception in axial compressors," *Journal of Propulsion and Power*, vol. 13, no. 1, pp. 31–38, 1997.

[61] F. Moore, "Theory of rotating stall of multistage axial compressors," in *In Von Karman Inst. for Fluid Dynamics Unsteady Flow in Turbomachines, Vol. 1 112 p (SEE N84-25960 16-34)*, vol. 1, 1984.

[62] E. Greitzer, "Surge and rotating stall in axial flow compressorspart i: Theoretical compression system model," *Journal of Engineering for Power*, vol. 98, p. 190, 1976.

[63] F. K. Moore, "A theory of rotating stall of multistage axial compressors," 1983.

[64] K. Botros, "Transient phenomena in compressor stations during surge," *Journal of Engineering for Gas Turbines and Power;(United States)*, vol. 116, no. 1, 1994.

[65] J. Haynes, G. Hendricks, and A. Epstein, "Active stabilization of rotating stall in a three-stage axial compressor," *ASME Transactions Journal of Turbomachinery*, vol. 116, pp. 226–239, 1994.

[66] O. Badmus, S. Chowdhury, K. Eveker, and C. Nett, "Control-oriented high-frequency turbomachinery modeling: single-stage compression system one-dimensional model," *Journal of turbomachinery*, vol. 117, no. 1, pp. 47–61, 1995.

[67] R. A. Adomaitis, "Spatially resolved compressor characteristics for modeling and control of blade-scale flow instabilities," DTIC Document, Tech. Rep., 1995.

[68] J. T. Gravdahl and O. Egeland, *Compressor surge and rotating stall: Modelling and control*. Springer, 1999.

[69] S. Koff and E. Greitzer, "Stalled flow performance for axial compressors. i-axisymmetric characteristic," in *29th International Gas Turbine Conference and Exhibit*, vol. 1, Netherlands, Amsterdam, 1984.

[70] K. Magnus, *Vibrations*. Blackie, 1965.

[71] AGARD Conference Proceeding No.293, *TURBINE ENGINE TESTING*. North Atlantic Treaty Organization, 1980.

[72] H. K. Khalil, *Nonlinear Systems*, 3rd ed. Prentice Hall, 2002.

[73] D. G. Luenberger and Y. Ye, *Linear and Nonlinear Programming*, 3rd ed. Springer, 2008.

[74] H. Royden, *Real Analysis*, 2nd ed. MACMILLAN, 1968.

[75] S. Boyd and L. Vandenberghe, *Convex optimization*. Cambridge university press, 2004.

[76] S. Casselman and L. Rodrigues, "A new methodology for piecewise affine models using voronoi partitions," in *Proc. 48th IEEE Conference on Decision and Control and 28th Chinese Control Conference*, Shanghai, China, 2009, pp. 3920 –3925.

[77] H. Guggenheimer, *Applicable Geometry: Global and Local Convexity*. RE Krieger Publishing Company, 1977.

[78] J. Roskam, *Airplane Flight Dynamics and Automatic Flight Controls, Part I*, 3rd ed. DARcorporation, 2001.

[79] E. Kreyszig, *Advanced engineering mathematics*. John Wiley & Sons, 2007.

[80] W. Kuhnel, *Differential Geometry: Curves - Surfaces - Manifolds*, 2nd ed. American Mathematical Society, 2006.

[81] S. Chern, W. Chen, and K. Lam, *Lectures on differential geometry*. World Scientific Publishing Company Incorporated, 1999, vol. 1.

[82] J. Löfberg, "YALMIP : A toolbox for modeling and optimization in MATLAB (Version 3 R2010b)," in *Proceedings of the CACSD Conference*, 2004.

[83] B. Samadi and L. Rodrigues, "Extension of local linear controllers to global piecewise affine controllers for uncertain non-linear systems," *International Journal of Systems Science*, vol. 39, no. 9, pp. 867–879, 2008.